Development of CRISPR/Cas-mediated gene editing in the retina

by

Fan Li

Bachelor of Medicine, Zhengzhou University

Master of Medicine (Ophthalmology), Sun Yat-sen University

Submitted in fulfilment of the requirements for the

Degree of Doctor of Philosophy (Medical Research)

Menzies Research Institute Tasmania

University of Tasmania

06/2020

DECLARATION OF ORIGINALITY

This thesis contains no material which has been accepted for a degree or diploma by the University or any other institution, except by way of background information and duly acknowledged in the thesis, and to the best of my knowledge and belief no material previously published or written by another person except where due acknowledgement is made in the text of the thesis, nor does the thesis contain any material that infringes copyright.

Fan Li

20th September, 2019

AUTHORITY OF ACCESS

The publisher of the paper comprising Chapter 3 holds the copyright for that content, and access to the material should be sought from the journal. The remaining non-published content of this thesis may be made available for loan and limited copying and communication in accordance with the Copyright Act 1968.

Fan Li

20th September, 2019

STATEMENT OF CO-AUTHORSHIP

The following people and institutions contributed to the publication of work undertaken as part of this thesis:

Fan Li, Sandy S.C. Hung, MohdKhairul Nizam Mohd Khalid, Jiang-Hui Wang, Vicki Chrysostomou, Vickie H.Y. Wong, et al. Utility of self-destructing CRISPR/Cas constructs for targeted gene editing in the retina. Hum Gene Ther. 2019 Aug. doi: 10.1089/hum.2019.021.

Author contributions:

F.L. (Candidate) performed experiments, analysed data, prepared the manuscript draft and was involved with the study design (contributed approximately 70% to the project); S.H, A.W.H. and G.S.L designed the study; M.N.M.K, K.W., R.W. provided assistance with laboratory work, J.H.W. V.C., V.W., L.T, B.V.B helped with the animal study, V.S. performed sequencing analysis, A.P., A.E.K., A.L.C. provided resources and critical reading of the manuscript, A.W.H. and G.S.L supervised, administered the project and provided the funding. All the authors contributed to the final manuscript preparation.

We the undersigned agree with the above stated “proportion of work undertaken” for each of the above published peer-reviewed manuscript contributing to this thesis:

Date: 20th September, 2019

Signed:

Prof Alex Hewitt
Supervisor
Menzies Institute for Medical Research
University of Tasmania

Prof Graeme Zosky
Deputy Director
Menzies Institute for Medical Research
University of Tasmania

Date: 20th September, 2019

STATEMENT OF ETHICAL CONDUCT

The research associated with this thesis abides by the international and Australian codes on human and animal experimentation, the guidelines by the Australian Government's Office of the Gene Technology Regulator and the rulings of the Safety, Ethics and Institutional Biosafety Committees of the University of Tasmania with Ethics Approval Number A14827 and St. Vincent's Hospital Melbourne with Ethics Approval Number AEC 014/15.

Fan Li

Date: 20th September, 2019

ABSTRACT

Many eye diseases have a distinct genetic etiology and collectively, these account for a large proportion of blindness, worldwide. Despite advances in molecular diagnostics and our understanding of genetic etiology, there are no definitive treatments available for many genetic eye diseases. Emerging technologies — such as gene augmentation therapy or stem cell-based replacement therapy — could help restore vision in a number of patients. Recently developed gene-editing techniques also hold great potential for treating blinding or potentially even life-threatening ocular diseases.

The Clustered Regularly Interspaced Short Palindromic Repeats (CRISPR)/CRISPR-associated system (Cas) is an adaptive, prokaryotic immune defense system that coordinates against viral intrusion; it has since been repurposed in a programmable fashion that allows us to very specifically target a gene locus via a user-specified guide RNA. Due to the ease of designing guide RNAs, CRISPR holds great potential for the study or treatment of inherited diseases. There have been a handful of *in vivo* CRISPR/Cas studies demonstrating the potential of not only modeling various diseases, but also treating genetic disorders or labeling live cells. Crucial considerations regarding somatic gene editing include adequate delivery to target cells *in vivo*, elimination of off-target effects and improved gene-editing efficacy via different CRISPR/Cas systems. As a proof-of-concept study, the overall aim of my PhD project was to use fluorescent proteins as a model to explore the efficacy of *in vivo* CRISPR editing in the retina. Based on our previous study using adeno-associated virus 2 (AAV2) to deliver CRISPR/Cas to modify genes in retinal cells in yellow fluorescent protein (*YFP*) transgenic mice, my PhD study first focused on developing and validating a self-destructive AAV2-mediated CRISPR/Cas system to improve the biosafety of genome editing *in vivo*. Next, I performed a direct head-to-head comparison of the *in vivo* gene-editing efficacy of different CRISPR/Cas systems.

My last aim was to use *in vitro* genome-scale CRISPR screens to identify critical genes underlying the ocular cancer, uveal melanoma.

To eliminate the possibility of inadvertent off-target effects of CRISPR/Cas9, we designed a novel self-destructing CRISPR/Cas system that disrupts the Cas enzyme itself with an extra guide targeting *SpCas9* along with the original *YFP*-targeting guide. After validation in a YFP-expressing cell line, I tested it in Thy1-YFP transgenic mouse retina using a dual AAV2 vector delivery system: one vector to deliver the SpCas9 transgene, and the other to deliver their cognate sgRNAs against SpCas9 and the target locus (*YFP*), as well as an mCherry transgene to validate retinal penetration of the AAV. After 8 weeks, the expression of SpCas9 and the efficacy of *YFP* gene disruption was quantified. SpCas9 messenger RNA (mRNA) was reduced in retinas treated with dual AAV2-mediated-YFP/SpCas9 targeting CRISPR/Cas compared to those treated with *YFP*-targeting CRISPR/Cas alone. We also showed that AAV2-mediated delivery of YFP/SpCas9 targeting CRISPR/Cas significantly reduced the number of YFP fluorescent cells among mCherry-expressing cells (~85.5% reduction compared to LacZ/SpCas9-targeting CRISPR/Cas) in the transduced retina of Thy1-YFP transgenic mice. Our data suggest that a self-destructive "kamikaze"-CRISPR/Cas system can be used as a robust tool for genome editing in the retina, without compromising on-target efficiency.

To determine the most efficacious CRISPR/Cas endonucleases for retinal editing *in vivo*, I designed and constructed *YFP*-targeting guide RNAs for different CRISPR/Cas systems, followed by *in vitro* validation and sgRNA selection in YFP-expressing cells. I then performed knockout tests across a range of different conditions, using the AAV2-based pseudotype AAV7m8 (single or dual vector delivery system) to deliver CRISPR/Cas constructs into retinal cells in CMV-Cre::Rosa26-YFP transgenic mice. For *in vitro* validation, SpCas9 and Cas12a achieved better knockout efficiency than SaCas9 (single and double vector) and CjCas9 in YFP-expressing cells. AAV7m8-mediated delivery of

CRISPR/Cas constructs achieved effective transduction into the outer retinal layer, and we found that SpCas9 achieved the highest knockout efficacy among all Cas endonucleases *in vivo*, which was consistent with the *in vitro* result. Other Cas endonucleases were observed to have low editing efficacy or variation in knockout efficacy.

Just as CRISPR/Cas can be applied to target a single gene, it is also possible to interrogate every possible gene in the genome. This genome-scale CRISPR/Cas screening approach can be used to identify novel gene targets in different cancers. I sought to then identify genes that are essential for uveal melanoma (UM), which is the most common malignant ocular cancer in adults. I employed a GeCKO (genome-wide CRISPR knockout) screening strategy in the UM cell line, OCM-1. By identifying the missing guide-RNA library after 12 passages using next-generation sequencing and bioinformatics analysis tools CRISPRAnalyzeR, we found 15 genes with three or more targeted sgRNA deletions during selection that are involved in critical biological pathways. By checking these 15 candidate genes based on open-access data from the Cancer Genome Atlas datasets, we found that there was elevated expression of the *SLC3A2* gene in UM patients in a pan-cancer view setting, and that the expression levels of three genes, *COQ2*, *MRPL22* and *POLR3K*, are associated with UM patient survival. Our work provides new insights into the molecular mechanisms of UM and may reveal new therapeutic targets for this deadly disease.

In summary, we developed a novel self-destructive CRISPR/Cas that can be used as a robust tool for genome editing in the retina of a YFP-expressing transgenic mice model. Moreover, we found that SpCas9 achieved the most efficient gene modification among the four CRISPR/Cas endonucleases that we tested in AAV7m8-transduced retinas. With a human UM cell line, we identified some novel gene targets using a genome-wide CRISPR/Cas9 library screening approach. These studies add new insight to the *in vivo* applications of CRISPR/Cas gene editing in the retina, which is crucial for optimizing the

"clinic ready" profile of CRISPR/Cas for impending application in the treatment of blinding eye diseases.

ACKNOWLEDGEMENTS

I want to thank my amazing team of supervisors Professor Alex Hewitt, Dr. Guei-Sheung (Rick) Liu and A/Prof Tony Cook for letting me join their group and helping me throughout my PhD study. I would like to thank my primary supervisor Alex for giving me such wonderful research opportunities and PhD training, for always being supportive, encouraging and helping, for pushing me when I needed to be pushed, and for setting feasible goals and plans to help me finish my thesis. I would also like to thank Rick for the laboratory and research training, for the support and guidance, for always being available for troubleshooting. Thanks to Tony for offering me support and valuable advice on presentation and writing, as well as wonderful suggestions during group meetings. I would like to thank my GRC Professor Heinrich Kerner for the help with my study and annual reviews.

I am so lucky to be working in such a great group with talented researchers and students around. I would like to give my sincere thanks to Vikrant Singh for helping me with bioinformatics analysis for uveal melanoma screen project. My thanks go to Kristof Wing, Mohd Khairul Nizam Mohd Khalid, Peter Lu, Qi Wang, Vivienne Lu, Jacqui Walker and Dr. Jana Talbot for their help with laboratory work and for always being supportive. My special thanks goes to Peter Tran, Kristof and Van Thi Tuong Nguyen for giving me great advice on the final PhD presentation.

Many thanks go to other researchers and students at Menzies and Wicking, the staff at Graduate Research Office for kind support, the laboratory management team and animal facility team who keep our projects going well, and the financial support from UTAS during my candidature. I would like to thank Professor Anna King, Professor Joanne L. Dickinson, A/Prof Kaylene Young, Professor Kathryn Burdon, Professor Changhai Ding and their

teams for support and help. A big thanks to James Bender for the assistance with animal work.

I did some of my lab training and animal work at the Centre for Eye Research Australia. I would like to give my special thanks to Dr. Helena Liang, Dr. Sandy Hung and Dr. Jiang-Hui (Sloan) Wang at CERA. I would like to thank Helena for being a wonderful mentor, for the enormous encouragement, support, and help and for cell culture training. Thanks to Sandy for the molecular biology laboratory training and patient teaching. I would like to thank Sloan for help with virus work and for giving me nice advice on PhD study. I would also like to thank A/Prof Chi Luu and Dr. Vicki Chrysostomou for helping with the animal study. Thanks to Dr. Raymond Wong, Professor Alice Pebay and her team for their help and support. Furthermore, I would also like to thank the whole Clinical Genetics Unit team at CERA for their support and friendship.

I would like to thank Dr. Vickie Wong and A/Prof Bang Bui at the Department of Optometry and Vision Sciences, University of Melbourne for their kind help with ERG and OCT for the animal study. I would also like to thank Dr. Leilei Tu and Jinying Chen, visiting PhD students from Jinan University for their assistance with experiments.

I would also like to mention a kind woman, Diane, who came to Menzies every Tuesday as a volunteer, helping in the clinic tearoom here and there. Her grandson, Jack Dyson, is a cystic fibrosis patient. Due to advances in modern medicine, he managed to pursue a career in bodybuilding while getting hospital treatment once or twice every year. In return, he and his family contributed to medical research or the community as volunteers in various ways. Other volunteers, such as those coming all the way to donate skin to our stem cell research, their involvement in research and their inspirational stories always remind me of the big picture of the research work — why we are doing medical research and who we are doing research for.

I would like to thank my “neighbors” who share the same study room with me, Jing Chen, Minakshi Nayak and Dr Aroub Lahham for being supportive and sharing with each other our mutual challenges and concerns despite the difference between laboratory-based research and epidemiology-related topics.

I got my specialist training in ophthalmology in Zhongshan Ophthalmic Centre, China, and I would like to thank my clinical training tutors for their help and support. In particular, I would like to thank Professor Keming Yu and Professor Jing Zhuang, supervisors for my Master’s degree, for bringing me into ophthalmology field. Thanks to Professor Shaochong Zhang and A/Prof Yantao Wei for vitreoretinal surgery training and helping me arrange flexible working time during my thesis writing.

Finally, I would like to thank my parents and the whole family for their support. They can barely understand my research project, but they believe what I have been doing is really important and they always feel proud of me. My deepest thanks go to my husband, Nianping, for supporting my every decision, for the understanding, and for sharing the childcare and chores. Without his full support, it would have been difficult to complete my study and thesis.

Pursuing a PhD is not without its fair share of challenges, especially at the start of candidature due to the steep learning curve and towards the finishing-up when multiple tasks need to be tackled. I am particularly grateful to everyone for their kind help and support along the way, not only for helping me with PhD study, but also for making this journey the most wonderful, fruitful and unforgettable life experience for me and my family.

PUBLICATIONS & PRESENTATIONS

Publications during PhD:

1. **Fan Li**, Sandy S.C. Hung, MohdKhairul Nizam Mohd Khalid, Jiang-Hui Wang, Vicki Chrysostomou, Vickie H.Y. Wong, et al. Utility of self-destructing CRISPR/Cas constructs for targeted gene editing in the retina. Hum Gene Ther. 2019 Aug. doi: 10.1089/hum.2019.021.

2. **Li, F.** A PhD is more than the sum of its publications. Nat Hum Behav 3, 1021 (2019). https://doi.org/10.1038/s41562-019-0719-y.

3. Lee JH, Wang JH, Chen J, **Li F**, Edwards TL, Hewitt AW, et al. Gene therapy for visual loss: Opportunities and concerns. Prog Retin Eye Res. 2019;68:31-53.

4. McCaughey T, Budden DM, Sanfilippo PG, Gooden GEC, **Fan L**, Fenwick E, et al. A need for better understanding is the major determinant for public perceptions of human gene editing. Hum Gene Ther. 2019;30(1):36-43.

5. Crombie DE, Daniszewski M, Liang HH, Kulkarni T, **Li F**, Lidgerwood GE, et al. Development of a Modular Automated System for Maintenance and Differentiation of Adherent Human Pluripotent Stem Cells. SLAS Discov. 2017;22(8):1016-25.

6. Hung SS, Chrysostomou V, **Li F**, Lim JK, Wang JH, Powell JE, et al. AAV-Mediated CRISPR/Cas Gene Editing of Retinal Cells *In Vivo*. Invest Ophthalmol Vis Sci. 2016;57(7):3470-6.

7. McCaughey T, Sanfilippo PG, Gooden GE, Budden DM, **Fan L**, Fenwick E, et al. A Global Social Media Survey of Attitudes to Human Genome Editing. Cell Stem Cell. 2016; 18(5):569-72.

8. Yang Y, Wu N, Tian S, **Li F**, Hu H, Chen P, et al. Lithium promotes DNA stability and survival of ischemic retinal neurocytes by upregulating DNA ligase IV. Cell Death Dis. 2016;7(11):e2473.

Book chapter:

Hung SS, **Li F**, Wang JH, King AE, Bui BV, Liu GS, and Hewitt AW. Methods for *In Vivo* CRISPR/Cas Editing of the Adult Murine Retina (2018). Methods Mol Biol. 1715:113-133.

Conference presentations:

Fan Li, Kristof Wing, Jiang-hui Wang, James Bender, Chi D. Luu, Jinying Chen, Vivienne Lu, Qi Wang, Qinyi Lu, Peter N. Tran, Kaylene Young, Anna King, Sandy S.C. Hung, Guei-Sheung Liu, Alex W. Hewitt. Comparison of CRISPR/Cas endonuclease gene editing efficiency of retinal cells *in vivo*. The Association for Research in Vision and Ophthalmology 2019 Annual Meeting, Vancouver. Oral presentation.

Fan Li, Vikrant Singh, Vivienne Lu, Jinying Chen, Sandy S.C. Hung, Joanne L. Dickinson, Phillippa Taberlay, Anthony L. Cook, Alex W. Hewitt, Guei-Sheung Liu. A Genome-Wide CRISPR/Cas9 Screen to Identify Novel Therapeutic Targets for Uveal Melanoma. 50th Annual Scientific Congress of the Royal Australian and New Zealand College of Ophthalmologists, Adelaide, 2018. Oral presentation.

Fan Li, Sandy S.C. Hung, Vicki Chrysostomou, Alice Pébay, Anna King, Alex W. Hewitt, Guei-Sheung Liu. Self-destructing CRISPR/Cas system for targeted genome editing in the retina. ACMD research week, Melbourne, 2016. Poster presentation.

ABBREVIATIONS

AAV	adeno-associated virus
ABEs	Adenine base editors
AMD	Age-Related Macular Degeneration
Cas	CRISPR-associated
CBEs	Cytosine base editors
cDNA	complementary DNA
crRNA	CRISPR RNA
CRISPR	Clustered Regularly Interspaced Short Palindromic Repeats
DEPC	Diethyl pyrocarbonate
DMEM	Dulbecco's Modified Eagle Medium
DMSO	Dimethyl Sulfoxide
DSB	double-strand break
ERG	Electroretinography
FACS	Fluorescence-activated cell sorting
FBS	fetal bovine serum
GCL	Ganglion Cell Layer
gDNA	Genomic DNA
GeCKO	genome-wide CRISPR knockout
GWASs	Genome-wide association studies
HA	hemagglutinin
HDR	homology directed repair
HEK293	Human Embryonic Kidney 293
HIF	hypoxia-induced factor
IMDM	Iscove's Modified Dulbecco's Medium
INL	Inner nuclear layer
LB	Luria broth
LCA	Leber congenital amaurosis
MOI	Multiplicity of infection
mRNA	messenger RNA
NGS	next-generation sequencing
NHEJ	non-homologous end joining
OCT	optical coherence tomography
ONL	outer nuclear layer
PAM	protospacer-adjacent motif
PBS	phosphate-buffered saline
PCR	polymerase chain reaction
PFA	paraformaldehyde
POAG	primary open angle glaucoma
RecA	recombinase A
RNP	ribonucleoprotein
RP	Retinitis pigmentosa
RPE	retinal pigment epithelium
sgRNA	Single guide RNA or guide RNA
SKCM	Skin Cutaneous Melanoma

T7E1	T7 Endonuclease I
TAE	Tris-acetate
TCGA	The Cancer Genome Atlas
tracrRNA	trans-activating crRNA
UM	uveal melanoma
WES	whole-exome sequencing
YFP	yellow fluorescent protein

TABLE OF CONTENTS

DECLARATION OF ORIGINALITY I
AUTHORITY OF ACCESS II
STATEMENT OF CO-AUTHORSHIP III
STATEMENT OF ETHICAL CONDUCT IV
ABSTRACT V
ACKNOWLEDGEMENTS IX
PUBLICATIONS & PRESENTATIONS XII
ABBREVIATIONS XIV
1 LITERATURE REVIEW 1
1.1 Introduction 1
1.2 Retinal degeneration 1
1.3 Overview of CRISPR-based gene editing 2
1.3.1 SpCas9 for genome editing 3
1.3.2 Cas12a for genome editing 4
1.3.3 CRISPR/Cas9 orthologs and variants for gene editing 5
1.3.4 Mechanisms of CRISPR/Cas gene editing 7
1.4 *In vivo* delivery to the retina 10
1.4.1 Electroporation to enhance CRISPR/Cas delivery to the retina 11
1.4.2 Viral vector-mediated CRISPR delivery to the retina 11
1.4.3 Non-viral vector-mediated CRISPR delivery to the retina 15
1.4.4 Surgical procedure to deliver CRISPR to the retina 15
1.5 Preclinical studies of CRISPR/Cas genome editing in the eye 17
1.5.1 Using CRISPR to model diseases and study gene function in the eye 17
1.5.2 Using CRISPR to treat Retinitis pigmentosa 18
1.5.3 Using CRISPR to treat Leber congenital amaurosis 19
1.5.4 Using CRISPR to treat age-related macular degeneration 20
1.5.5 Using CRISPR to treat glaucoma 21
1.5.6 Off-target detection of CRISPR/Cas genome editing in the retina 22
1.5.7 Retinal integrity and function change with CRISPR/Cas genome editing 22
1.5.8 Summary of CRISPR/Cas genome editing in the retina 24
1.6 Challenges and future perspective 24
1.6.1 Safe and efficient *in vivo* delivery 24
1.6.2 Reducing off-target 25
1.6.3 Improving precise repair 25
1.7 Aims of PhD project 26
2 GENERAL MATERIALS AND METHODS 28
2.1 Methods 28
2.1.1 Guide RNA design 28
2.1.2 DNA/RNA quantification 28
2.1.3 CRISPR/Cas plasmid cloning 29
2.1.4 *In situ* testing for SpCas9 sgRNAs 34
2.1.5 Cell culture and plasmid DNA transfection 35
2.1.6 Western blot 36
2.1.7 Genomic DNA extraction from cells 37
2.1.8 Gene-editing efficiency with Sanger sequencing and T7E1 assay 38
2.1.9 AAV production and titration 40
2.1.10 Animal ethics, maintenance, anesthetics and intravitreal injection 43
2.1.11 Electroretinography (ERG) 44
2.1.12 Optical Coherence Tomography (OCT) 45
2.1.13 Retinal collection 45
2.1.14 Flow cytometric analysis 45
2.1.15 Retinal flat mount, cryosection, imaging and cell counting 46
2.1.16 SpCas9 expression in retina by qPCR 48
2.1.17 Genome-wide CRISPR/Cas9 screen for uveal melanoma OCM-1 cells 49
2.1.18 Whole-exome sequencing to detect off-target by CRISPR/Cas9 in the retina 56
2.1.19 Statistical Analysis 56
2.2 Materials 57

3 UTILITY OF SELF-DESTRUCTING CRISPR/CAS CONSTRUCTS FOR TARGETED GENE EDITING IN THE RETINA 58
3.1 Introduction 58
3.2 Results 60
3.2.1 Validation of four *SpCas9*-targeting sgRNA 60
3.2.2 Validation of kamikaze-CRISPR/Cas construct in YFP-expressing cells 64
3.2.3 Kamikaze-CRISPR/Cas reduced potential off-target *in vitro* 69
3.2.4 Time course of SpCas9 expression *in vivo* 70
3.2.5 YFP knockout quantification *in vivo* 72
3.2.6 Kamikaze CRISPR/Cas didn't affect retinal structure or thickness by OCT 76
3.2.7 Functional test of retina following AAV-mediated CRISPR/Cas editing by ERG 78
3.2.8 Kamikaze CRISPR/Cas didn't aggravate off-target effect *in vivo* 86
3.3 Discussion 86
4 COMPARISON OF CRISPR/CAS ENDONUCLEASE GENE-EDITING EFFICIENCY OF RETINAL CELLS *IN VIVO* 90
4.1 Introduction 90
4.2 Results 92
4.2.1 sgRNA selection by *in vitro* validation 92
4.2.2 Cas endonuclease construct cloning and validation 95
4.2.3 *In vivo* AAV7m8 delivery of CRISPR/Cas in the mouse retina 96
4.2.4 Comparison of *in vivo* YFP knockout in the mouse retina by FACS 99
4.3 Discussion 104
5 A GENOME-WIDE CRISPR/CAS9 SCREEN TO IDENTIFY NOVEL THERAPEUTIC TARGETS FOR UVEAL MELANOMA 106
5.1 Introduction 106
5.2 Results 108
5.2.1 Quality control for uveal melanoma screening 108
5.2.2 15 genes were identified by CRISPR/Cas9 screen analysis in UM *in vitro* 110
5.2.3 Major pathways identified by functional enrichment analysis using g:Profiler 113
5.2.4 Different expression levels of each candidate gene on different cancer stages and its effect on uveal melanoma patient survival 113
5.3 Discussion 119
6 GENERAL DISCUSSION AND CONCLUSIONS 123
Conclusions 127
7 REFERENCES 128
8 Appendixes 143
Appendix 1 Plasmid cloning and primers 143
Appendix 2 Materials and experiment set up 149
Appendix 3 AAVs and titration 156
Appendix 4 Animal groups 157
Appendix 5 Uncropped agarose gel and western blot images. 158

1 LITERATURE REVIEW

1.1 Introduction

Inherited retinal diseases are disabling disorders of visual function that affect millions of people worldwide. With the development of next-generation sequencing and better molecular diagnostic techniques, numerous genetic variants across many loci have been definitively associated with inherited retinal diseases[1,2]. Despite this increase in our understanding of the genetic etiology and potential therapeutic targets, there remains no effective treatment for the majority of inherited retinal diseases.

Although significant progress in gene therapy has been achieved over the last two decades, there are few sustained, safe and effective ocular gene therapy for inherited retinal diseases[3–5]. Despite the reported improved visual function in certain Leber congenital amaurosis patients treated with *RPE65* gene replacement therapy[6–8], several significant obstacles hinder its clinical translation, including the limits of viral vector capacity.

Advances in genome-editing techniques, particularly in CRISPR/Cas, has renewed excitement in ocular gene-based therapy. This literature review summarizes *in vivo* applications of CRISPR/Cas gene editing in the retina, including an overview of current progress and diversity of CRISPR system; *in vivo* delivery vectors and methods; and CRISPR-based gene editing as a potential therapeutic in various ocular disease models. It highlights the main challenges of CRISPR-based retinal-genome editing and potential ways to tackle these concerns.

1.2 Retinal degeneration

Retinal degeneration underlies a group of blinding diseases, including hereditary diseases such as retinitis pigmentosa (RP), Leber congenital amaurosis (LCA), Stargardt's disease, choroideremia, and Usher syndrome, and non-hereditary ocular diseases such as age-

related macular degeneration (AMD). To date, over 250 genes (Figure 1.1) have been implicated in retinal diseases. However, treating these ocular disorders remains challenging.

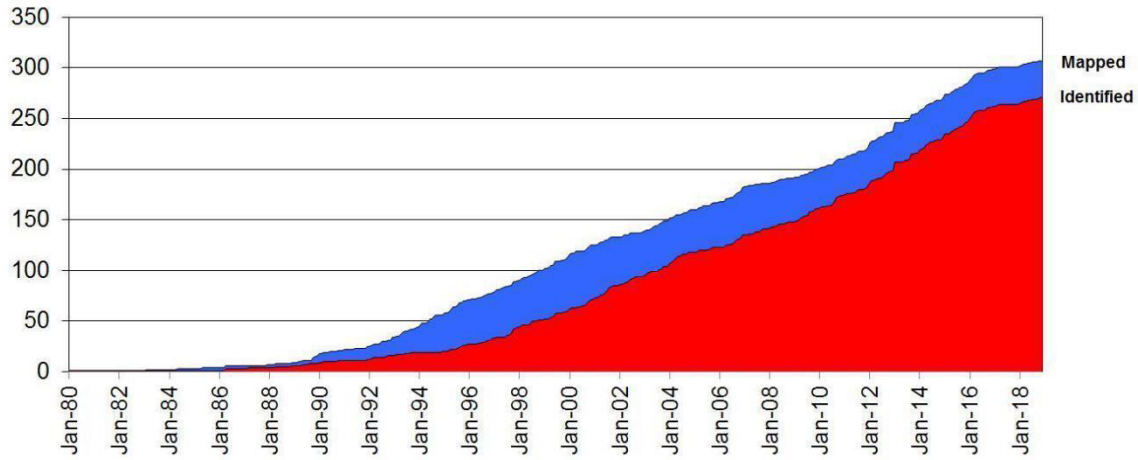

Figure 1.1 Mapped and identified retinal disease genes 1980-2019 (from RetNet).

Up to now, much gene therapy work has been focused on bringing an ectopic functional gene into cells via viral or non-viral vectors to restore loss-of-function caused by mutations. The limitation of gene replacement therapy is that its efficacy may decrease over time. What is more, it is not feasible to package certain large-sized genes using currently available viral vectors. A recently developed CRISPR-based gene-editing approach holds great potential to tackle these challenges and treat these blinding eye diseases.

1.3 Overview of CRISPR-based gene editing

The CRISPR/Cas system was discovered as part of a prokaryotic bacterial immune system and has anti-viral activity[9,10]. It has been repurposed as a potent tool for gene editing in mammalian cells[11,12]. CRISPR/Cas systems are diverse; the system with the most utility consists of two main components—a Cas endonuclease that can act as molecular scissors to cut or nick the DNA strands, and its programmable guide RNA sequence (referred to as sgRNA), which can localize the Cas endonuclease protein to the exact genomic region of interest. Recently CRISPR/Cas systems have been categorized

as Class 1 or Class 2[13–16]. The Class 1 CRISPR/Cas system is subdivided into types I, VI, III, and Class 2 is subdivided into types II, V, VI. While Class 1 systems involve multiple Cas endonucleases, Type II and Type V in Class 2 have been engineered to perform robust RNA-guided gene editing in eukaryotic cells, which have simpler components with a single Cas endonuclease.

1.3.1 SpCas9 for genome editing

In Type II systems, Cas 9[12,17,18], the sole DNA endonuclease, is guided by two RNAs: a specificity determining CRISPR RNA (crRNA), complementary to the target DNA sequence, and an auxiliary trans-activating crRNA (tracrRNA), complementary to crRNA sequence. The protospacer-adjacent motif (PAM) is an essential targeting component, which differs among many different Type II systems. The most commonly engineered system, CRISPR/SpCas9 (from *Streptococcus pyogenes*), requires a PAM with sequence 5'-NGG-3', where N represents any nucleotide. Cas9 contains two domains: the HNH domain cleaves the complementary DNA strand, while the RuvC-like domain cleaves the non-complementary DNA strand[18]. Target DNA is cut 3-5 bases upstream of the PAM sequence, generating blunt ends. The crRNA and tracrRNA duplexes can also be fused into a chimeric single guide RNA (sgRNA) that can not only mimic the natural crRNA-tracrRNA hybrid but also make this system simpler in the experimental setting (Figure 1.2). Due to its high efficiency and simplicity, the CRISPR-Cas9 system has become the most widely used genome-editing tool.

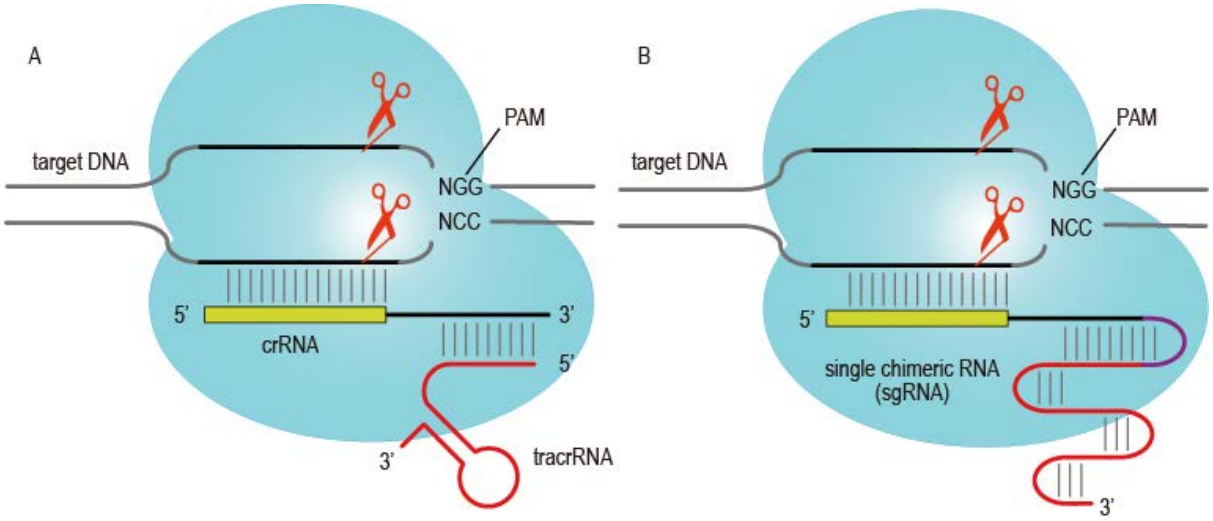

Figure 1.2 Targeted DNA cleavage by CRISPR/Cas9.

Cas programmed by crRNA and tracrRNA duplex (A), Cas9 programmed by single chimeric RNA (sgRNA) (B). The cleavage occurs near a PAM site with the sequence of 5'-NGG-3'.

1.3.2 Cas12a for genome editing

Cas12a (originally called cpf1), classified as a Type V CRISPR system[14], is a single RNA-guided endonuclease lacking tracrRNA and recognizing a T-rich PAM. Unlike Cas9, Cas 12a has only one domain, RuvC domain, which cleaves both DNA strands at the distal end of the PAM in a staggered pattern[13]. Among Cas12a families, two Cas proteins, AsCpf1 (from *Acidaminococcus*) and LbCpf1 (from *Lachnospiraceae*), have shown efficient genome editing in human cells[14]. The major characteristics of Cas9- and Cas12a-based gene editing are shown in Figure 1.3 based on published papers[14].

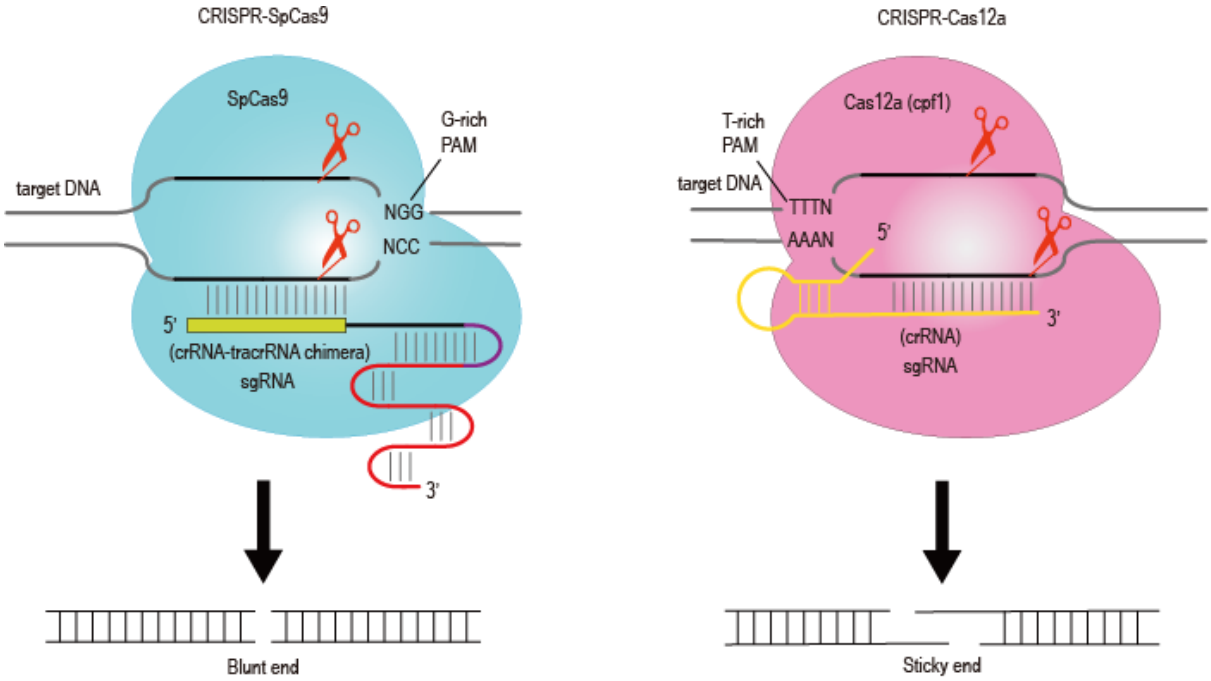

Figure 1.3 Main characteristics of CRISPR/SpCas9- and CRISPR/Cas12a-based DNA cleavage.

1.3.3 CRISPR/Cas9 orthologs and variants for gene editing

1.3.3.1 Main Cas9 orthologs for *in vivo* gene editing

Apart from SpCas9, several Cas9 orthologs have been discovered from different origins with distinct features. Out of hundreds of currently available Cas9 orthologs, a few of them, e.g. SaCas9 (*Staphylococcus aureus*), CjCas9 (*Campylobacter jejuni*) and NmCas9 (*Neisseria meningitidis*), have been developed for *in vivo* ocular genome engineering. The differences between these Cas9 orthologs lies in the size of Cas endonuclease, PAM requirements, editing efficacy, crystal structure, etc. The main Cas endonucleases for *in vivo* genome editing in the retina are compared in Table 1.1.

Table 1.1 Comparison of main Cas orthologs for *in vivo* retinal gene editing application

Cas orthologs	origins	PAM (5'-3')	Size (Kb)	*In vivo* retinal gene editing application Ref
SpCas9	*Streptococcus pyogenes*	NGG	*~4.2*	[19–27]
SaCas9	*Staphylococcus aureus*	NNGRRT	*~3.2*	[28]
CjCas9	*Campylobacter jejuni*	NNNNRYAC, NNNNACA	*~2.9*	[29,30]
Cas12a (Cpf1)	*Acidaminococcus*, *Lachnospiraceae*	TTTN	~3.9 (AsCpf1) ~3.7 (LbCpf1)	[31]
NmCas9	*Neisseria meningitidis*	NNNNGATT	*~3.2*	[32]

1.3.3.2 Cas9 variants

To address customizable experimental needs and expand CRISPR-based application, a handful of engineered Cas9 variants have been developed based on natural Cas nucleases. Those that have been used for *in vivo* applications are listed below.

i D10A Cas9 nickase

D10A Cas9 was created by mutating the catalytic domains of Cas9 while retaining its specificity, so it can nick a single DNA strand without creating double-strand break (DSB). A pair of nickases targeting opposite DNA strands[33] improves genome editing specificity and reduces off-target activity.

ii SpCas9 VQR

The D1135V/R1335Q/T1337R triple SpCas9 mutant protein (referred to as Cas9-VQR) was engineered to recognize the novel PAM site 5'-NGA-3' instead of 5'-NGG-3' in wild-type SpCas9. Serena G et al[34] employed Adeno-Associated Virus 9 (AAV9) delivery of CRISPR/SpCas9-VQR to target P23H mutation in murine retina and effectively disrupt the P23H *Rho* mutant.

iii Catalytically dead Cas9 (dCas9)

The dCas9 was created by inactivating the catalytic nuclease domains while maintaining the recognition domains of Cas9 that allow RNA-guided targeting without cleavage ability[35]. It can be used to activate or repress gene expression (CRISPRa and CRISPRi) by fusing to gene activators or inhibitors. Alternatively, combined with sgRNA scaffolds binding fluorescent protein, dCas9 can be used to label living cells[36].

iv CRISPR Base Editors

Two types of base editors have also been developed based on dCas9: Cytosine base editors (CBEs)[37] and Adenine base editors (ABEs)[38]. Base editing allows for single nucleotide exchange in the genome without DSB. In CBEs, a cytidine deaminase such as APOBEC1 was fused with dCas9, which enabled cytosine (C) to thymine (T) conversion at target sites with high specificity[37]. Another ABEs system was further developed to allow A/T to C/G conversion, expanding the scope of precise genome engineering of point mutations. *In vivo* base editing has been demonstrated in preclinical animal models[39–41], and the same approach could be potentially applied to retinal disease associated with point mutation in future studies.

1.3.4 Mechanisms of CRISPR/Cas gene editing

1.3.4.1 DNA repair pathways

Despite the differences between CRISPR/Cas systems, when the CRISPR/Cas complex

makes targeted breaks, the resulting DSB is then repaired by one of the two general repair pathways (Figure 1.4): the efficient but error-prone non-homologous end joining (NHEJ) repair pathway or the less efficient but precise repair homology directed repair (HDR) pathway[42,43]. NHEJ results in random insertions or deletions (indels), and indel formation leads to the disruption of the open reading frame of the gene (frameshift mutation), which can be used to create gene knockout. On the other hand, precise modification through HDR can be activated with a DNA repair template containing the desired sequence provided. The efficiency of HDR is usually low, as HDR occurs primarily during the S/G2 phase, thus limiting its use to actively dividing cells. For postmitotic cells such as retinal cells, NHEJ is the major repair pathway involved and HDR efficiency is usually low.

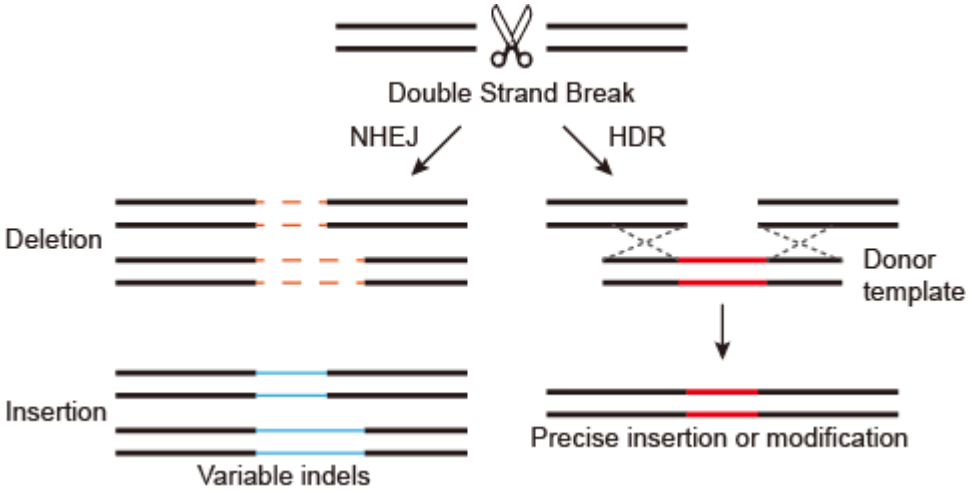

Figure 1.4 CRISPR/Cas mediated DSB followed by two repair pathways: NHEJ and HDR.

1.3.4.2 CRISPR-based NHEJ approach to disrupt gene in retinal cells *in vivo*

Overall, reported CRISPR/Cas-mediated gene disruption efficiencies through NHEJ in the retina are high, with variation in different studies or individual animals. Kim et al. reported indels in retinal pigment epithelium (RPE) cells reached 25±3% three days after subretinal injection of Cas9 ribonucleoprotein (RNP)[44]. The same group[29] reported a single AAV-CjCas9:Vegfa achieved indels with frequencies 22%~30% in a period of 14 to 42 days post-intravitreal injection, and they found the indels were lasting and increased in the

mouse retina for up to 14 months after injection[30]. With different lentiviral vectors, up to 84% of indel formation efficacy was achieved in mouse RPE cells[45]. Some groups didn't directly use indel rates but rather the phenotype change to indicate high genome-editing efficacy. Our group observed a reduction of YFP-positive cells of approximately 84.0% (95% CI: 81.8–86.9) in Thy1-YFP transgenic mouse 5 weeks after administration of a dual AAV CRISPR/Cas9 construct[20]. This level of gene modulation *in vivo* is similar to that reported for other tissues, such as brain (~ 68% using AAV)[46] and liver (80–90% using adenovirus)[47].

1.3.4.3 CRISPR-based HDR approach in retinal cells *in vivo*

Although studies have illustrated a high efficiency of CRISPR/Cas-mediated NHEJ repair in retinal cells, this gene repair pathway is error-prone. The HDR repair pathway is preferable in order to correct gene mutations precisely. As the occurrence of HDR is largely restricted to the dividing stage of cells, applying this strategy in non-dividing postmitotic cells, such as neurons or retinal cells, remains challenging. As the retina is part of the central nervous system, reported methods to improve HDR in the brain could be potentially applied to genome editing in the retinal. Nishiyama and colleagues[48] achieved around 15% knockin efficiency in the brain by CRISPR-based HDR delivered by single AAV-CRISPR in Cas9 mice or dual AAV-CRISPR in wild-type adult mice. Suzuki and colleagues[49] demonstrated the efficiency of a NHEJ-based homology-independent targeted integration method to correct *Mertk* mutations in a mouse model of retinitis pigmentosa (RP). Both groups reported comparable efficiency of precise sequence insertion in postmitotic cells, using different strategies. The only *in vivo* study addressing a CRISPR-based HDR approach in the retina was reported by Xue's group[50], which developed a Cas9/bacteria recombinase A (RecA) system to precisely correct a *pde6b* gene mutation with increased HDR efficiency in a RP mouse model (rd1 mouse).

1.3.4.4 CRISPR-based gene knockdown in retinal cells *in vivo*

Engineered dCas9 variants fused with a gene repressor protein (i.e., the KRAB protein) or a gene transcription activator (i.e., VP16), could shut down or up-regulate target genes. Xia et al.[32] used AAV-nuclease null NmCas9-mediated knockdown of the *Slc9a8* gene in the mouse eye by subretinal injection to study the function of sodium/proton exchange 8 (NHE8) in RPE and photoreceptor cells.

1.4 *In vivo* delivery to the retina

Although CRISPR-based editing has proven to be robust in a variety of eukaryotic cells *in vitro*[11,12], *in vivo* gene editing cannot be applied unless efficient *in vivo* delivery of CRISPR/Cas constructs into the target cells in an organism is achieved. Using various packaging formats, advances in the *in vivo* delivery of CRISPR/Cas system are key to the clinical translation of CRISPR-based therapy.

Theoretically, current techniques used for gene delivery could be used to deliver CRISPR/Cas components to the retina. The eye has unique structures and is immune-privileged, making local delivery not only feasible but also more effective than systemic delivery. *In vivo* gene editing requires local viral or non-viral vector delivery of CRISPR/Cas constructs via intravitreal injection or subretinal injection. Sometimes, electroporation is used along with subretinal injection to enhance retinal intake, especially in newborn animals.

A handful of viral and non-viral vectors have been developed to deliver CRISPR/Cas components to retinal cells *in vivo*. Overall, viral vectors have better transduction efficacy to the living organism and relatively longer expression time while non-viral vectors stimulate less immune response and are easier to scale up but have a lower transduction rate. With these distinct advantages as well as drawbacks, a combination of both vectors or the development of novel vectors with improved features are still needed to deliver

CRISPR/Cas tools safely and effectively to allow efficient editing in the retinal cells *in vivo*.

1.4.1 Electroporation to enhance CRISPR/Cas delivery to the retina

Before the application of viral vector for CRISPR/Cas delivery to the retina, Wang et al. applied CRISPR/Cas9 genome editing in neonatal mice retina by subretinal injection followed by electroporation, thereby identifying the *Blimp1* gene as essential for rod-bipolar function. Later, this approach was applied by other groups[19,21,34,51] for efficient genome editing in the retina in mouse or rat models. As a single plasmid with both Cas endonuclease and sgRNA cassettes, the transduction efficiency to the retina is relatively high. The limitation of this approach is that it is only applicable in newborn animals with retinal cells at the mitotic stage and therefore is not practical for editing the adult retina. Moreover, electroporation is not a clinically feasible treatment as it can negatively affect retinal integrity[34]. Considering that most retinal diseases develop gradually in childhood or as an adult, studies of *in vivo* genome editing in adult animals via different delivery methods will be more relevant for future clinical application.

1.4.2 Viral vector-mediated CRISPR delivery to the retina

Viral vectors have been widely used in gene therapy clinical trials and also show great promise in preclinical *in vivo* gene editing for the treatment of various retinal diseases. Among these different viral vector types, adenoviral vectors, adeno-associated viral (AAV) vectors and Lentiviral vectors are the leading platforms for gene therapy delivery, with different features fit for different target tissues/cells and diseases.

AAVs are the leading platform for *in vivo* gene therapy delivery. As AAVs can transduce both dividing and non-dividing cells efficiently with rare genomic DNA integration, it is a clinical safer vehicle for ocular gene therapy. Nearly 70% of ocular gene therapy uses AAVs[5,52] . Also, the most widely used viral vector for *in vivo* CRISPR/Cas delivery to the retina is AAV (Table 1.2).

Lentiviral vectors, on the other hand, may not be ideal for many gene therapy applications in the clinical setting, mainly due to the risks associated with random genome integration. Instead of *in vivo* application, Lentiviral vectors have been applied for *ex vivo* use to treat diseases such as β-thalassemia, in which lentiviral delivered modified cells are reinfused intravenously and engraft in the bone marrow to eventually express functional β-globin gene[53]. As for *in vivo* ocular gene therapy, Lentiviral vector-mediated delivery only accounts for around 10% of total clinical trials[5,54].

Adenoviral vectors are derived from Adenoviruses and have limited application in ocular therapy, mostly due to its transient expression as well as higher immune response.

These viral vectors have been widely reviewed previously[55,56] as gene therapy tools and the main features and their application for *in vivo* CRISPR/Cas delivery are listed in Table 1.2

Table 1.2 Viral vectors for *in vivo* CRISPR/Cas delivery in the eye

Viral vector	Packaging capacity	Dividing or non-dividing cells	Integration to host genome	immunogenicity	Duration of expression	References of *in vivo* ocular CRISPR application
AAV	~5 Kb	both	rare	low	long	[20,22–24,26,28–31,51,57]
Lentivirus	~9 Kb	both	yes	low	prolonged	[45]
Adenovirus	~8 Kb	both	no	high	transient	[25]

1.4.2.1 AAV-mediated CRISPR/Cas delivery to the retina

AAV-mediated CRISPR delivery to the mouse brain was first reported by Swiech et al.[46]. With a dual AAV delivery system delivery SpCas9 and sgRNA targeting single gene (*Mecp2*) as well as multiple genes (*Dnmt1*, *Dnmt3a* and *Dnmt3b*), a high co-transduction

efficiency (~75%) and efficient gene editing in the adult mouse brain was achieved. Our group first adopted a similar approach for CRISPR/Cas9 genome editing in adult retina[20]. By delivering SpCas9 and *YFP*-targeting sgRNA in a dual AAV2 system through intravitreal injection, we achieved high CRISPR/SpCas9-mediated gene editing in the inner retina, indicated by 84% reduction of YFP-expressing cells compared with *LacZ*-targeting control CRISPR constructs. A number of applications of AAV vectors for CRISPR/Cas delivery are listed in Table 1.2.

The advantages of AAV vectors as a gene delivery tool are not limited to high *in vivo* efficiency, but also a wide range of tissue or cell tropism with different serotypes, making CRISPR/Cas tissue/cell specific delivery and targeting possible. A variety of serotypes have been used in retinal CRISPR/Cas genome editing, including AAV1[24], AAV2[20,57], AAV5[22,28], AAV8[23], AAV9[30–32,34,44] AAV2/8 hybrid[26]. AAV2 delivery of CRISPR/Cas9 constructs mainly infect the inner layer of retina, especially in the ganglion cells through intravitreal injection[20,57] while AAV9-mediated CRISPR/Cas achieved efficient gene editing in RPE or photoreceptors with intravitreal injection[30–32,34,44], indicating AAV9 has better retinal transduction. Apart from serotype and injection method, different tissue-specific promoters have been used to achieve tissue- or cell-specific genome editing in the retina. Photoreceptor-specific promoters, such as photoreceptor-specific human rhodopsin kinase (RK) promoter[23], hRho promoter[32], and GRK1 promoter[28], have been used to limit CRISPR/Cas-mediated genome editing to photoreceptors, which are the main therapeutic target for inherited retinal diseases. Huang et al. adapted an endothelial-specific promoter of intercellular adhesion molecule 2 (pICAM2) to drive SpCas9 expression in vascular endothelial cells in the retina[24].

To overcome the limited packaging capacity of AAV vectors, a dual delivery system was used to deliver SpCas9 and sgRNA cassettes in two separate vectors. Even though efficient gene disruption in the retina was reported[20,22–24,26,51,57], this dual vector delivery approach requires co-transduction, which may reduce gene-editing efficiency. Some Cas9 orthologs with smaller size facilitate an all-in-one AAV vector to package both Cas

endonuclease and sgRNA together. CjCas9[29,30], Cas12a[31], SaCas9[28] and their respective sgRNA was used in a single viral vector for *in vivo* gene knockout in the retina.

1.4.2.2 Lentivirus-mediated CRISPR/Cas delivery to the retina

The major limitation of AAV for *in vivo* CRISPR delivery is its cargo capacity is less than 5 kb. Lentivirus, on the other hand, can deliver exogenous DNA up to 9 Kb to both dividing and non-dividing cells, making it a versatile tool for packaging both SpCas9 and its sgRNA together in one vector. Andreas et al.[45] demonstrated a single subretinal injection of lentivirus-delivered SpCas9 and *Vegfa*-targeting sgRNA resulted in robust knockout (indel formation up to 84%) of expression of *Vegfa* in mouse retina.

Potential risks associated with random genome integration of Lentiviral vectors limit its clinical application in CRISPR-based gene editing in the eye. However, the feature of long-lasting gene expression via Lentiviral delivery can be used for CRISPR/Cas screen, another important application of CRISPR/Cas system. Because lentivirus can deliver DNA stably into the genome of host cells, which can express for a long time and pass down to the next passage, a CRISPR/Cas screen library can be delivered using lentivirus. This lentivirus-mediated CRISPR/Cas screen has been used to study cancer genetics and has potential applications in ocular cancer research (Chapter 5).

1.4.2.3 Adenovirus-mediated CRISPR/Cas delivery to the eye

Because adenovirus has transient expression and provokes relatively higher immune response, it is not widely used for CRISPR/Cas delivery in the retina. Adenoviral vector-mediated CRISPR/Cas gene editing has been applied mainly in liver diseases[47,58–61] , lung cancer[62], and pancreatic cancer[63]. Ranran Cheng et al. [58] developed an adenovirus-delivered CRISPR/Cas9 system, with transient expression and rapid decay of Cas protein, that demonstrated persistent genome editing in the liver of adult mice. Jain et al.[25] used adenovirus to deliver *MYOC*-targeting CRISPR assembly to mouse trabecular meshwork via intravitreal injection. They noticed mild self-limiting anterior segment inflammation even

with Ad5-null vector, indicating the inflammation arose from Adenovirus rather than from the CRISPR constructs. No further detrimental effect to the eye was observed.

1.4.3 Non-viral vector-mediated CRISPR delivery to the retina

Non-viral vectors have been used in gene therapy clinical trials and have the potential for lower immunogenicity, larger packaging payloads, and greater scale-up capacity for clinical use[64]. Compared to viral vectors, non-viral vectors have lower delivery efficiency[65] as they are synthesized rather than evolving via natural selection.

Non-viral vectors have also been successfully used to deliver CRISPR/Cas constructs to various cells *in vivo*. The anionic nature of sgRNA allows Cas9 protein–sgRNA complexes to be integrated into cationic liposomes, a commonly used tool for DNA, RNA, and protein delivery. Lipid-mediated Cas9 protein-sgRNA complexes have been successfully delivered to achieve efficient gene editing in the mouse ear[66,67], with the goal of developing a treatment for inherited hearing loss.

Cationic lipid-mediated Cas9 RNPs[44] was delivered to the mouse eye via subretinal injection in a laser-induced choroidal neovascularization model. Promoted genome editing in the RPE cell was observed, with Cas9 protein degraded three days post-injection. This “hit and go” approach can minimize the expression of SpCas9 and thereby the off-target effect or the immune response caused by overexpression of Cas endonuclease.

In summary, there are still challenges and limitations for currently available viral and non-viral vectors for *in vivo* CRISPR/Cas delivery. The development of novel viral serotypes with retinal tropism, advances in nanotechnology, and the combined application of both viral and non-viral vectors will tackle the challenges for *in vivo* delivery of CRISPR/Cas to the retina for future clinical success.

1.4.4 Surgical procedure to deliver CRISPR to the retina

CRISPR/Cas constructs packaged by different vectors or naked plasmid DNA can be delivered to the retinal cells either via intravitreal or subretinal injection (Figure 1.5), with differing advantages and disadvantages.

1.4.4.1 Intravitreal injection

In a clinical setting, intravitreal injection is a common approach to deliver therapeutic agents to patients with eye diseases, maximizing therapeutic local delivery and minimizing systemic complications. Intravitreal injection is one of the most commonly performed procedures in ophthalmology at present. It has also been used to deliver therapeutic vectors in gene replacement therapy. The procedure is easier and probably has fewer surgical complications compared with subretinal injection. The drawback, however, is that for this purpose, transduction to the outer layer of the retina is limited as vectors degrade along the transduction, in part due to the inner limiting membrane. As observed before, AAV2-mediated CRISPR transduces mainly to the inner layer of the retina, mostly within the ganglion cells[20]. Therefore, it has been used mainly to treat diseases affecting the inner retina, such as ganglion in Leber's hereditary optic neuropathy. Other AAV serotypes or AAV2-based variants, such as AAV9 or AAV7m8, however, have better transduction in the retina. Our group used AAV7m8 to deliver CRISPR/Cas construct via intravitreal injection and found sufficient transduction to the outer layer of the retina (Figure 4.7, 4.8, Chapter 4).

1.4.4.2 Subretinal injection

AAV vector-packaged CRISPR/Cas constructs or naked CRISPR plasmid DNA can be administered into the potential space between the PRE layer and the photoreceptor outer segments via subretinal injection. Compared with intravitreal injection, therapeutic vector delivery via subretinal injection has better photoreceptor transduction efficiency and triggers less immune response, especially in inherited retinal diseases in which the photoreceptors or the RPE cells are involved. This procedure, however, is technically challenging, with potentially more complications including retinal detachment and vitreous hemorrhage. Although no severe complications of subretinal injection were reported with *in vivo* CRISPR/Cas studies in the retina, an optimized delivery procedure with minimum invasion, high safety and reproducibility would be preferred for future clinical application.

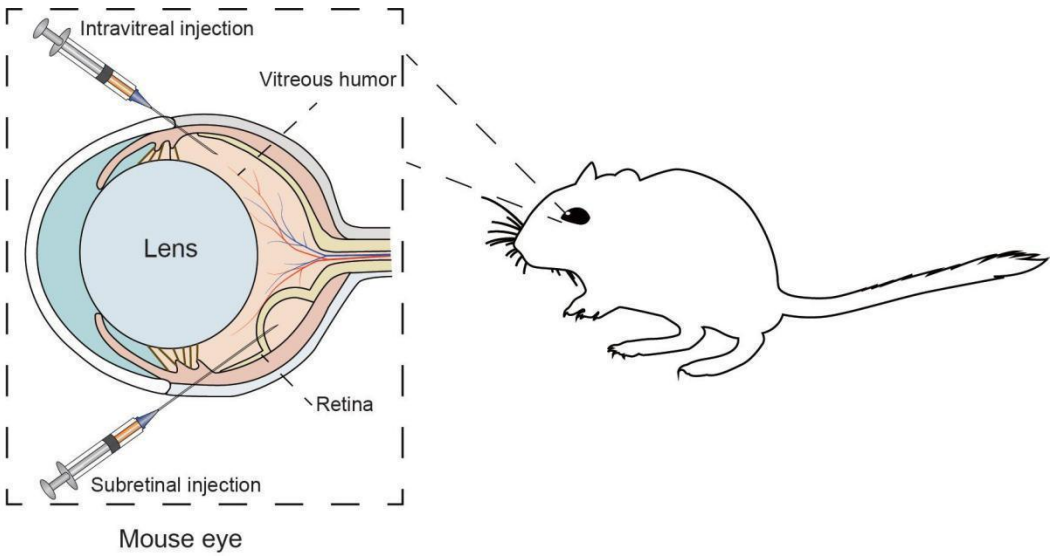

Figure 1.5 *In vivo* delivery of CRISPR/Cas9 to the mouse retina by intravitreal injection or subretinal injection.

1.5 Preclinical studies of CRISPR/Cas genome editing in the eye

1.5.1 Using CRISPR to model diseases and study gene function in the eye

CRISPR/Cas gene editing is a useful tool for modelling ocular diseases and studying gene function. Congenital cataract rabbit models[68,69], a retinal disease rat model[70] and a corneal dystrophy mouse model[71] were created via injection of CRISPR/Cas animal zygotes.

One of the ways to study gene function is by germline disruption or conditional knockout of a specific gene. Germline gene knockout sometimes causes embryo death; conditional knockout based on the Cre/loxP system is feasible but also time-consuming and complicated. Therefore, *in vivo* gene disruption using CRISPR is an alternative way to study functional genetics. Genes playing a critical role in photoreceptors have been studied this way. To study the role of the regulators of the *Blimp1* gene, which may determine rod versus the cone fate, Wang et al.[72] caused deletion of a small element B108 (a cis-regulatory module of *Blimp1* gene) using CRISPR/Cas9 in a neonate mouse retina by electroporation. Knockout of B108 led to more bipolar cell formation, similar to *Blimp1* conditional knockout by Cre. This study revealed that B108 is crucial for *Blimp1* expression,

providing a deeper understanding of the development of rodent retina. Gong's group[32] illustrated the role of sodium/proton exchange 8 (NHE8), with nuclease null NmCas9-mediated knockdown of the *Slc9a8* gene in the mouse eye retina. Campla and colleagues[73] showed CRISPR-based deletion of the binding site of NRL and CRX, two rod-specific differentiation factors of *Frmpd1* gene, eliminated or significantly reduced *Frmpd1* gene expression in rods or rod bipolar cells, respectively. These studies demonstrate the feasibility of studying gene function in the retina using CRISPR/Cas genome editing *in vivo*.

1.5.2 Using CRISPR to treat Retinitis pigmentosa

RP is one of the most common of the inherited retinal diseases, affecting about 2.5 million people world-wide[74]. For recessive RP with a mutated gene such as *RPE65*, gene replacement therapy via AAV vector-delivered healthy copy of *RPE65* could be used although it likely wouldn't be long-lasting and treatment may need to be repeated. Gene replacement therapy is not applicable for autosomal dominant RP, which would require both allele-specific knockout of mutated gene and restoration of wild-type gene to produce functional protein.

Mutations in *Rhodopsin* (*RHO*) account for 30% of dominant RP. CRISPR/Cas system was applied to target mutated *RHO* genes in rodent RP model, as a treatment strategy for adRP. The challenge in CRISPR-based treatment for *RHO*-related adRP is to design sgRNA that targets the mutated allele but not the wild-type allele. Bakondi et al.[19] designed sgRNA targeting a PAM unique to the mutation, with a single nucleotide difference from the wild-type sequence. Through subretinal delivery of CRISPR/Cas9 by *in vivo* electroporation in a S334ter-3 rat model of RP allele-specific disruption of S334ter was achieved, which prevented RP and improved visual function in the rat. Another group[21] reported non-allele-specific gene editing of CRISPR/Cas9 in P23H (p.Pro23Hist)-mutant PHO transgenic mice, with the designed sgRNA recognizing both the mutant and the wild-type allele. Nonetheless, significant reduction of the mutant RHO protein was observed,

and this level of reduction was sufficient to prevent photoreceptor degeneration. Allele-specific CRISPR/Cas gene editing was achieved by different research groups[34,51] in a P23H mutation mouse model. CRISPR-mediated “ablate-and-replace” strategy has been developed by Tsai and colleagues[26], using a dual AAV2/8 vector system — one vector to carry SpCas9 and the other to package double sgRNAs and also human RHO cDNA to create a large deletion of mutated *RHO* gene and compensate for the lost endogenous RHO protein simultaneously. This approach could potentially be used to treat other autosomal dominant ocular diseases. Yu and colleagues[23] used a different approach to treat RP. They disrupted the neural retina leucine zipper (*Nrl*) gene, a rod fate determinant gene, by AAV-mediated CRISPR/Cas9 delivery via subretinal injection in three different retinal degeneration mouse models. NRL expression was significantly reduced in rods in mouse retina following AAV8-mediated CRISPR/Cas delivery, resulting in partial loss of rods function and gain of cone function, consequently preserving cone function and improving cone survival.

1.5.3 Using CRISPR to treat Leber congenital amaurosis

Leber congenital amaurosis (LCA) represents the most severe form of inherited retinal dystrophy, affecting vision as early as childhood. The most common form of LCA, LCA10 is an autosomal recessive disorder caused by *CEP290* loss-of-function mutations in both alleles. Currently, there is no effective treatment for LCA10. Gene replacement therapy for LCA10 has been hindered partly due to the large size of *CEP290*, which is around 7440 bp and makes *in vivo* delivery challenging. One of the most common forms of *CEP290* mutation in many western countries, is an adenine to guanine point mutation in intron 26 of the *CEP290* gene referred as “IVS26 splice mutation” of *CEP290* gene[75–77]. Zhang and colleagues managed to use a truncated version of CEP290 cDNA[78] packaged by AAV in neonatal Cep290^{rd16} mice and reported marked improvement in photoreceptor survival and function. Although this mini-transgene delivery method can partly mitigate *CEP290*-associated retinal disease, the treatment effect was transient and partial.

Similarly, therapeutic benefit of an antisense oligonucleotides (AONs)-based approach is effective but transient[79,80].

Therefore, a direct CRISPR-based gene-editing approach is particularly intriguing for treating LCA10. Ruan et al.[22] used a dual AAV system to deliver SpCas9 and a specific pair of sgRNAs in a LCA cellular model. The two cleavages upstream and downstream of the mutation resulted in a reduction of mutant CEP290 expression, precise excision in the intronic fragment flanking the IVS26 mutation, and rescue of the expression of wild-type CEP290. Interestingly, with a single AAV-SaCas9 system, although the expression of mutant CEP290 mRNA was reduced, rescue of wild-type CEP290 wasn't achieved as with SpCas9. In addition, the researchers demonstrated that this dual AAV system with SpCas9 could effectively delete an intronic fragment of the CEP290 gene in the wild-type mouse retina, providing hope that CRISPR/Cas9-based treatment strategies could be used for patients with LCA10. More recently, Maeder and colleagues[28] moved one more step further by testing similar CRISPR/SaCas9-mediated *CEP290* gene editing in human cells, retinal tissues, and a humanized *CEP290* mouse model as well as in non-human primates. Subretinal injection of AAV5-packaged CRISPR/SaCas9 editing (referred as EDIT-101) in both species showed rapid and long-term *CEP290* editing rates in more than 10% of photoreceptors, which proved to be sufficient for near-normal vision in early studies[81,82]. A Phase I/II clinical trial of EDIT-101 for the treatment of LCA10 is now ongoing, the first ever *in vivo* study of CRISPR-based genome editing in patients (ClinicalTrials.gov; identifier: NCT03872479).

1.5.4 Using CRISPR to treat age-related macular degeneration

Unlike RP, Age-Related Macular Degeneration (AMD) is a multifactorial retinal disease that affects a larger population[83–85]. Risk factors for AMD include aging, family history, smoking and genetic factors. In neovascular AME (nAMD) or wet AMD, pathological choroidal neovascularization is involved and results in bleeding and severe vision loss. A number of factors including vascular endothelial growth factor (VEGF), platelet-derived

growth factor (PDGF), and hypoxia-induced factor (HIF) play an important role in ocular neovascularization and therefore are promising therapeutic targets for these blinding diseases. In fact, anti-VEGF drugs have been the standard treatment for AMD for a long time. However this approach requires ongoing invasive injections.

Disruption of *Vegf* gene (*vegfa*) or receptor gene (*vegfr2*) using CRISPR/Cas provides an alternative and longer-lasting treatment strategy for AMD. Huang et al.[24] reported that rAAV1-mediated CRISPR/SpCas9 genome editing depleted the expression of *vegfr2* by 30% *in vivo* in the retina, reducing angiogenesis in the mouse models of laser-induced choroidal neovascularization or oxygen-induced retinopathy. In line with Huang's study, Kim's group showed efficient *in vivo* disruption of *Vegfa* or *hif1a* gene by Cas9 orthologs (CjCas9[29] and Lbcpf1[31]), resulting in a reduced area of neovascularization in a mouse model. In addition to viral vector-mediated CRISPR editing in ocular neovascularization, a non-viral vector delivery of Cas9 RNPs was developed by the same group[44] to initiate immediate genome editing in the RPE cells *in vivo*.

These studies demonstrate the potential clinical application of CRISPR/Cas gene editing in nAMD, and a broader application in other neovascular ocular diseases including retinopathy of prematurity, diabetic retinopathy and corneal neovascularization.

1.5.5 Using CRISPR to treat glaucoma

Like AMD, primary open-angle glaucoma (POAG) is a complex, blinding eye disease triggered by both environmental and genetic risk factors. *MYOC*, which encodes for myocilin, was the first among many glaucoma genes identified and mutations in *MYOC* may play a causative role in some forms of POAG[86].

Jain et al.[25] performed CRISPR-Cas9-mediated genome editing in primary human trabecular meshwork cells, a transgenic *MYOC* mouse model and also *ex vivo* human eyes. They used adenovirus-delivered CRISPR/Cas to knock down *MYOC* gene in a transgenic mouse model with the human mutant *MYOC* gene, resulting in reduced mutant protein expression in the trabecular meshwork, lowered intraocular pressure and improved ganglion cell function. Mild inflammation in the anterior chamber was noticed due to the

adenovirus injection, without any negative effect on the iridocorneal angle, intraocular pressure, or the aqueous humor drainage system.

1.5.6 Off-target detection of CRISPR/Cas genome editing in the retina

Reducing the potential off-target mutation associated with CRISPR/Cas genome editing is critical for translating CRISPR/Cas from bench to bedside. Therefore a sensitive method for detecting off-target effects *in vivo* is crucial. In most studies of *in vivo* CRISPR/Cas genome editing in the retina, sgRNAs were designed and selected by online tools based on optimal off-target and on-target scores, and no significant off-target mutagenesis was reported on predicted top ranking off-target sites in each study. However, most studies either used a cell-based off-target detection method or applied an *in vitro* method such as Digenome-seq[28–30] or GUIDE-Seq[28] along with Cas-OFFinder, which is not sensitive enough to identify off-target mutations with frequencies less than 0.1%. Other more sensitive *in vitro* off-target tools, like CIRCLE-seq[87], or recently developed *in vivo* off-target detection methods referred as VIVO[88] and DISCOVER-Seq[89] could be applied for detecting genome-wide CRISPR/Cas off-targets in the retina in future studies.

1.5.7 Retinal integrity and function change with CRISPR/Cas genome editing

Safety is one of the major concerns in translating CRISPR/Cas genome engineering into clinical application. Multiple factors, such as immune response, off-target effect or delivery method, may contribute to functional or morphological change in the retina. To assess the effect of *in vivo* CRISPR/Cas gene editing in the retina, optical coherence tomography (OCT), histological assessment and electroretinography (ERG) can be performed.

Our group and another team[20,24] showed no statistically significant change in retinal morphology or function confirmed by ERG 4-5 weeks after intravitreal injection of AAV-delivered CRISPR/Cas9 constructs. To evaluate the relatively long-term effect of self-destructive CRISPR/Cas constructs[57] on retinal function and structure, our group recorded ERG and OCT in Thy1-YFP mice at Week 8 post-intravitreal injection. Although retinal structure was not negatively affected, unexpected reduction in retinal function was

observed 8 weeks after injection of self-destructive *YFP*-targeting CRISPR/Cas9 and conventional *YFP*-targeting CRISPR/Cas9, the same CRISPR/Cas9 constructs we used previously but which hadn't shown any detrimental impact on retinal function 5 weeks after intravitreal injection[20].

Partial restoration of retinal function in a retinal degeneration or glaucoma animal model following CRISPR/Cas treatment was reported. Yu et al.[23] reported high efficiency of AAV-mediated CRISPR/Cas9 disruption of Nrl gene in three different mouse models of retinal degeneration, and found CRISPR-Nrl treated eyes had better ERG waveforms and higher outer nuclear layer (ONL) cell density compared with CRISPR-EGFP-treated control. Giannelli and colleagues[34] also showed that the ONL and outer segment (OS) of retina were partially preserved in Cas9-VQR-treated eyes 3 months after subretinal injection, despite the damage to retinal integrity and function due to electroporation. Similarly, another group[50] reported improvement in ERG a-wave by *ex vivo* ERG recording in *rd1* mouse 14 days after Cas9/RecA treatment. Jain et al. [25] demonstrated improved retinal ganglion cell function in eyes treated by adenovirus-delivered *MYOC*-targeting CRISPR/Cas in a myocilin-associated glaucoma mouse model. These studies showed that therapeutic CRISPR/Cas gene editing could partially improve retinal integrity or function with the disruption of a disease-causing mutation.

The longer-term effect of CRISPR/CjCas9 genome editing in the mouse retina was assessed 8 weeks[29] or 14 months [30] after intravitreal injection. At 8 weeks post-injection, ERG showed no significant decrease in cone function represented by b-wave of photopic response whether in AAV-CjCas9:Hif1a or AAV-CjCas9:Vegfa-treated mice. At 14 months it was observed that while disruption of *Hif1a* gene by AAV-CjCas9:Hif1a didn't induce any change in retinal integrity or retinal function, administration of AAV-CjCas9:Vegfa caused a serious change in retinal morphology, indicating that AAV-CjCas9-mediated gene editing in *Hif1a* rather than *Vegfa* might be a safer strategy for treating ocular angiogenesis diseases.

Overall, current studies illustrate that *in vivo* CRISPR/Cas gene editing in the retina does not affect retinal function or integrity within a period of 4 to 5 weeks; the long-term effect may be different and must be investigated further. The negative effect on retinal function or structure may arise from electroporation[34] or mutated proteins resulting from CRISPR/Cas editing[57] or directly from the disruption of certain genes that are essential to the retina, such as *Vegfa*[30].

1.5.8 Summary of CRISPR/Cas genome editing in the retina

The majority of *in vivo* studies have focused on developing therapies for retinal degenerative diseases including RP, LCA10, AMD and glaucoma, while some groups adopted the CRISPR/Cas genome editing tool to study gene function in the retina. Among the currently available Cas endonucleases, SpCas9 remains the most commonly used CRISPR/Cas system for *in vivo* genome editing in the retina, with minimal studies examining the *in vivo* application of other Cas orthologs, such CjCas9, SaCas9, NmeCas9 and Cas12a (LbCpf1). High efficiency genome editing with different CRISPR/Cas systems has been reported, without direct comparison to determine which works best in the retina. Although current *in vivo* studies have addressed potential off-target cleavage with CRISPR-based retinal genome editing, more sensitive *in vivo* off-target detection methods need to be further investigated and the long-term effects of gene editing observed.

1.6 Challenges and future perspective

1.6.1 Safe and efficient *in vivo* delivery

Currently, viral vectors, especially AAV, are the most widely used for *in vivo* delivery of CRISPR/Cas in ocular gene therapy. The major limitation of AAV vectors is their cargo capacity, and a dual vector system is required to deliver Cas endonuclease, especially SpCas9, and sgRNA separately. A single AAV delivery of other smaller Cas9 orthologs including CjCas9, Cas12a and SaCas9 has been applied to *in vivo* genome editing in rodent retina. As the PAM sequence of some Cas9 orthologs is not as prevalent in the

human genome as SpCas9, *in vivo* retinal genome editing with other smaller and novel Cas9 orthologs or engineered Cas9 variants urgently need to be applied more broadly.

Non-viral vectors are not extensively used for *in vivo* CRISPR delivery to the adult retina, partly due to their lower transfection in the retina compared with viral vectors. The only tested non-viral delivery of CRISPR/Cas constructs to the retina is lipid-mediated Cas9 RNPs; other vectors like nanoparticles, or a combined viral and non-viral delivery of CRISPR/Cas system to the retina, require further investigation before this gene-editing tool can be applied to the clinical treatment of ocular diseases.

1.6.2 Reducing off-target

Several strategies have been employed in an attempt to avoid off-target cleavage, including improved guide-RNA design[33,90] or modification of Cas9 enzymes[91,92], e.g. the high-fidelity variant, SpCas9-HF1. Limiting the Cas9 expression could be achieved via chemical[93,94] and biophysical[95] modulation of Cas9, which were extensively reviewed by Doudna et al.[96]. Alternatively, our group[57] and some others[22,97–99] applied a self-destructive CRISPR/Cas system that disrupts the CRISPR/Cas enzyme itself after the active protein has been expressed. Developing ways to minimize unwanted off-target cut remains critical for therapeutic application in the future.

1.6.3 Improving precise repair

At present, using the NHEJ pathway following CRISPR-mediated gene knockout is the more commonly used approach in *in vivo* CRISPR application in the retina. As gene disruption can only address a limited number of retinal diseases with specific disease-causing mutations, the broad application of CRISPR-based *in vivo* genome editing requires improved precision in repair efficiency through HDR. As HDR is restricted to actively dividing cells, HDR efficiency is usually low in post-mitotic cells such as the retina. Small molecules might be used to improve HDR in the retina, including SCR7-Pyrazine, a potent DNA ligase IV inhibitor[100]; L755507, a β_3-adrenergic receptor partial agonist[101]; RS-

1, a RAD51 stimulator[102], and i53, an inhibitor of 53BP1[103]. Tests of their efficacy, delivery methods and safety in the retina in animal models are needed.

Base editing is a recently developed dCRISPR-based approach for precise repair in inherited diseases with point mutations. Although this recently developed base-editing approach has only been used for a limited number of *in vivo* studies[39,40,104], it provides an attractive alternative therapeutic as it is associated with little or no off-target or indels compared to CRISPR/Cas gene editing. Ocular diseases with a point mutation, such as LCA10 (with A>G mutation in the intron 26 of *CEP290* gene) or RP with a proline to histidine substitution at codon 23 (P23H), could be good candidates to test *in vivo* base-editing efficiency in the retina.

In summary, with ongoing rapid breakthroughs in this area and challenges and concerns fully addressed, CRISPR/Cas-based gene editing tools hold great potential in treating inherited retinal diseases.

1.7 Aims of PhD thesis

Prior to CRISPR/Cas being used in the clinical setting, the following principal issues need to be fully addressed regarding somatic retinal gene editing: efficient and efficacious CRISPR/Cas editing in the retina, elimination of potential off-target effects and cellular immune responses and improvement in HDR precise repair in retinal cells.

My whole PhD focuses on the optimization and validation of a “clinic ready” *in vivo* CRISPR/Cas system for impending application in treatment of ocular diseases. The main aim of this thesis is to validate the feasibility and efficacy of AAV-mediated CRISPR/Cas gene editing in the retina, and a minor aim is to use CRISPR screen tool to look for potential therapeutic target in an ocular cancer, uveal melanoma, which could lead to more translational application in the future.

As the CRISPR/Cas system can be used to target any sequence with a relevantly designed PAM site, rather than focusing on any particular single gene related to inherited retinal diseases, we chose, as proof-of-concept, yellow fluorescent protein transgenic

mice models as a rapidly quantifiable method to assess *in vivo* CRISPR/Cas gene editing, as it has an easily identifiable phenotype.

Three specific aims with were included in my PhD study:

1. **To improve efficiency and reduce off-target:** to validate a self-destructing CRISPR/Cas construct to reduce potential off-target effects delivered by AAV2.
2. **To compare gene editing efficacy of currently available CRISPR/Casy systems:** to compare and find out the most efficacious CRISPR/Cas endonucleases in retinal genome editing.
3. **To apply CRISPR/Cas screening to identify novel therapeutic targets for uveal melanoma:** to use a Genome-Scale CRISPR Knockout (GeCKO) screen to identify essential genes that are involved in the survival of uveal melanoma.

2 GENERAL MATERIALS AND METHODS

2.1 Methods

2.1.1 Guide RNA design

Websites used for guide design are listed in Appendix 2, Table 8.16. Initially, we used the Zhang lab CRISPR tool to design YFP sgRNA for SpCas9 (http://crispr.mit.edu/, the website was shut down). Alternatively, Benchling was used. The following factors were considered for guide RNA design: the availability and difference of PAM sequencing in different CRISPR/Cas systems, the homology of the target sequence to other genes as it may cause off-target effects, and the orientation of the target locus, i.e. whether it encodes the sense or the antisense sequence.

The specific guide-RNA design is listed Results. Briefly, the designing procedure using Benchling was as follows: the sequence of the target gene was imported, guide parameters (target region, guide length, PAM) were set and the results provided guide RNA sequence along with an on-target and off-target score. The top three of four guides with higher on-target and off-target scores were selected, and oligonucleotides were ordered from IDT.

2.1.2 DNA/RNA quantification

2.1.2.1 Measurement by NanoDrop spectrophotometer

DNA/RNA was measured by NanoDrop 1000 spectrophotometer. The purity of the sample DNA/RNA was assessed by calculating the ratio of absorbance at 260 nm and 280 nm.

2.1.2.2 Measurement by Qubit assay

The Qubit dsDNA BR assay kit was used to measure DNA concentration, following manufacturer's instructions. Briefly, master mix was prepared as 199 µL of Qubit buffer+1 µL of Qubit reagent per sample and two standards. Samples were prepared in Qubit assay

tubes and incubated at room temperature for 2 min. Tubes were then loaded into the Qubit fluorometer to be read.

Sample	Master mix (µL)	DNA (µL)
Standard 1	190	10
Standard 2	190	10
DNA sample	198	2

2.1.3 CRISPR/Cas plasmid cloning

Different plasmid-cloning strategies were applied for insert-DNA cloning, including cloning by restriction enzyme digest, cloning by PCR and plasmid modification by annealed oligo cloning or gBlocks. Insert DNA was then ligated with digested vector backbone by the T4 DNA ligase enzyme. Plasmid DNA was then introduced into competent cells through transformation. 5-10 colonies were picked and cultured. The correct plasmid cloning was identified by restriction digest or Sanger sequencing. Plasmid-cloning methods and procedures are listed below.

2.1.3.1 Vector/Insert digest, purification and ligation

i Plasmid cloning by restriction enzyme digest

a. Restriction enzyme digest

Component	50 µL reaction
Plasmid DNA	~2 µg
Restriction enzyme A	1 µL
Restriction enzyme B*	1 µL
10 x buffer	5 µL
Nuclease-free water	Add to 50 µL

Only one restriction enzyme was needed in certain cases. Both recipient and donor plasmids were digested by the same restriction enzyme(s).

The digest was incubated at the enzyme's active temperature for 3 h or overnight. 1 µL CIP was added to the recipient plasmid digest and incubated at 37ºC for 1 h.

b. Gel purification for insert and vector

Digested DNA was loaded onto a 0.8% Tris-acetate (TAE) gel to run at 80 V for 1 h. The desired band with the right size was cut under UV visualization and purified using a commercial gel purification kit following the manufacturer's protocol. DNA was eluted in 30 µL nuclease-free water and DNA concentration was measured by nanodrop.

c. Ligation

Component	**20µL reaction**
Purified vector backbone DNA	100 ng
Purified insert DNA	*
T4 DNA ligase	1 µL
10 x T4 ligase buffer	2 µL
Nuclease-free water	Add to 20 µL

Required mass insert was calculated using NEBioCalculator (insert: vector ratio=3:1 unless otherwise specified)

Ligation was incubated at 16ºC overnight.

The list of plasmids cloned by the restriction enzyme digest method is presented in Appendix 1 (Table 8.1)

ii Plasmid cloning by PCR

Polymerase chain reaction (PCR)-based cloning was used to introduce restriction sites when no restriction enzyme digest sites could be found in donor plasmid.

PCR reaction:

Component	**50 µL reaction**
10 x KOD Buffer	5 µL
2 mM dNTPs	5 µL
Template DNA	~10 ng
10 µM forward primer	1.5 µL
10 µM reverse primer	1.5 µL
KOD Hot start DNA Polymerase	1 µL
Nuclease-free water	Add to 50 µL

Thermal cycle varied depending on the length of PCR fragment, CG% of primers, etc.

PCR product was purified by gel purification kit according to the manufacturer's protocol. PCR product and recipient plasmid were then digested by restriction enzymes, followed by gel purification as mentioned above. DNA ligation was performed as described previously. The list of plasmids cloned by PCR and PCR primer sequences is presented in Appendix 1 (Table 8.2, Table 8.5).

iii Plasmid cloning by annealed oligo

a. Insert oligo anneal

Component	**10 µL reaction**
Forward oligo (100 µM)	1 µL
Reverse oligo (100 µM)	1 µL
T4 PNK	1 µL
10 x T4 DNA ligase buffer	1 µL
Nuclease-free water	6 µL

Thermal cycle: 37ºC 30min, 95ºC 5 min ramp down to 25ºC (hold).

b. Recipient plasmid DNA digestion and purification

Recipient plasmid DNA was digested by restriction enzymes and purified as described above.

c. Ligation

Component	**20 µL reaction**
Purified linearized vector	25 ng
Annealed oligo (1:50 dilution)	1 µL
T4 DNA ligase	1 µL
10 x T4 DNA ligase buffer	1 µL
Nuclease-free water	Add to 20 µL

Ligation was incubated at 16ºC overnight.

A list of plasmids cloning by oligo annealing and oligo sequences are presented in Appendix 1 (Table 8.3, Table 8.6).

iv Plasmid cloning by gBlocks gene fragments

a. Resuspension of gBlocks

gBlock fragment was centrifuged at 3000 g for 3-5 sec, and TE buffer was then added to reach a final concentration of 10 ng/µL. Diluted gBlock was incubated at 50ºC for 20 min following a brief spin.

b. gBlocks digest

Component	**30 µL reaction**
gBlock fragment (10 ng/µL)	10 µL
Restriction enzyme A	1 µL
Restriction enzyme B*	1 µL
T4 DNA ligase	1 µL
10 x CutSmart buffer	3 µL
Nuclease-free water	15 µL

*Digest separately if active temperatures were different.

gBlock digest was incubated for 3 h or overnight.

c. gBlocks purification

Following digestion, the gBlock DNA fragment was purified using PCR purification kit and eluted in 30 µL nuclease-free water.

d. Ligation

Component	**20 µL reaction**
Purified linearized vector	50 ng
Purified digested gBlocks fragment	3:1 ratio to vector
T4 DNA ligase	1 µL
10 x T4 DNA ligase buffer	2 µL
Nuclease-free water	Add to 20 µL

Ligation of purified linearized vector plasmid and digested gBlock fragment was incubated at room temperature for 5 min.

gBlocks gene fragments were ordered from IDT. Plasmid cloning by gBlcoks method and gBlocks sequences are listed in Appendix 1 (Table 8.4, Table 8.7)

v Plasmid cloning by Gibson assembly method

pX551-miniCMV-CjCas9 was cloned using Gibson assembly method. CjCas9 (template using pX404-CMV-CjCas9) was PCR amplified and inserted into pX551-miniCMV-SpCas9 backbone using Gibson assembly method according to manufacturer's protocol.

2.1.3.2 Transformation

Competent cells (DH5a) were transformed with plasmid cloning using the heat shock method according to manufacturer's protocol. Briefly, 10 µL of ligation reaction was added to 50 µL DH5a cells and incubated on ice for 30 min. The cells were heat shocked at 42ºC for 20 seconds in a digital dry bath and then incubated on ice for 2 min. 500ul of pre-warmed SOC medium was added to the cells, followed by incubation in a 37ºC shaking incubator for 1 h. The cells were spread on Luria broth (LB) agar plates (ampicillin) and incubated at 37ºC overnight. 5-10 single colonies were picked and cultured in 5mL liquid LB supplemented with ampicillin for miniprep. The correct plasmids were identified by restriction enzyme digest, Sanger sequencing, or *in vitro* validation in Human Embryonic Kidney 293A (HEK293A) cells. Plasmids were stored in two forms for longer-term use: glycerol stock of overnight bacterial culture and purified high concentration plasmid from Maxiprep or Megaprep.

2.1.3.3 Plasmid purification

i Small-scale plasmid DNA purification

Plasmid DNA was isolated using the Qiaprep spin miniprep kit according to the manufacturer's instructions. In brief, single bacterial colonies were picked and cultured in 5 mL of LB supplemented with ampicillin (100 µg/mL) in 14 mL round-bottom polypropylene, loosely capped tubes. Cultures were incubated at 37ºC in a shaker for around 12~14 h. 3 mL of bacteria culture was centrifuged in Eppendorf tube at 10000 g

for 3 min. The bacteria pellet was resuspended, lysed, neutralized and finally eluted in 30 µL of nuclease-free water. The plasmid DNA concentration was measured and recorded.

ii Large-scale plasmid DNA purification

Plasmid DNA was isolated using the Qiagen Maxiprep or Megaprep Kit according to the manufacturer's instructions. Single bacterial colonies were picked and cultured in 5mL of LB media with ampicillin as described previously. For Maxiprep, 500 µL of the culture was inoculated in 500 mL LB supplemented with ampicillin (100 µg/mL), and a total of 4 flasks of 500 mL bacteria culture were used for Megaprep. The bacterial culture was incubated overnight in a shaker at 37ºC (except pXX6 at 32ºC) at 225 rpm. The culture was centrifuged at 3,000 g for 30 min at 4ºC. The bacteria pellet was then resuspended, lysed, and neutralized and eluted in elution buffer. Plasmid DNA concentration was measured and recorded.

2.1.3.4 Plasmid verification by Sanger sequencing

Plasmids were verified by Sanger sequencing after cloning at Australian Genome Research Facility (AGRF, Melbourne) or in-house at Menzies Institute for Medical Research.

Component	**12 µL reaction**
Plasmid DNA	~1000 ng
Sequencing primer (10 µM)	1 µL
Nuclease-free water	Add to 12 µL

A list of sequencing primers is presented in Appendix 1 (Table 8.5).

2.1.3.5 Glycerol stock

To make a glycerol stock, 500 µL LB with plasmid was mixed with 500 µL 50% sterile glycerol and stored at -80ºC.

2.1.4 *In situ* testing for SpCas9 sgRNAs

CRISPR/Cas *in situ* testing was carried out by incubating the individual synthetic SpCas9 sgRNA or LacZ sgRNA alone with the recombinant SpCas9 protein and the pX551

plasmid. Samples were loaded to run on a 0.8% TAE agarose gel to visualize their cleavage efficiency for SpCas9. AgeI enzyme digested pX551 plasmid was used as a positive control.

2.1.5 Cell culture and plasmid DNA transfection

Cells were maintained in sterile cell culture flasks or petri dishes in a humidified 37ºC incubator with 5% CO_2. Cells were maintained in 75 cm^2 flasks. For large-scale cell expansion, 175 or 225 cm^2 flasks were used.

2.1.5.1 Thawing cells

A vial of frozen cells was taken from the liquid nitrogen tank. A "QUICK THAW" method in 37ºC water bath was applied by shaking the vial rapidly in water till approximately 3/4 thawed. Fresh complete growing medium was added into the vial, and the cell suspension was transferred into a 15 mL centrifuge tube filled with 5-8 mL complete medium. The cell suspension was centrifuged at 300 g at room temperature for 3 min. Supernatant was aspirated, and the cell pellets were resuspended in 10 mL fresh culture medium and transferred into a tissue culture treated flask by adding medium up to 15mL. Cells were placed into a cell culture incubator and maintained on a regular basis.

2.1.5.2 Passaging cells

Old culture medium was aspirated, and the cells were washed with ~10 mL phosphate-buffered saline (PBS). 2mL of 0.25% Trypsin-EDTA was added and cells were incubated at 37°C for 1-2 min. Cells were checked periodically under a microscope. The plate was tapped to loosen cells. 8 mL of complete growing medium was added to neutralize trypsin. Cell suspension was transferred to a sterile 15 mL centrifuge tube and the cell pellet was formed by centrifuging at 300 g for 3 min at room temperature. Cells were seeded at 1:4~1:5 ratio (for a specific amount of cells, count cells before seeding), and passaged again every two to three days before reaching 95% confluence.

2.1.5.3 Cell counting

Cell suspension (20 µL) was mixed well with equal volume of trypan blue solution and 10 µL was transferred to Cell Counting Chamber Slides and read by an Automated Cell Counter. The cell suspension was diluted and cell density calculated accordingly when the original cell density exceeded the counting range of the cell counter.

2.1.5.4 Making frozen stocks for cells

Cells were harvested in the same way as described previously. Cells were counted and suspended in freezing medium with a final concentration of $1x10^6$ cells/mL. Cryovial tubes with cell suspension were placed in a Mr. Frosty freezing container at -80ºC temporally and transferred to a freezing box in a liquid nitrogen tank.

2.1.5.5 Plasmid DNA transfection

$2.5x10^5$ cells per well were seeded onto a 6-well plate one day prior to transfection. The following day, cell culture medium was replaced with 1 mL Dulbecco's Modified Eagle Medium (DMEM)/10% fetal bovine serum (FBS) per well. The transfection complex was prepared as follows.

Component	**For 6-well plate per well**
Plasmid DNA*	1.5 µg
OptiMEM	150 µL
Fugene HD transfection reagent	Add to 12 µL

*750 ng/plasmid was used in dual plasmid transfection

Transfection complex was added to cells. Cells were maintained and collected for further analysis at certain time points after transfection.

2.1.6 Western blot

2.1.6.1 Sample preparation and protein assay

Cells or retinal tissues were lysed in 100~200 µL of cell lysis buffer on ice, followed by sonication for 5-10 sec by an ultrasonic cell disruptor. The cell lysate was centrifuged at 12000 rpm at 4ºC for 15 min, and the supernatant was collected. The concentration of

protein was measured in a microplate reader using Pierce™ BCA Protein Assay Kit according to the manufacturer's protocol.

Component	Volume per sample (µL)
Sample lysate	65
4 x NuPAGE LDS Sample Buffer	25
500 mM DTT	10

Sample was heated at 85ºC in a heat blocker for 10 min.

2.1.6.2 Protein blotting, membrane blotting and antibody incubation

15 µL of sample and 10 µL of prestained molecular weight marker (Novex® sharp pre-stained protein standard) were loaded onto NuPAGE™ Novex™ 4-12% Bis-Tris Protein Gels and run at 160 V for 1 h. Gels with protein were then transferred to polyvinylidene fluoride membranes using the XCell II™ Blot Module. Membranes were blocked with 5% skim milk in TBS-T at room temperature for 1 h and then incubated with mouse monoclonal SpCas9 antibody (1:1000 dilution) or HA-probe (F-7) (1:1000 dilution) at room temperature for 1 h. Membranes were washed and further incubated with horseradish peroxidase-conjugated goat anti-mouse secondary antibody (1:5000 dilution) at room temperature for 1 h. For detection of housekeeping protein, mouse monoclonal β-actin antibody (1:2000 dilution) was used.

2.1.6.3 Detection of protein and western blot analysis

Membrane was incubated in chemiluminescence buffer (a mixture of 500 µLreagent A with 500 µL reagent B, Amersham ECL Prime Western Blotting Detection kit). Images were captured by Amersham Imager 600. For *in vitro* SpCa9 time course analysis, the relative levels of SpCas9 protein of each sample were quantified using Image J with normalization to β-actin.

2.1.7 Genomic DNA extraction from cells

For less than $5x10^6$ cells, genomic DNA was extracted using the Quick-DNA Miniprep Plus Kit (Zymo Research) according to the manufacturer's instructions. Genomic DNA was eluted in 30~50 µL nuclease-free water and concentration was measured using nanodrop.

For larger sample volumes, the Quick-DNA Midiprep Plus Kit (Zymo Research) was used. DNA was eluted in 200 µL DNA elution buffer.

2.1.8 Gene-editing efficiency with Sanger sequencing and T7E1 assay

Briefly, HEK293A-YFP cells were transfected with CRISPR/Cas plasmids and cells were collected as described previously. Genomic DNA was extracted and used as a direct PCR template for amplification with primers specific to the targeted region in the *YFP* gene. The PCR product was purified and sequenced for indel analysis, or alternatively the PCR product was denatured and reannealed to produce heteroduplex mismatches, which were recognized and cleaved by T7 Endonuclease I (T7E1), and the cleavage was detected by gel analysis.

A detailed protocol follows.

2.1.8.1 Genomic DNA amplification by PCR

Component	**Master mix (10x)**
Nuclease-free water	55.5 µL
10 µM Forward primer (CMV Seq-FWD)	10 µL
10 µM Reverse primer (EYFP SURVEYOR REV)	10 µL
KAPA HiFi Fidelity Buffer	20 µL
dNTPs	3 µL
KAPA HiFi HotStart DNA Polymerase (1U/µL)	1.5 µL
Total volume	100 µL

Sequence of primers:

CMV Seq-FWD	CGCAAATGGGCGGTAGGCGTG
EYFP SURVEYOR REV	CTGGTAGCTCAGGTAGTGGTTG

9 µL of master mix was mixed with 1µL genomic DNA sample or water as negative control.

Thermal cycles:

Step	**Temperature (ºC)**	**Time (min:sec)**	**Cycles**
Denature	95	5:00	1
Denature	98	0:20	30
Anneal	67	0:15	
Extend	72	0:30	

Extend	72	2:00	1

9 µL of master mix was mixed with 1 µL genomic DNA sample or water as negative control.

2.1.8.2 Sanger sequencing for indel analysis

Genomic DNA was extracted from HEK293A-YFP cells transfected with mismatch-containing guide RNAs. PCR amplification from genomic DNA was purified using a DNA Clean & Concentrator kit and was sequenced in-house on the Applied Biosystems 3500 Genetic Analyzer (Thermo Fisher Scientific) using YFP reverse sequencing primer. Sanger files were analyzed for insertions and deletions using the inference of CRISPR edits (ICE) tool.

2.1.8.3 Form heteroduplexes for T7EI digestion

Component	**Amount per sample (µL)**
PCR product	10
10X NEBuffer 2	1.5
Nuclease-Free Water	1.5
Total volume	13

Thermal conditions:

Step	**Temperature (°C)**	**Time**
Denature	95	10 min
Ramp 1	95 to 85	Ramp rate -2°C /sec
Ramp 2	85 to 25	Ramp rate -0.3°C/sec

2.1.8.4 T7E1 digestion

Component	**Amount per sample (µL)**
PCR heteroduplexes from above	13
T7 Endonuclease I (diluted to 1 U/µL in NEBuffer 2)	2
Total volume	15

T7E1 digestion was performed at 37°C for 1 h.

2.1.8.5 T7E1 results visualization

Digested samples were loaded on 2% TAE agarose gel and run at 100 V for 1 h. The cleavage was further quantified by gel analysis using Image J.

2.1.9 AAV production and titration

2.1.9.1 AAV2 production

Recombinant AAV2 viruses were produced in HEK293D cells packaging desired plasmid as described previously [105]

i Seeding HEK293D cells

A week before AAV production, a sufficient amount of HEK293D cells were maintained and passaged in T175 flasks. One day prior to transfection, HEK293D cells were harvested and seeded into 50 dishes (100 x 20mm) at 7×10^6 cells/dish in growing medium (DMEM/10% FBS).

ii Producing AAV2 utilizing calcium phosphate transfection

2 h before transfection, old growing medium was aspirated leaving around 1 mL to cover the cells and around 9 mL transfection medium (IMDM/10%FBS) was added to each dish of HEK293D cells. Triple plasmid transfection was then performed using the Calcium Phosphate method. For each dish, a total of 25 µg DNA was used including 5 µg packaging/capsid plasmid (pXX2), 15 µg helper plasmid (pXX6) and 5 µg AAV construct (SpCas9 or guide RNA). Transfection solutions A and B were prepared in 50 mL falcon tubes, respectively, as listed below.

Order of adding reagents	**Reagents**	**Amount for 50 dishes**
Transfection solution A		
1	2 x HBS	24.75 mL
2	NaH_2PO_4	0.25 mL
Transfection solution B		
1	10% TE	Add to 25 mL
2	AAV construct	250 µg
3	pXX2	250 µg
4	pXX6	750 µg
5	2M $CaCl_2$	3.125 mL

2 mL of transfection solution A and B were aliquoted to separate 14 mL poly-propylene round-bottom tubes, respectively. Then solution B was added dropwise to solution A to

form a transfection cocktail. The cocktail was incubated at room temperature for 20–30 min and 1 mL was added to each of the 50 dishes of HEK293D cells.

iii Change medium with maintenance medium

One day after transfection, old medium was aspirated leaving around 1 mL to cover the cell and 11 mL of maintenance medium (DMEM/2%2 FBS) was added to each dish.

iv AAV2 vector extraction, purification and concentration

TaKaRa AAVpro Purification Kit (AAV2) was used for AAV2 extraction, purification and concentration using modified manufacturer's instructions. Briefly, transfected HEK293D cells were harvested and centrifuged at 3000 g for 10 min at 4ºC. Supernatant was removed and cell pellets were collected into one tube. Cells were resuspended in 10 mL AAV Extraction Solution A and incubated at room temperature for 5 min. Extracts were centrifuged at 3000 g for 10 min at 4ºC and supernatant was transferred to a new falcon tube. 1 mL AAV Extraction Solution B was added to the supernatant. 1 mL of SD Solution was added and the mixture was incubated for 30 min at 37ºC, and then centrifuged at 3000 g for 10 min at 4ºC. Supernatant was collected as crude AAV2 vector solution. Then the crude viral vector was purified in AAV purification column and further concentrated in the Filter Device by centrifuging. The final solution recovered in a sterile collection tube was purified and concentrated rAAV2 particles in 200~250 µL suspension buffer.

2.1.9.2 AAV7m8 production

Recombinant AAV2-based variant AAV7m8 was produced in HEK293D cells packaging desired plasmid in a similar way as AAV2 production, with the following modifications regarding packaging/capsid plasmid and viral purification.

For triple plasmid transfection, 5 µg of 7m8 was used per dish instead of pXX2. TaKaRa AAVpro Purification Kit (All Serotypes) was used for AAV7m8 extraction, purification and concentration. After AAV Extraction Solution B step, 1/100 volume of Cryonase Cold-active Nuclease was added and then incubated at 37ºC for 1 h. 1/10 volume of Precipitator

A plus and 1/20 volume of Precipitator B were added, respectively. The mixture solution was centrifuged, and the supernatant was filtered using a Millex-HV 0.45 μm filter. The filtrate containing AAV vector was then concentrated using an Amicon Ultra-15 (100 kDa filter) and transferred to a new sterile tube.

2.1.9.3 AAV titration

i Preparation for standard

1 μg of linearized vector plasmid was prepared by restriction enzyme digest and purified with a purification kit (Promega gel and PCR clean-up systems). The concentration was measured by nanodrop. 1 x 10^9 vg/5 μL of the standard in 500 μL of TE buffer was prepared following the formula below.

The amount of linearized plasmid in 500 μL TE buffer

$$= \frac{vector\ plasmid\ length\ X\ 660}{6.022\ X\ 1000}$$

A total of eight dilutions in TE buffer were prepared as shown below.

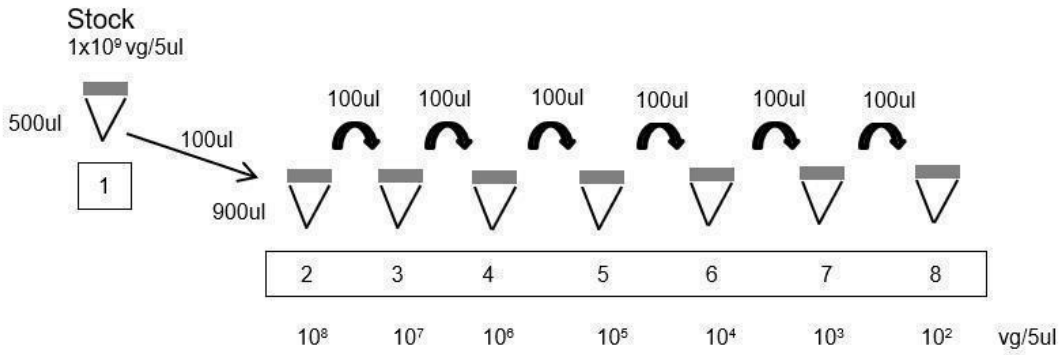

ii AAV titration by quantitative PCR (qPCR)

1/10^4 and 1/10^5 virus were prepared, and qPCR was set using SYBR green.

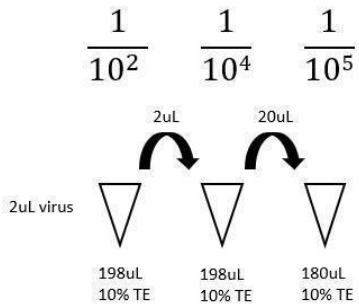

Component	Volume (µL)
Nuclease-free water	7.3
Fast SYBR green master mix	12.5
Forward primer (100 µM)	0.1
Reverse primer (100 µM)	0.1
Template (Standards or diluted vectors)*	5.0

*Four replicates for diluted vectors, duplicates for standards and negative control (water)

Thermal cycles:

Cycle number	Denature	Anneal/extend
1	95ºC, 10 min	
40	95ºC, 15 s	60ºC, 60 s

List of AAV and titration were presented in Appendix 3.

2.1.10 Animal ethics, maintenance, anesthetics and intravitreal injection

2.1.10.1 Animal ethics and maintenance

All procedures were conducted according to the Association for Research in Vision and Ophthalmology Statement for the Use of Animals in Ophthalmic and Vision Research and the requirements of the National Health and Medical Research Council of Australia (Australian Code of Practice for the Care and Use of Animals for Scientific Purposes). Ethics approval was obtained from the Animal Ethics Committees of the University of Tasmania (A14827) and St. Vincent's Hospital Melbourne (AEC 014/15). Animals were housed under standard conditions (20°C, 12/12-hour light/dark cycle) with *ad libitum* access to food and water.

2.1.10.2 Anesthetics

For intravitreal injection or electrophysiological assessment, mice were anesthetized by intraperitoneal injection of ketamine (60 mg/kg) and xylazine (10 mg/kg). 0.5% proxymetacaine was applied for corneal anesthesia. Animals were sacrificed under CO_2 euthanasia according to approved animal ethics.

2.1.10.3 Intravitreal injection

Intravitreal injection was performed under a surgical microscope. A small puncture was made at the superior-temporal quadrant behind the limbus using a 30-gauge needle. A hand-pulled glass micropipette was inserted into the vitreous cavity, which was connected to a 10 µL Hamilton (Bio-Strategy, Broadmeadows, VIC, Australia) and the injection rate was controlled by a UMP3-2 Ultra Micro Pump. Based on AAV titration by qPCR, AAV vectors were diluted to include similar viral genome. A total of 1 µL dual-viral suspension (AAV-Cas endonuclease: AAV-guide RNA=1:1) was injected into the mouse eye. A list of animal groups with injection detail is provided in Appendix 4.

2.1.11 Electroretinography (ERG)

Mice were kept under overnight dark-adaptation conditions for 12 h prior to ERG assessment. ERG was performed following the protocol outlined previously[105–107]. In brief, mouse pupils were dilated with 0.5% tropicamide. A pair of specially made loop electrodes were placed around each eye, and a needle electrode was inserted into the tail of the mouse. A small drop of ocular lubricant (Alcon Systane®) was used to maintain corneal hydration and improve electrical contact. Different levels of stimuli were delivered, and signals were recorded simultaneously for both eyes. ERG analysis was performed as previously described, with three major components of the ERG waveform returned: the photoreceptor (a-wave), bipolar cell (b-wave), and ganglion cell dominated (scotopic threshold response, STR).

2.1.12 Optical Coherence Tomography (OCT)

Following ERG recordings, retinal images were obtained using a spectral domain-OCT as previously described[20,105]. Mice were positioned to capture Optic Nerve Head (ONH) centered 1.4 mm-wide horizontal B-scans (consisting of 1000 A-scans per B-scan) from both eyes. Eyes were aligned to place the optic nerve at the center of the image. Image analysis was undertaken using FiJI software (https://fiji.sc/) in a masked fashion, via manual segmentation of the inner boundary of the retinal nerve fiber layer (inner limiting membrane), the outer boundary of the retinal nerve fiber layer, the inner plexiform layer and Bruch's membrane. Total retinal thickness (from the inner limiting to Bruch's membrane), retinal nerve fiber layer thickness (from the inner limiting membrane to the inner aspect of the inner plexiform layer) and outer retinal thickness (from Bruch's membrane to the outer plexiform layer) were measured in each eye.

2.1.13 Retinal collection

Eyes were popped out of sockets with applied force. A fine needle was used to the disturb aqueous humor to relieve intraocular pressure. The cornea was grasped with forceps and an elliptical opening was created using small surgical scissors. Iris, lens and vitreous body were extracted. Incisions were made along four sides of the eye and the retina was separated from the choroid. The retina was kept in an Eppendorf tube chilled PBS (4°C) until ready for dissociation.

2.1.14 Flow cytometric analysis

2.1.14.1 Cell preparation for flow cytometry

YFP-expressing HEK293A cells were trypsinized and harvested in PBS. Cells were resuspended in Fluorescence-activated cell sorting (FACS) buffer and stained with DAPI (5 µg/mL) to exclude dead cells.

2.1.14.2 Retina dissociation for flow cytometry

Freshly collected retina was dissociated using a papain dissociation kit according to the manufacturer's instructions. In brief, papain solution with a final concentration of approximately 20 units/mL and 0.005% DNase was prepared. Freshly dissected retinal tissue was placed in the papain solution and incubated at 37°C in a rocker platform for 1 h. The mixture was vigorously triturated and cell suspension was transferred to a sterile tube, followed by centrifuge to form retinal cell pellets. Pelleted cells were resuspended in a mixture of 0.9 mL EBSS with 100 µL reconstituted albumin-ovomucoid inhibitor solution in a sterile tube. The supernatant was discarded, and the cells were immediately resuspended in PBS. After washing with PBS several times, retinal cells were resuspended in FACS buffer and stained with DAPI (5 µg/mL) to exclude dead cells.
The percentage of YFP-positive cells and mCherry-positive cells were then analyzed from the live cell population with a Flow Cytometer (BD FACS Canto II) and data were analyzed using FlowJo.

2.1.15 Retinal flat mount, cryosection, imaging and cell counting

2.1.15.1 Flat mount

Enucleated eyes were fixed in ice-cold 4% paraformaldehyde (PFA) for 1 h prior to dissecting under a microscope. A fine needle was used to disturb the aqueous humor to relieve intraocular pressure. The cornea was grasped with forceps and an elliptical opening was created from the same incision using small surgical scissors. Cornea, iris and lens were removed, and four equally spaced radial relaxing incisions were made, extending two-thirds of the way from the retinal periphery to the ONH. The sclera and choroid were then removed along with residual vitreous body, leaving only the retina on a slide. The retina was fixed with 75% ethanol at 4ºC for 30 min in a dark slide staining box. The retina was washed with PBS and incubated with 1% Triton-X at room temperature for 20 min. The retina was washed with PBS and then stained with NucBlue™ Live ReadyProbes™ Reagent for 20 min at room temperature. The slide was then washed

thoroughly with PBS and dried with Kimwipe, followed by mounting with Dako Fluorescent mounting medium and covered with a coverslip. Slides were stored at 4ºC in the dark until images were taken.

2.1.15.2 Retinal cryosection

Enucleated eyes were fixed in 4% PFA for 1 h and embedded in optimal cutting temperature compound prior to frozen sectioning on a microtome cryostat. Serial 10-um-thick sections were cut, mounted on FLEX glass slides, and then stained with NucBlue™ Live ReadyProbes™ Reagent. Slides were then mounted with Dako Fluorescent mounting medium, covered with coverslip and stored at 4ºC in the dark until images were taken. For longer-term storage, slides with mounted retinal sections (without staining) were transferred directly in a slide storage box at -80ºC. Retinal cryosection images were taken by an Olympus VS120 Slide Scanner.

2.1.15.3 Retinal imaging and cell counting

For YFP-knockout counting, retinal images were captured by a fluorescence microscope (Zeiss Axio Imager Microscope; Carl-Zeiss-Strasse, Oberkochen, Germany) equipped with a charge-coupled digital camera (AxiocamMRm, Zeiss) and image acquisition software (ZEN2, Zeiss). Retinal cell quantification was performed as previously described20. Briefly, images of retinal flat mount were taken with filters fit for mCherry (605 nm, Zeiss Filter set 64HE) and YFP (495 nm, Zeiss Filter set 38HE). Retinal cells were manually quantified using ImageJ with individual fluorescent images captured at ×400 magnification from different retinal quadrants. The efficiency of YFP knockout was determined by calculating the proportion of YFP-negative cells among these mCherry-expressing cells.

2.1.16 SpCas9 expression in retina by qPCR

2.1.16.1 Total RNA extraction from mouse retina

Enucleated mouse eyes were stored in RNAlater RNA stabilization reagent, and retinas were dissected immediately under a microscope as described previously. Total RNA from mouse retinas was extracted and purified using commercial kits (RNeasy Mini Kit) in accordance with the manufacturer's instructions. Briefly, retinas were disrupted and homogenized. Ethanol was then added to the lysate to promote RNA binding to the RNeasy membrane. The sample was then transferred to the RNeasy Mini spin column. Total RNA was bound to the membrane of the column, with contamination washed away by desired washing buffers. RNA was then eluted in RNase-free water and measured by Nanodrop. A 260/280 ratio of <2.0 was considered pure. The RNA samples were stored at -80ºC.

2.1.16.2 Reverse transcription for mRNA

RNA was subsequently reverse-transcribed into complementary DNA (cDNA) using a high-capacity RT kit (Taqman RNA Reverse Transcription Kit) according to the manufacturer's instructions. For each retinal sample, 80ng of total RNA eluted in 5 µL of Diethyl pyrocarbonate (DEPC)-treated water was reversely transcribed following the protocol listed below.

Component	**volume (µL)**
10 x RT Buffer	1.0
25 x dNTP Mix (100 mM)	0.4
10 x RT Random Primers	1.0
MultiScribe ™ Reverse Transcriptase	0.5
Nuclease-free water	2.1
RNA (80 ng)	5.0
Total per reaction	10.0

Thermal cycling condition

	Step 1	**Step 2**	**Step 3**	**Step 4**
Temperature (°C)	25	37	85	4
Time (min)	10	120	5	∞

After the reverse transcription, cDNA was diluted with 90µl of DEPC-treated water for quantitative PCR.

2.1.16.3 qPCR to detect SpCas9 expression

qPCR was performed using a Fast SYBR Green Master Mix with the SpCas9 forward and reverse primers as well as mCherry forward and reverse primers. For each sample, a 10µL reaction was prepared containing 8µL master mix (as shown in the table below) and 2µL diluted cDNA sample. The relative expression levels of SpCas9 were calculated using the ΔΔCt method[108] with normalization to mCherry. *GAPDH* was used as a housekeeper gene.

Component	25 µL reaction (µL)
Nuclease-free water	7.25
Fast SYBR green master mix	12.5
Forward primer (100 µM)	0.125
Reverse primer (100 µM)	0.125
Diluted cDNA	5.0
Total per reaction	25.0

2.1.17 Genome-wide CRISPR/Cas9 screen for uveal melanoma OCM-1 cells

We used a Genome-Scale CRISPR Knockout (GeCKO) lentiCRISPR v2 library (a gift from Feng Zhang, Catalog#1000000048) that targets around 19050 genes throughout the whole human genome, with a total of 1233411 sgRNAs pooled together (6 gRNAs per targeted gene, 1000 control sgRNAs designed not to target the genome, and over 1000 sgRNAs targeting microRNA). First, a lentiCRISPR v2 plasmid library was amplified and packaged with lentivirus. Uveal melanoma (UM) cell line OCM-1 was transduced with lentiCRISPR v2 library and puromycin was added to maintain a low Multiplicity of infection (MOI) to ensure each cell received only one sgRNA. A large volume of transfected OCM-1 cells (more than $1x10^8$) were cultured to maintain enough sgRNA coverage, and cells were collected at two time points: once immediately after transduction, and finally after 12 passages. Genomic DNA was extracted, and the presence of the guide RNA library was identified using next-generation deep sequencing. Web-based tools CRISPRAnalyzeR

and g:Profiler were then employed for bioinformatics and functional analysis. Detailed protocols are listed below based on previous studies[109–111].

2.1.17.1 Amplification of pooled sgRNA library

Pooled sgRNA library (GeCKO v2.0 DNA plasmids) for screening was amplified as previously described[111]. Briefly, diluted half-library of lentiCRISPR v2 (Library A and Library B) was electroporated in Endura ElectroCompetent Cells and recovered in SOC medium. A 40000 dilution of transformation was plated for overnight growth and transformation efficiency was calculated by multiplying the number of colonies by dilution fold. Colonies were harvested, bacteria pellets were weighed, and plasmid DNA was generated using Maxiprep Kit.

2.1.17.2 Lentivirus generation for pooled sgRNA library (lentiCRISPR v2)

Lentivirus was produced in HEK293FT cells packaging amplified GeCKO v2.0 DNA plasmids (Library A+ Library B).

One day prior to transfection: Seeding $2x10^7$ cells per T175 flask, 2 flasks in total.

The reaction mixture was set up as below.

Tube A:

Component	**Per T175 flask**
Library A+B (1:1 ratio)	22.5 µg
pMD2.G	7.9 µg
pCMV D8.91	14.6 µg
Opti-MEM	4.5 mL

Tube B:

Component	**Per T175 flask**
Lipofectamine 2000	130 µL
Opti-MEM	4.5 mL

Tube A and Tube B were incubated at room temperature for 10 min separately, then mixed evenly and incubated at room temperature for another 10 min. Medium was aspirated with only 1 mL left to cover cells. 9 mL of the transfection mixture was added per flask. The medium was changed after 4-6 h. Cells along with medium were collected to a 50 mL

centrifuge tube 48 h later. The cell suspension was centrifuged for 5 min at 300g, and the supernatant was transferred to a new sterile centrifuge tube, followed by flowing through a 0.45 μm sterile filter. 5x PEG virus precipitation solution was added to concentrate the virus and the mixture was placed at 4ºC overnight. Supernatant was discarded followed by centrifuge at 4ºC at 1500 g for 30 min. The lentivirus particle was resuspended in 2mL Opti-MEM and an aliquot was stored at -80ºC.

2.1.17.3 Kill-curve with puromycin selection for OCM-1

$2x10^5$/well OCM-1 cells were seeded in 6-well plates to reach 80% confluency the next day. Different puromycin concentrations (0, 0.25, 0.50, 1, 2 and 2.5 μg/mL) was added to the wells. Cells were examined under microscope 24 h after puromycin treatment. The lowest concentration of puromycin that killed all the cells within two days was selected as the concentration for CRISPR screen for OCM-1. The selected concentration of puromycin was then tested in OCM-1 cells seeded in similar confluency in T175 flask before applying to large-scale cell culture.

2.1.17.4 Lentiviral transduction and screening in OCM-1 cell

i Lentiviral transduction

One day before lentiCRISPR v2 transduction, $2x10^5$/well OCM-1 cells were seeded in 6-well plates. Before infection, the medium was replaced with 1ml RPMI with 10% FBS, and polybrene was added (final concentration 8 μg/mL). A series of different volumes of lentiCRISPR v2 virus (0, 0.1, 0.25, 0.5, 1 and 2.5 μL) were added to each well. Two days after infection, cell culture medium was replaced with 2 mL of fresh medium supplemented with the selected concentration of puromycin. Two wells of cells without Lentivirus infection were used as controls (positive control: with puromycin, negative control: without puromycin). Two days after puromycin treatment, live cells were collected and counted. MOI was calculated as the number of live cells in puromycin selection condition/number of live cells in the negative control. The amount of Lentivirus with a MOI around 0.3 was

selected for pooled screens. Lentiviral transduction and puromycin selection were further tested in larger cell numbers using the selected puromycin concentration and Lentiviral volume in proportion.

ii Knockout screening in large-scale expansion of OCM-1 cells

A total of 30 T225 flasks of OCM-1 cells ($1x10^7$ cells per flask) were seeded one day before Lentiviral transduction. Cells were transduced with lentiCRISPR v*2* in medium supplemented with polybrene (8 µg/mL). Puromycin was added two days after lentiviral transduction. Cells were harvested two days after puromycin treatment and $1x10^8$ cells were maintained in puromycin selection condition, with the remaining infected cells collected and stored in a freezer (referred to as UMP0). The cells in culture were maintained in puromycin condition for 1 week in total and then $1x10^8$ cells were cultured and passaged in puromycin-free medium for 12 passages. OCM-1 cells were collected at P12 and stored in the freezer (referred to as UMP12). Three biological replicates of CRISPR knockout screening were performed in UM cell line OCM-1. Sample ID for P0 were listed as UMP0_1, UMP0_2, UMP0_3, and P12 as UMP12_1, UMP12_2, UMP12_3.

2.1.17.5 Next-generation sequencing (NGS)

i gDNA preparation for NGS analysis

Frozen cell pellets of OCM-1 P0 and OCM-1 P12 were stored at -80ºC until use. Over $1x10^8$ cells were used to maintain a coverage of >500. Genomic DNA was extracted using the Zymo Research Quick-DNA Midiprep Plus Kit according to the manufacturer's instructions. sgRNA library was PCR amplified for NGS. PCR reaction and conditions were as follows.

Component	**50 µL reaction (µL)**	**Final concentration**
NEBNext High Fidelity PCR master mix, 2x	25	1x
Pooled sgRNA library sample/gDNA of OCM-1	1	0.4 ng/µL

NGS_Lib_Fwd primer	1.25	0.25 µM
NGS_Lib_KO_Rev primer (barcode)	1.25	0.25 µM
Nuclease-free water	21.5	
Total	50	

Thermal cycling condition:

Cycle number	**Denature**	**Anneal**	**Extend**
1	95ºC, 5 min		
2-13	98ºC, 20 s	60ºC, 15 s	72ºC, 15 s
14			72ºC, 1 min

PCR products were purified using a QIAquick PCR purification kit according to the manufacturer's protocol. NGS was performed in two stages: Stage 1, after amplification of pooled sgRNA library to determine sgRNA distribution; Stage 2, at the end of the screen.

ii NGS analysis

Sequencing was performed on the NOVOSEQ™ 6000 Sequencing system at the Ramaciotti Centre for Genomics, University of New South Wales, Australia. The FastQ files were generated using bcl2fastq2 Conversion Software v2.20.

iii Quality control

Data from the FastQ files were assessed by FastQC, a quality control tool for high throughput sequence data, to ensure that all the reads have phred score over 25. An interactive report was provided including basic statistics (reads quality score), adapter contents, etc.

iv Adapter/Quality trimming

The adapter content was removed by BBTools using the bbduk module, which filters or trims reads for adapters and contaminants using k-mers. It was developed to do quality filter trimming and remove adapter content via different parameters including GC filtering, k-mers matching and length filtering. Less than 9.78% of poor reads were removed along with the adapter contents from our FastQ files data.

2.1.17.6 Bioinformatic analysis using CRISPRAnalyzeR

CRISPR/Cas9 Knockout screening analysis was performed using the CRISPRAnalyzeR[112], a web-based analysis platform that features eight different algorithms to compare the hit calling including DESeq2[113] , MAGeCK[114], edgeR[115], sgRSEA (Jungsik Noh et al, 2015), Mann-Whitney[116] , ScreenBEAM[117] and BAGEL[118]. In our analysis, five different programs were used with default parameters to identify the ranked-based possible hits as follows:

i DESeq2

DESeq2 is a differential expression analysis method implemented in R as a package. It uses read counts of all sgRNAs/genes for given different experimental conditions to estimate the differential effects based on negative binomial model. Enrichment and depletion of the sgRNAs/genes were estimated on log2 fold change between the two different groups by using the Wald test[113].

ii MAGeCK

MAGeCK is a model-based CRISPR/Cas9 knockout method to identify the negative and positive selected sgRNAs and genes across different experimental conditions. The program uses the median-normalized method to adjust the effective size of libraries and read-count distribution and then uses the mean variance estimation model and negative binomial to determine the significant sgRNAs and genes across the different conditions.

Finally, the robust ranking aggregation (RRA) algorithm[119] is used to rank the significant genes in negative and positive selection, respectively[114] .

iii edgeR

edgeR is another method using differential expression analysis implemented in R. In this program, read count data were modelled by using an over-dispersed Poisson model. Gene dispersion was estimated by the conditional maximum likelihood method and adapted Fisher's exact tests were used for assessing the differential expression for sgRNAs/genes[115].

iv Wilcox

The Wilcox method was implemented on the two-sided Mann-Whitney-U test[116], a test for comparing two different groups on fold change for each gene. Later, the corrected *p* value was calculated by using the Benjamini-Hochberg method to correct for multiple testing.

v sgRSEA

Single-guide RNA Set Enrichment Analysis (sgRSEA) is another program implemented on the R programming language for enrichment analysis of CRISPR/Cas9 Knockout Screen Data. It ranks the sgRNA on the signal-to-noise ratio and calculates sgRNA ranking by enrichment score (which is one-sided Kolmogorov Smirnov statistic method) and reflects the enriched and depleted sgRNA, respectively.

2.1.17.7 Assessment of gene expression of hit candidates using ULCAN

The tumor subgroup expression on our hit candidates was then assessed using online portal ULCAN[120]. The expression level of each gene at different cancer stages and its effect on UM patient survival was checked based on genomic data from TCGA datasets.

2.1.17.8 Functional analysis using gProfiler

The functional analysis was done by using gProfiler[121,122], a web-based tool for functional profiling for significant genes from high throughput data. A list of significant genes was

supplied and statistically significant gene ontology and pathways were identified. Cytoscape[123] and Enrichment map[124] were used for visualizing statistically significant pathways as mentioned previously[125].

2.1.18 Whole-exome sequencing to detect off-target by CRISPR/Cas9 in the retina

2.1.18.1 Genomic DNA extraction from mouse retina

Genomic DNA was extracted from mouse retina using the Gentra Puregene Tissue Kit according to the manufacturer's instructions. Briefly, a retina sample was completely lysed in Cell Lysis Solution by incubating at 55ºC overnight with Puregene Proteinase K. RNase A solution was added and the mixture was incubated at 37ºC for 1 h. Proteins were precipitated by adding Protein Precipitation Solution. Genomic DNA was precipitated from the supernatant by adding isopropanol. DNA pellet was washed with 70% ethanol, air dried and finally eluted in 50~100 µl DNA Hydration Solution. DNA was dissolved by incubating at 65ºC for 1 h.

2.1.18.2 Whole-exome sequencing and analysis.

Genomic DNA from retina was extracted and dissolved in DNA Hydration Solution. Whole-exome sequencing (WES) and standard bioinformatics analyses were performed by the Beijing Genomics Institute (BGI). Raw reads were filtered, and the resulting high-quality, clean data were aligned to the mouse reference genome (mm10). For indel analysis, homology between the sgRNA sequence and sequences around the indel site in the mouse reference genome were evaluated. Off-target effects were considered when MAFFT showed ungapped alignment between these sequences[126], with fewer than five nucleotide mismatches and correct PAM sites present in the reference sequence.

2.1.19 Statistical Analysis

All statistical analyses were performed using Prism 7 software (GraphPad Software, Inc., La Jolla, CA, USA). Group data are presented as mean ± SEM, and mean data were analyzed with unpaired t-tests, one-way or two-way analysis of variance (ANOVA)

followed by post-hoc analysis (GraphPad Prism 7.0) unless otherwise specified. A value of $p<0.05$ was taken to be statistically significant.

2.2 Materials

A complete list of reagents, cell lines, animal stains and their suppliers used for all experiments, experimental setup, software and online resources described in this thesis is provided in Appendix 2.

3 UTILITY OF SELF-DESTRUCTING CRISPR/CAS CONSTRUCTS FOR TARGETED GENE EDITING IN THE RETINA

3.1 Introduction

In our previous study, we achieved high-efficiency genome editing in mouse retina using a dual AAV2-mediated CRISPR/Cas9 system[20]. Other groups also reported promising results of CRISPR/Cas application in various animal models for pre-emptive therapy for well-characterized monogenic ocular diseases[19,21,23,28]. Despite advances in efficient gene editing *in vivo*, extended over-expression of CRISPR/Cas endonuclease including elevated off-target cleavage[127,128] and cellular immune responses[60] remain key safety hurdles to clinical application.

To address this, we designed a self-destructive “kamikaze”-CRISPR/Cas system that disrupts the CRISPR/Cas gene after active protein expression (Figure 3.1). To determine the efficacy of *in vivo* genome editing by our “kamikaze”-CRISPR/Cas construct, a *SpCas9*-targeting sgRNA module, together with a *YFP*-targeting sgRNA, were packaged into a dual AAV2 vector system for intravitreal delivery in Thy1-YFP transgenic mice. Our hypothesis was that by inserting a second gRNA-targeting Cas endonuclease itself, CRISPR constructs would be degraded and Cas protein expression would be reduced without compromising the on-target efficacy of *YFP*-targeting sgRNA.

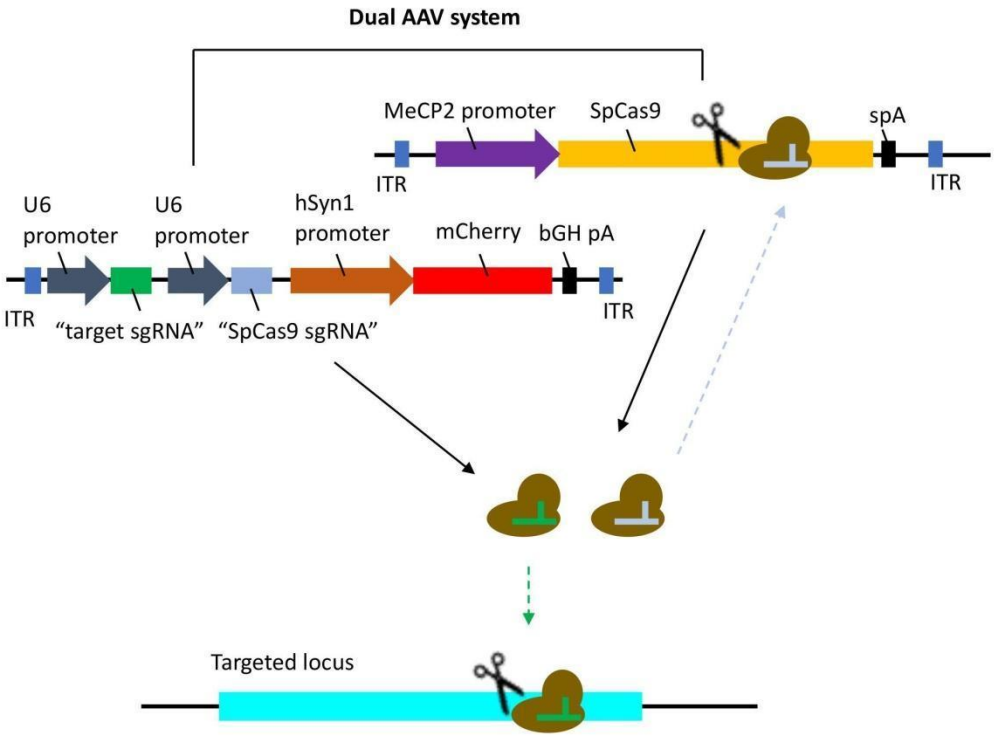

Figure 3.1. Schematics of Kamikaze CRISPR/Cas system.

A dual AAV vector system was used, with one viral vector delivering SpCas9 and the other delivering sgRNAs against SpCas9 and the target locus (YFP), in the presence of mCherry. The workflow of this study was to first design *SpCas9*-targeting sgRNAs (Figure 3.2), select the best-performing SpCas9 sgRNA with the least off-target profile, and then insert this SpCas9 sgRNA into the original *YFP*-targeting sgRNA AAV vector. Differences in SpCas9 expression and YFP knockout efficiency were compared in HEK293-YFP cells transfected with this self-targeting *YFP*-targeting CRISPR and the regular *YFP*-targeting CRISPR, followed by an *in vivo* test in Thy 1-YFP mouse retina using a dual AAV2 delivery system. Retinal functional and structural assessment were also performed to investigate whether this kamikaze-CRISPR/Cas system would cause extra burden to the retina compared with a regular CRISPR/Cas system.

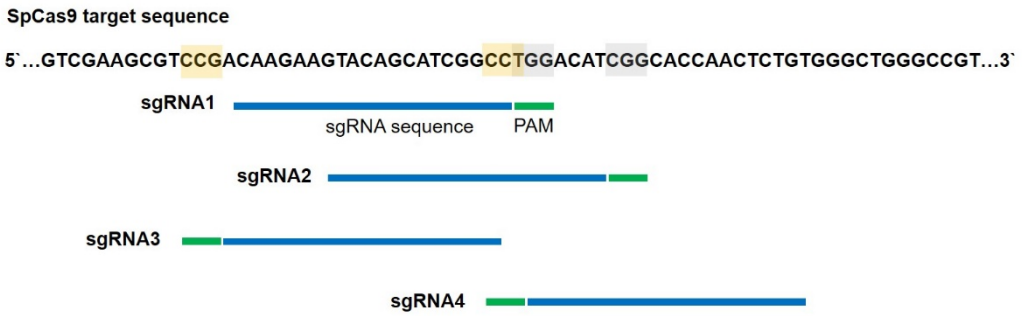

Figure 3.2 Schematic diagram of SpCas9 sgRNA design.

Blue: selected SpCas9 sgRNA targeted sites. Green: PAM sequences.

3.2 Results

3.2.1 Validation of four *SpCas9*-targeting sgRNA

3.2.1.1 *In situ* validation of SpCas9 sgRNAs

To validate our designed four sgRNAs for SpCas9 targeting, we first used an *in situ* cleavage assay by incubating the individual synthetic SpCas9 sgRNA or LacZ sgRNA alone with the recombinant SpCas9 protein and the pX551 plasmid. Cleavage pattern for SpCas9 was visualized on 0.8% TAE gel.

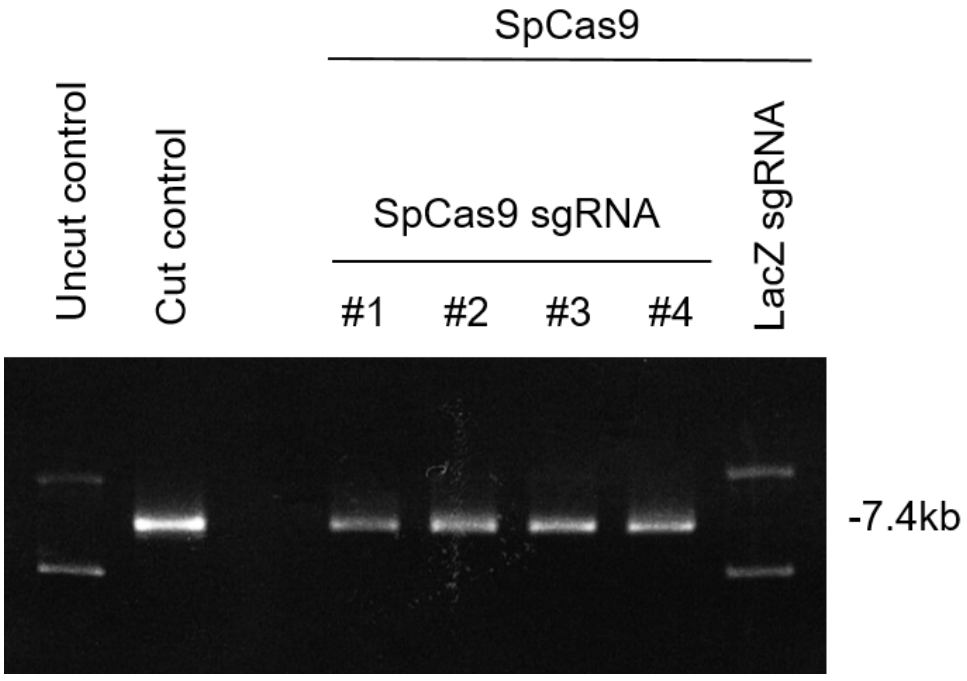

Figure 3.3 *In situ* validation of SpCas9 sgRNAs.

Robust cleavage of the SpCas9 plasmid (pX551) was found when each of the four designed SpCas9-targeting sgRNAs （SpCas9 sgRNA #1, #2, #3, #4) were introduced to recombinant SpCas9 protein (Figure 3.3). The same cleavage pattern was found when pX551 plasmid was digested by restriction enzyme (AgeI), which served as a positive control. No cleavage was found in negative control and *LacZ*-targeting sgRNA control. Uncropped agarose gel images are presented in Appendix 5.

3.2.1.2 SpCas9 sgRNA selection by western blot

SpCas9-targeting sgRNA plasmids were generated. We further confirmed the efficacy of *SpCas9* gene perturbations by transfection of the plasmid with SpCas9 (pX551-CMV-SpCas9) together with plasmid with *SpCas9*-targeting sgRNA (pX552-SpCas9 sgRNA #1, #2, #3, #4) into HEK293A cells. SpCas9 sgRNA #4 had a clear destructive effect on SpCas9 (Figure 3.4) with reduction of SpCas9 protein by western blot, as well as having a lower off-target score against the human genome as predicted by a web-based CRISPR design program (http://crispr.mit.edu). Therefore, SpCas9 sgRNA#4 was selected and it is referred to as SpCas9 sgRNA in the following experiment.

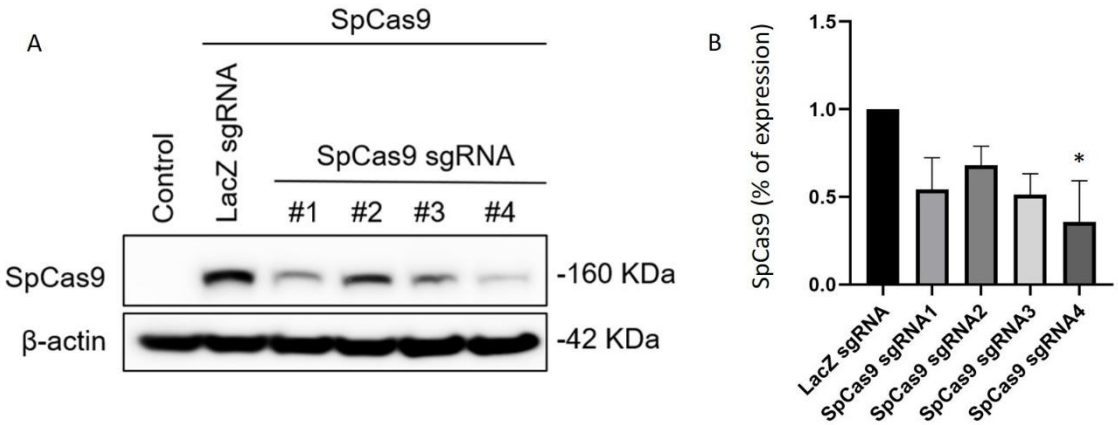

Figure 3.4 *In vitro* validation of SpCas9 sgRNAs by western blot.

Representative western blot of SpCas9 protein expression in HEK293A cells co-transfected with SpCas9 and SpCas9 sgRNA plasmids (A). Relative fold change of SpCas9 expression normalized to β-actin. Significant reduction of SpCas9 expression was found in cells transfected with SpCas9 and SpCas9 sgRNA4 plasmids compared with LacZ sgRNA control (B). Data are presented as mean ± SEM for three independent replicates. Statistical analysis between groups was performed using one-way ANOVA (*p<0.05).

3.2.1.3 Time course of SpCas9 expression *in vitro*

We further confirmed the efficacy of SpCas9 sgRNA in *SpCas9* gene perturbations by a time-course analysis of SpCas9 protein expression in HEK293A cells co-transfected with SpCas9 plasmid and SpCas9 sgRNA plasmid. SpCas9 protein was progressively reduced in cells transfected with *SpCas9*-targeting CRISPR/Cas plasmids (pX551-CMV-SpCas9 + pX552-CMV-GFP-SpCas9 sgRNA4) and also cells transfected with LacZ sgRNA control plasmids (pX551-CMV-SpCas9 + pX552-LacZ sgRNA) by western blot (Figure 3.5). A time-course analysis showed that at each time point, SpCas9 protein expression was lower in cells transfected with *SpCas9*-targeting CRISPR/Cas plasmids compared with LacZ sgRNA control, and the difference in SpCas9 expression was significant at certain time points (p<0.01 at day 1, p<0.05 at day 2; Figure 3.6).

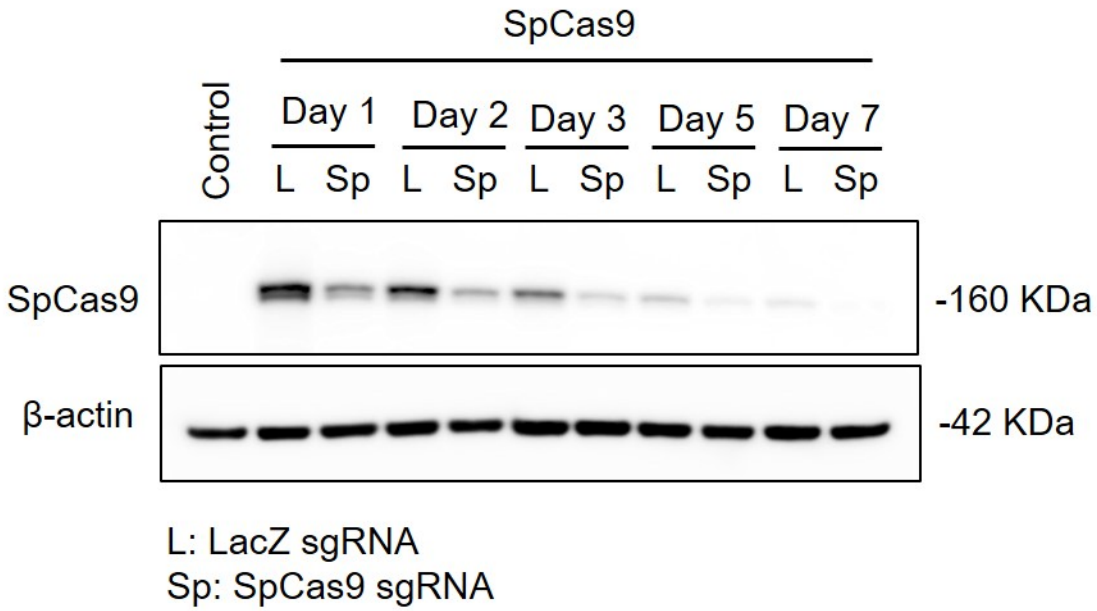

Figure 3.5 Representative western blot of the time course of SpCas9 protein expression.

Cells were harvested at day 1, 2, 3, 5, 7 after transfection. A time course analysis by western blot showed that SpCas9 protein was progressively reduced in cells following the transfection of selected *SpCas9*-targeting CRISPR/Cas construct (pX552-SpCas9 sgRNA4) compared to LacZ sgRNA control.

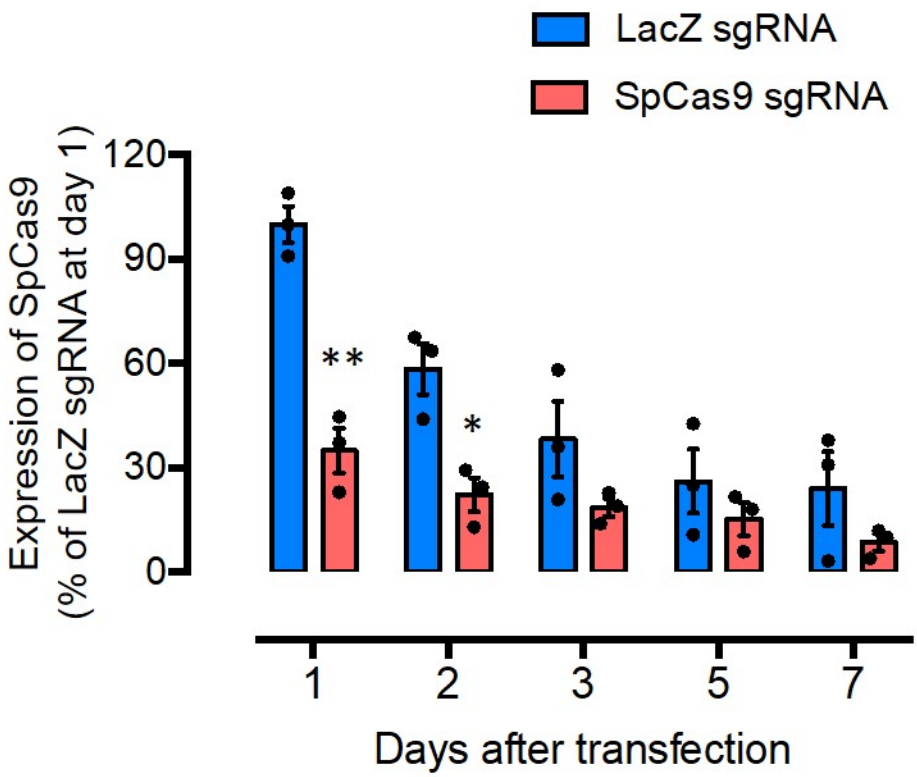

Figure 3.6 Analysis of time course of SpCas9 protein expression.

Relative fold change of SpCas9 expression normalized to β-actin. Data are presented as mean ± SEM for three independent replicates. Statistical analysis between groups was performed using two-way ANOVA followed by Tukey's multiple comparisons test (*p<0.05, **p<0.001).

3.2.2 Validation of kamikaze-CRISPR/Cas construct in YFP-expressing cells

We next re-engineered our kamikaze-CRISPR/Cas construct with *YFP*-targeting sgRNA or a *LacZ*-targeting sgRNA. The schematics of kamikaze-CRISPR/Cas constructs used for *in vitro* test are shown in Figure 3.7. To strengthen the result, we generated kamikaze-CRISPR/Cas construct based on two *YFP*-targeting guide RNAs, one termed YFP sgRNA2 and the other referred to as YFP sgRNA6. Their cleavage efficacy in YFP-expressing cells was tested in our previous study (data not shown) and used as vector backbone for this kamikaze-CRISPR project.

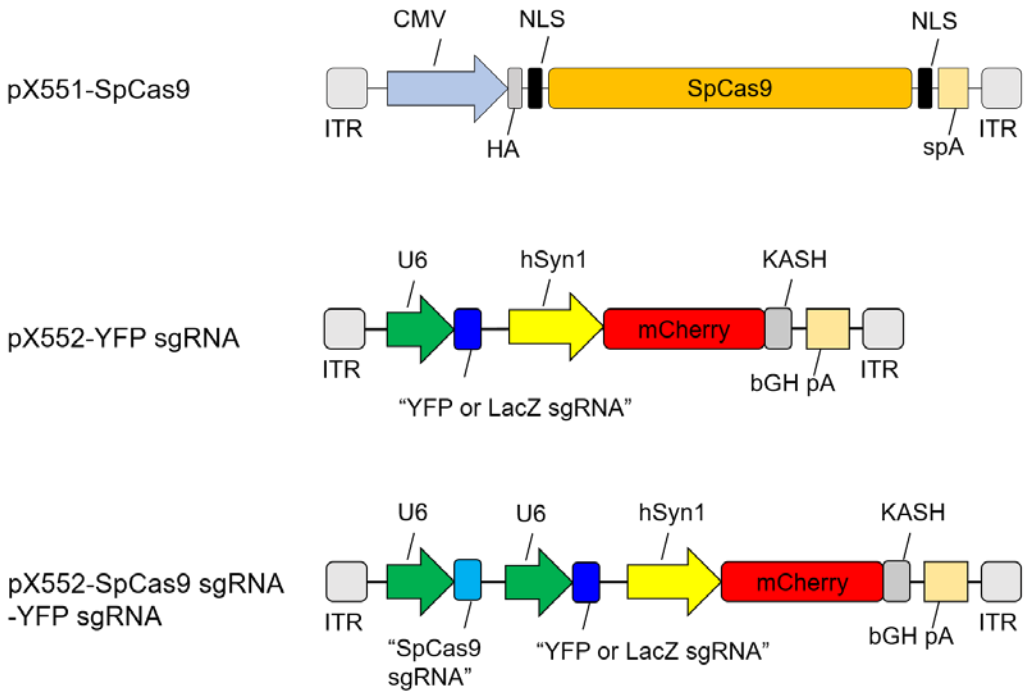

Figure 3.7 Schematics of Kamikaze CRISPR/Cas constructs for *in vitro* validation.

SpCas9 was driven by CMV promoter, sgRNA was driven by U6 promoter, and mCherry cassette was driven by a neuron-specific promoter hSyn1.

3.2.2.1 SpCas9 reduction *in vitro*

To validate the reduction of SpCas9 in cells treated with Kamikaze CRISPR/Cas constructs, HEK293A cells were transfected with either Kamikaze CRISPR/Cas constructs or conventional CRISPR/Cas constructs, followed by western blot analysis two days after transfection. We observed a reduction of SpCas9 protein in cells that had received the kamikaze-CRISPR/Cas construct (SpCas9 + SpCas9 sgRNA/LacZ sgRNA, SpCas9 + SpCas9 sgRNA/YFP sgRNA) compared to those cells that had received the regular CRISPR/Cas construct (SpCas9 + pX552-LacZ sgRNA, SpCas9 + pX552-YFP sgRNA) (Figure 3.8).

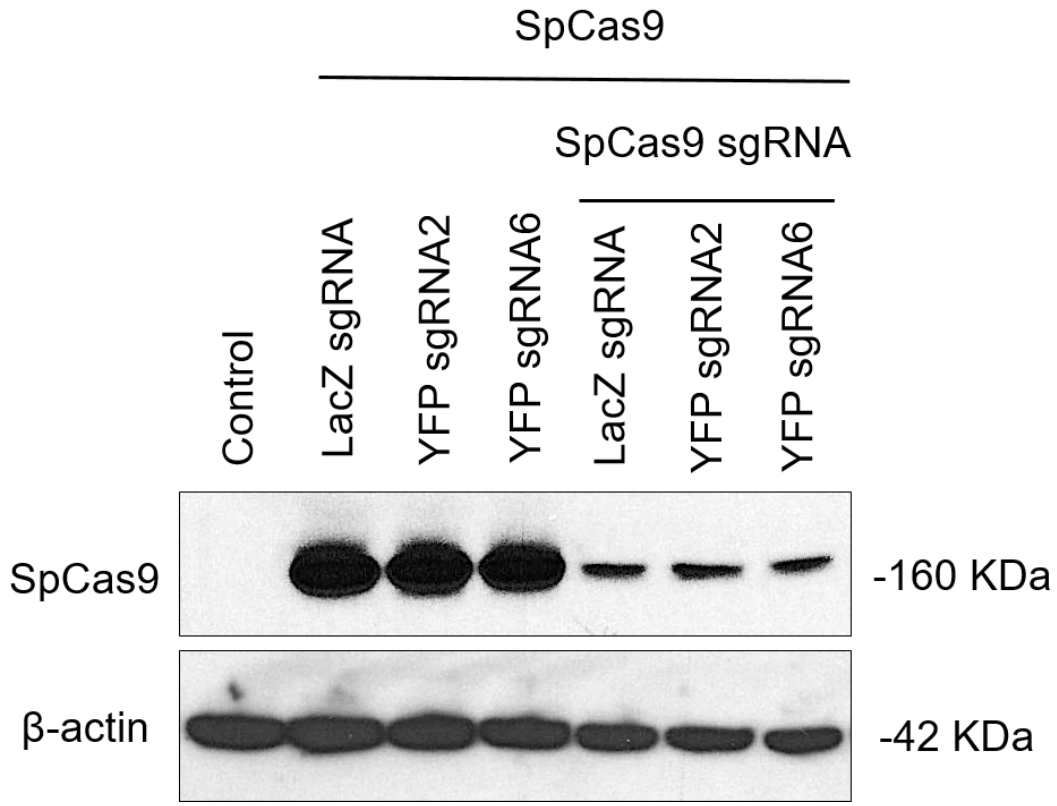

Figure 3.8 SpCas9 reduction in cells transfected with Kamikaze-CRISPR/Cas9.

Representative western blot of SpCas9 protein expression in cells transfected with kamikaze-CRISPR/Cas9 construct or non-kamikaze CRISPR/Cas9 constructs. Two days after transfection in 6-well plates, HEK293A cells were lysed and subjected to western blot analysis with antibodies against SpCas9 and β-actin.

3.2.2.2 YFP disruption *in vitro*

To test the efficacy of *YFP* gene disruption, HEK293A-YFP cells were transfected with *YFP-targeting* Kamikaze CRISPR/Cas constructs or conventional *YFP-targeting* CRISPR/Cas9 constructs. YFP expression was checked under a fluorescence microscope. A marked reduction of percentage of YFP-expressing cells was detected from 5-7 days after transfection (data not shown). Ten days after transfection, a marked reduction in YFP expression in HEK293-YFP cells transfected with *YFP*-targeting CRISPR/Cas constructs (SpCas9 + YFP sgRNA) and also *YFP*-targeting kamikaze-CRISPR/Cas constructs (SpCas9 + SpCas9 sgRNA/YFP sgRNA). No obvious reduction

could be found in cells transfected with *LacZ*-targeting controls (kamikaze and non-kamikaze).

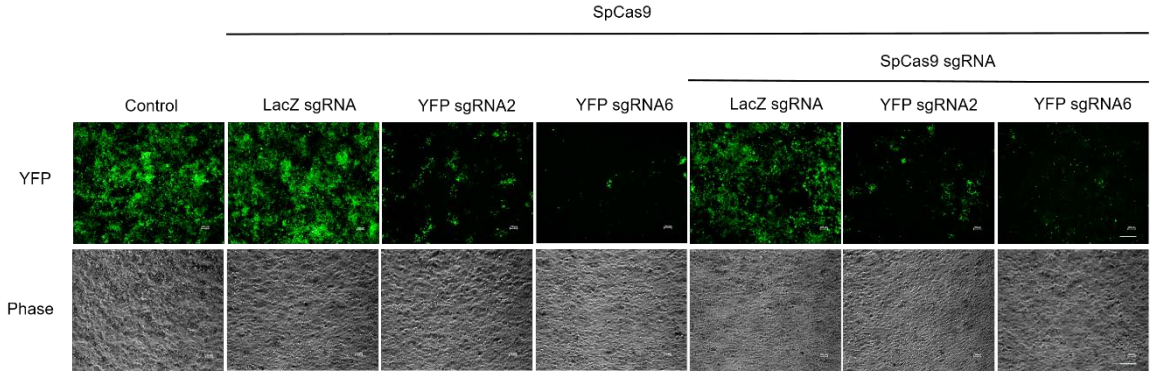

Figure 3.9 Fluorescence microscopy image showing reduction in YFP expression. Representative images of YFP expression in cells transfected with kamikaze (SpCas9 sgRNA-YFP sgRNA and SpCas9 sgRNA-LacZ sgRNA) or non-kamikaze (YFP sgRNA and LacZ sgRNA) constructs. *Scale bar: 100 µm.* Cells were collected at day 10 post transfection.

YFP-knockout efficiency was further quantified by flow cytometry analysis at day 10 post-transfection (Figure 3.10 and 3.11). The percentage of YFP-expressing cells was significantly reduced in cells transfected with *YFP*-targeting kamikaze-CRISPR/Cas constructs (SpCas9 sgRNA-YFP sgRNA2: 10.0±1.0% and SpCas9 sgRNA/YFP sgRNA6: 5.6±0.4%, respectively), compared to *LacZ*-targeting kamikaze (SpCas9sgRNA/LacZ sgRNA: 85.9±1.3%) or *LacZ*-targeting (LacZ sgRNA: 86.0±1.4%) CRISPR/Cas construct at 10 days after transfection. Similarly, a lower percentage of YFP-expressed cells was also found in cells transfected with the *YFP*-targeting CRISPR/Cas construct (YFP sgRNA2: 16.7±2.7% and YFP sgRNA6: 7.4±1.4% respectively).

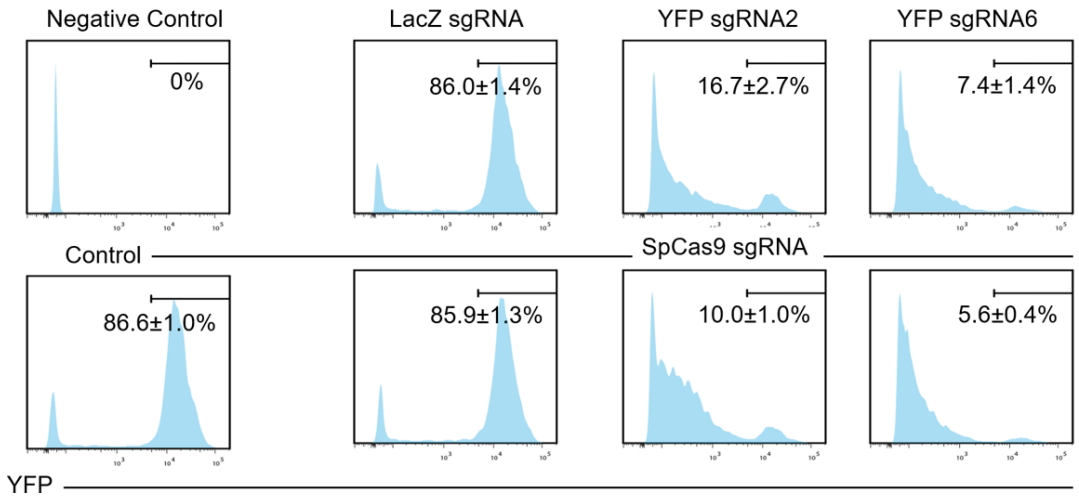

Figure 3.10 Flow cytometry demonstration plot.

Representative flow cytometry plots of HEK293A-YFP cells receiving CRISPR/Cas plasmids (upper panels) or Kamikaze-CRISPR/Cas plasmids (lower panels).

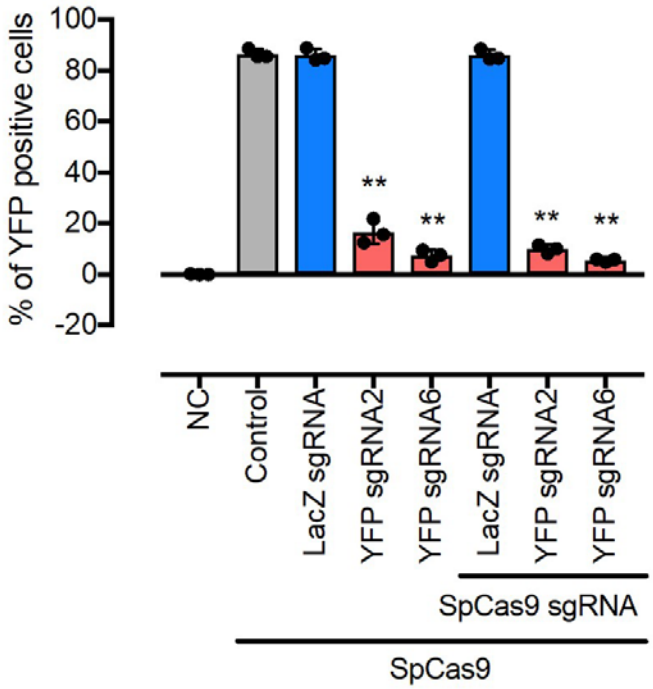

Figure 3.11 Flow cytometry analysis.

Data are presented as mean ± SEM for three independent replicates. Statistical analysis between groups was performed using one-way ANOVA followed by multiple comparisons test (**$p < 0.001$, compared with control) NC, using HEK293A cells as negative control. Control, HEK293A-YFP cells without transfection. Cells were collected at day 10 post transfection.

3.2.3 Kamikaze-CRISPR/Cas reduced potential off-target *in vitro*

To assess the off-target effect of Kamikaze CRISPR/Cas, *in silico* prediction tool Cas-OFFinder was used, and no off-target sites for YFP sgRNA and SpCas9 sgRNA were identified. An alternative method was introduced to verify if Kamikaze CRISPR/Cas could reduce potential off-target. To this end, we created a series of putative off-target sites by introducing single-nucleotide mismatch along YFP sgRNA6 sequence and compared the editing activity of non-kamikaze and kamikaze-CRISPR/Cas systems (Figure 3.12 A). Almost all guide RNAs with single-nucleotide mismatches (in kamikaze and non-kamikaze) displayed editing activity at day 10 (Figure 3.12 B), with the highest editing introduced by a mismatch located distal to the PAM (M18) at day 10. A statistically significant reduction in editing activity at M2-M8 and M20 mutant guide RNA positions was observed with our kamikaze-CRISPR/Cas system compared to the non-kamikaze CRISPR/Cas system (Figure 3.12 C).

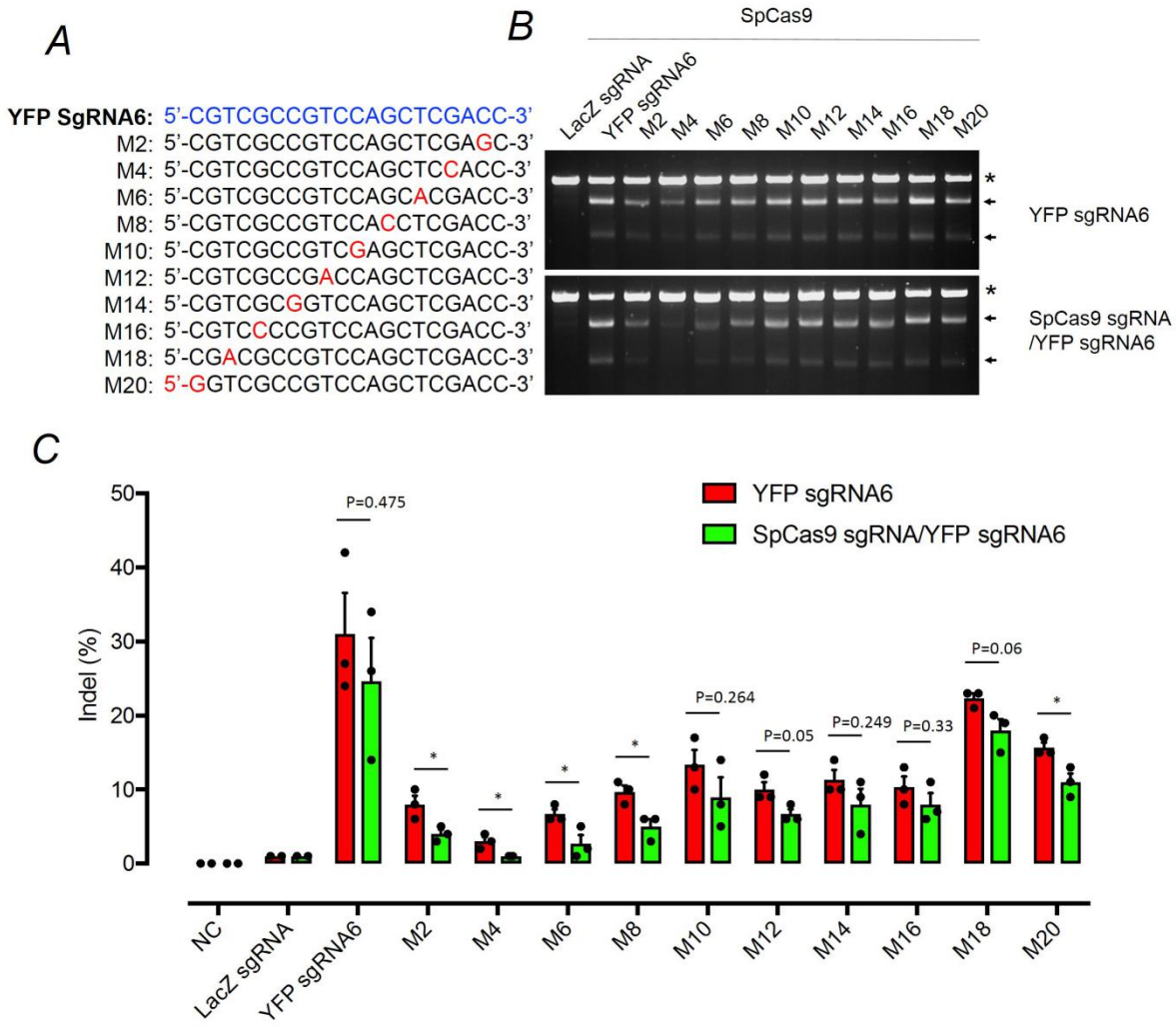

Figure 3.12 Off-target analysis *in vitro*.

(A) Sequences of single-nucleotide mismatch containing *YFP*-targeting guide RNAs. (B) CRISPR/Cas9 editing activity of these single-nucleotide mismatches at day 10 after transfection by T7E1 assay. (C) Difference in mismatch related CRISPR editing between kamikaze *YFP*-targeting CRISPR/Cas system and non-kamikaze *YFP*-targeting CRISPR/Cas system, by analysis of indel using ICE tool. Mean ± SEM for three independent replicates (*p<0.05).

3.2.4 Time course of SpCas9 expression *in vivo*

To test whether SpCas9 expression would be reduced in retinas receiving AAV2-kamikaze, initially we tested SpCas9 protein expression by western blot analysis, but

SpCas9 protein was undetectable in all three groups (Figure 3.13).

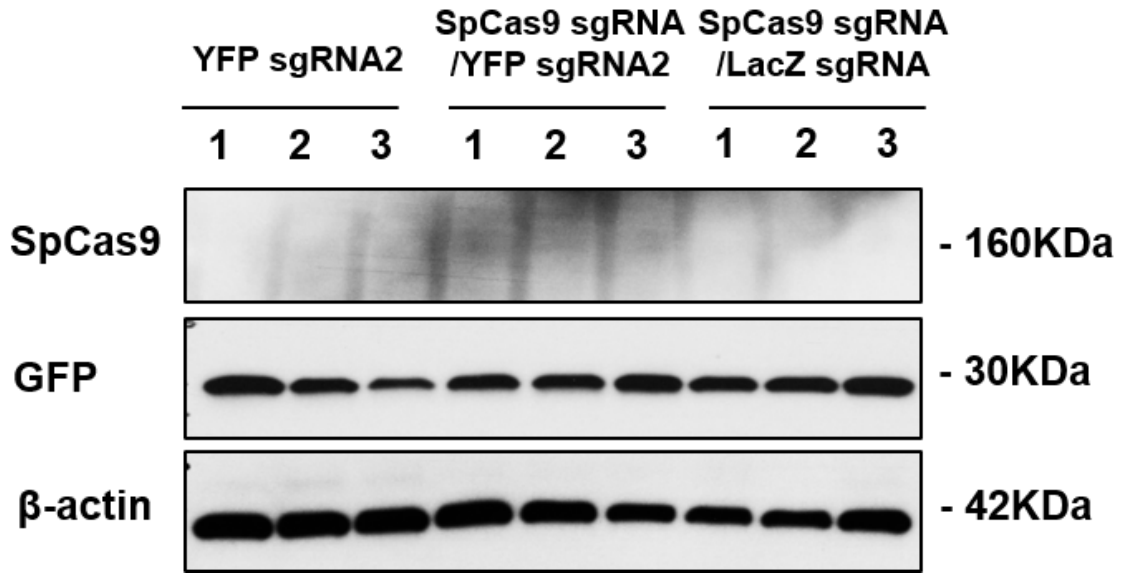

Figure 3.13 Western blot of SpCas9 protein expression *in vivo*.

No expression of SpCas9 protein was detected in retinas receiving AAV2-YFP sgRNA2, AAV2-SpCas9 sgRNA/YFP sgRNA2, AAV2-SpCas9 sgRNA/LacZ sgRNA, while YFP protein expression was detected using GFP (B-2). (Protein in each group was prepared from three retinas pooled together).

Next, we tested the *SpCas9* gene perturbation in the retinas by qPCR instead. A time-course analysis (Figure 3.14) showed that SpCas9 mRNA levels in retinas treated with AAV2-YFP sgRNA2 were stable for 4 weeks after viral injection before increasing and fluctuating, while the SpCas9 mRNA level in retinas treated with AAV2-SpCas9 sgRNA/YFP sgRNA2 remained low for 6 weeks and increased at week 8. At most time points, SpCas9 mRNA was lower (week 3, 4, 5, 6, 8) or similar (week 1, 2) in retinas treated with AAV2-mediated-*YFP/SpCas9*-targeting CRISPR/Cas compared to those treated with *YFP*-targeting CRISPR/Cas alone. At week 8, the difference in SpCas9 expression was statistically significant between these two groups ($p<0.05$).

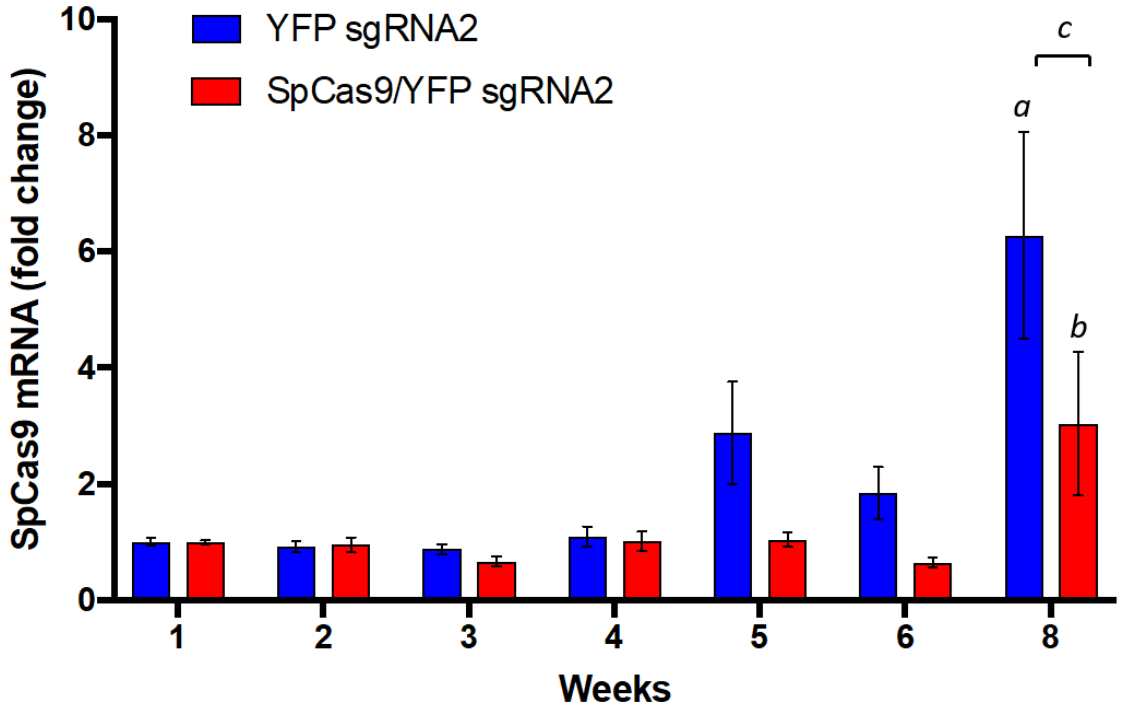

Figure 3.14 Time course of SpCas9 mRNA expression in the mouse retina.

SpCas9 mRNA was isolated from C57BL/6 mice mouse retinas receiving AAV2-SpCas9 sgRNA/YFP sgRNA2 or AAV2-YFP sgRNA2 at 1, 2, 3, 4, 5, 6 and 8 weeks after intravitreal injection. Relative fold change of SpCas9 expression was normalized by week 1 in each treatment group. Representative data are shown for 5-6 retinas per group/time point and expressed as mean ± SEM. Statistical analysis between groups was performed using two-way ANOVA followed by Sidak's multiple comparisons test. (a, YFP sgRNA2: 1 vs 8 weeks, p=0.002. b, SpCas9/YFP sgRNA: 1 vs 8 weeks, p=0.7043. c, YFP sgRNA2 vs SpCas9/YFP sgRNA, p=0.0142).

3.2.5 YFP knockout quantification *in vivo*

To evaluate whether the reduction of SpCas9 expression by the kamikaze-CRISPR/Cas construct would compromise on-target editing (YFP disruption) efficiency, Thy1-YFP mice received a single intravitreal injection of a dual viral suspension of AAV2-SpCas9 along with the *YFP*-targeting kamikaze-CRISPR/Cas construct (AAV2-SpCas9 sgRNA/YFP sgRNA), the *LacZ*-targeting kamikaze- CRISPR/Cas construct (AAV2-SpCas9

sgRNA/LacZ sgRNA) or a single *YFP*-targeting CRISPR/Cas construct (AAV2-YFP sgRNA). The timeline for *in vivo* YFP knockout study is shown in Figure 3.15.

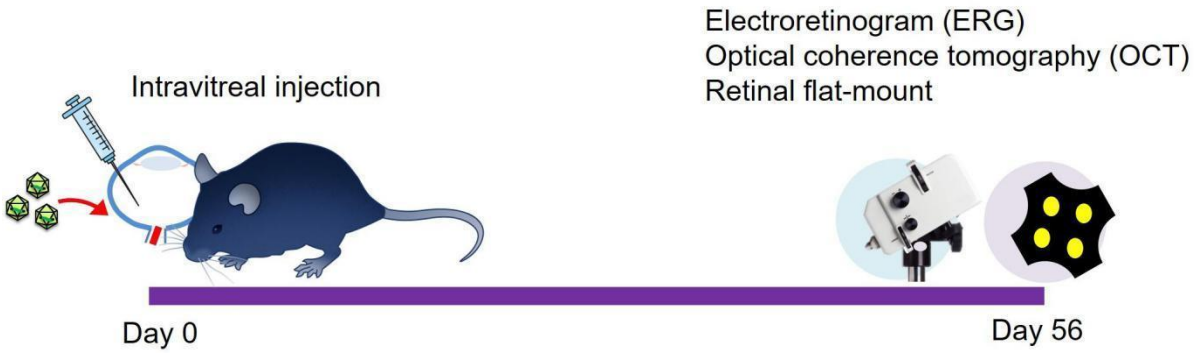

Figure 3.15 Timeline for YFP knockout *in vivo*.

Each Thy1-YFP mouse received an intravitreal injection of 1 µL dual-viral suspension ($2.5x10^9$ vg AAV2-SpCas9 and $2.5x10^9$ vg AAV2-sgRNA) in the left eye, and the contralateral right eye (no injection) was used as control. Animal groups are listed in Appendix 4.

Eight weeks following injection, retinal flat mount images revealed a lower number of YFP-positive cells among mCherry-expressing cells in mice treated with AAV2-SpCas9 sgRNA/YFP sgRNA or AAV2-YFP sgRNA compared to AAV2-SpCas9 sgRNA/LacZ sgRNA control (Figure 3.16) or contralateral non-injected control eyes. A marked decrease in the number of YFP-positive cells in the inner retina was found in both kamikaze and non-kamikaze *YFP*-targeting CRISPR/Cas-treated eyes compared to controls upon quantification of YFP disruption. Specifically, the proportion of retinal YFP (-) /mCherry (+) cells was reduced to 5.5±1.4% in AAV2-SpCas9 sgRNA/YFP sgRNA2-treated retina and 7.3±1.3% in AAV2-YFP sgRNA2-treated retina, compared with 38.2±1.7% in AAV2-SpCas9 sgRNA/LacZ sgRNA treated eyes. Overall there was an 85.5% (95% CI: 78.4-92.6) and 80.9% (95% CI: 74.3-87.5) reduction in YFP-positive cells in AAV2-SpCas9 sgRNA/YFP sgRNA- and AAV2-YFP sgRNA2-treated retinas, respectively, compared to AAV2-SpCas9 sgRNA/LacZ sgRNA-treated eyes (Figure 3.17). No significant difference in YFP disruption was found between AAV2-YFP sgRNA2- and AAV2-SpCas9 sgRNA/YFP sgRNA2-treated retinas (p=0.62; Figure 3.17). Similar results were found

using an alternate *YFP*-targeting sgRNA (YFP sgRNA6), where the proportion of retinal YFP (-) /mCherry (+) was 17.0±1.3% in AAV2-SpCas9 sgRNA/YFP sgRNA6-treated retina and 20.6±1.2% in AAV2-YFP sgRNA6-treated retina, compared to 40.8±2.0% AAV2-SpCas9 sgRNA/LacZ sgRNA-treated eyes (Figure 3.18). This represents a relative reduction of 49.5% (95% CI: 43.5-55.5) and 58.3% (95% CI: 56.4-62.0) in AAV2-SpCas9 sgRNA/YFP sgRNA6- and AAV2-YFP sgRNA6-treated retinas compared to those that had received AAV2-SpCas9 sgRNA/LacZ sgRNA, respectively (Figure 3.18).

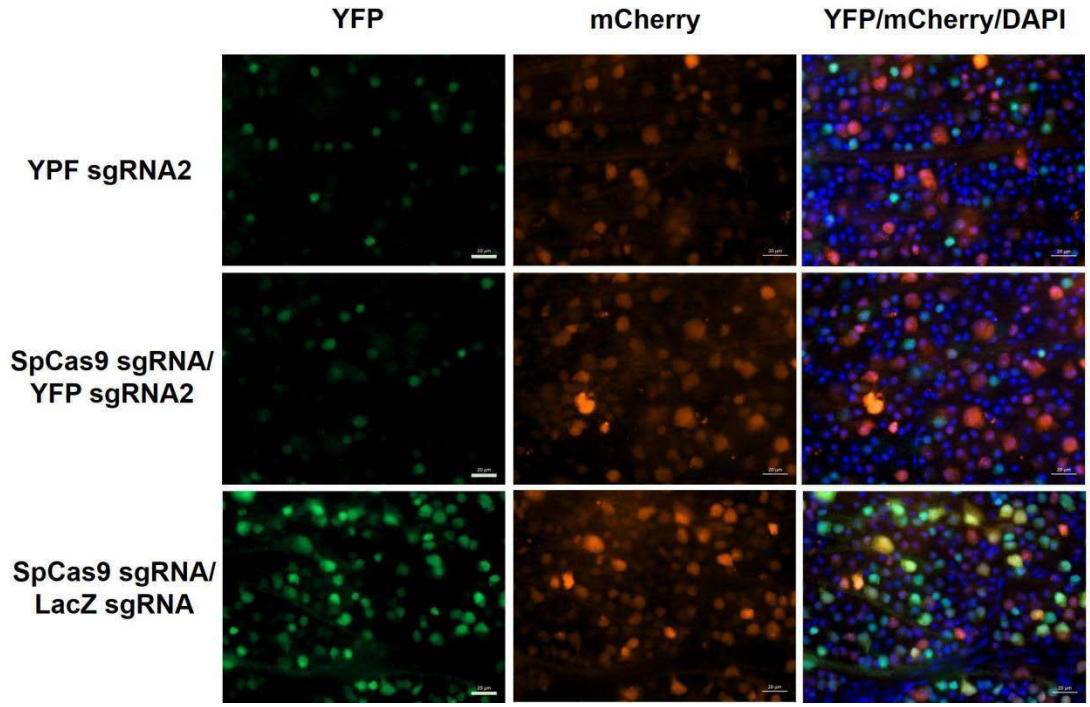

Figure 3.16 High magnification of retinal flat-mount images showing YFP disruption *in vivo*.

Scale bar: 20 µm.

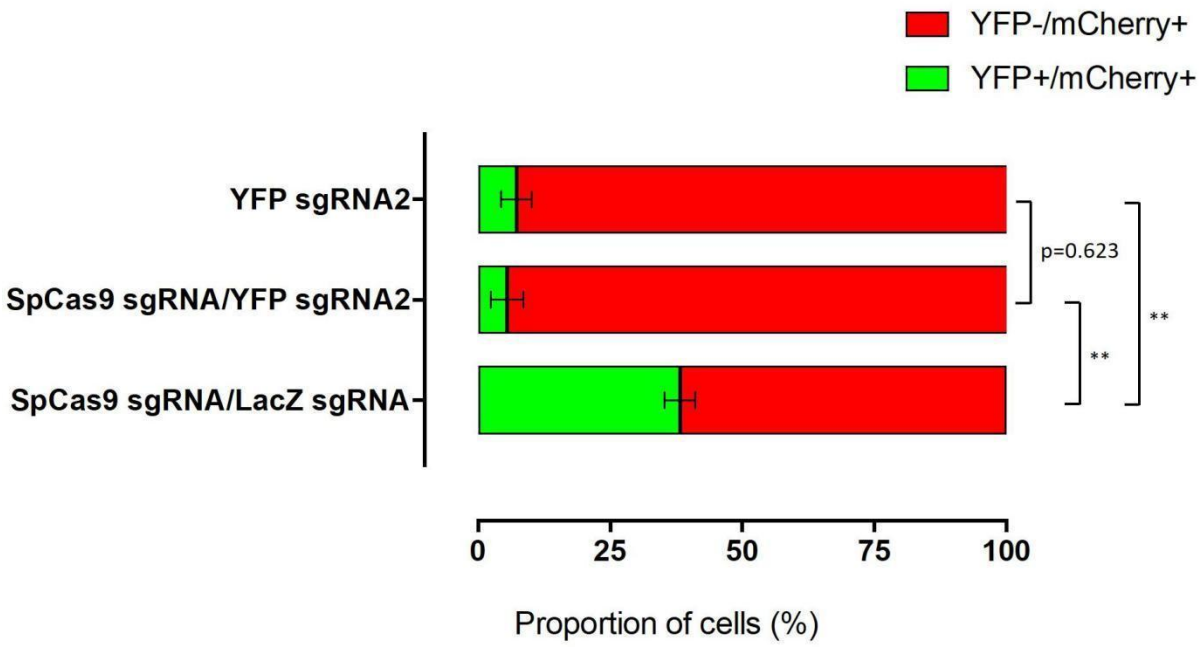

Figure 3.17 Quantification of YFP disruption in the retina (YFP sgRNA2).

Differences were found in YFP expression following AAV2-mediated delivery of SpCas9 sgRNA/YFP sgRNA2 (n=5), YFP sgRNA2 (n=5) or SpCas9 sgRNA/LacZ sgRNA (n=3). Mean ± SEM for 3-5 independent replicates. Statistical analysis between groups was performed using one-way ANOVA followed by Tukey's multiple comparisons test (**$p < 0.001$).

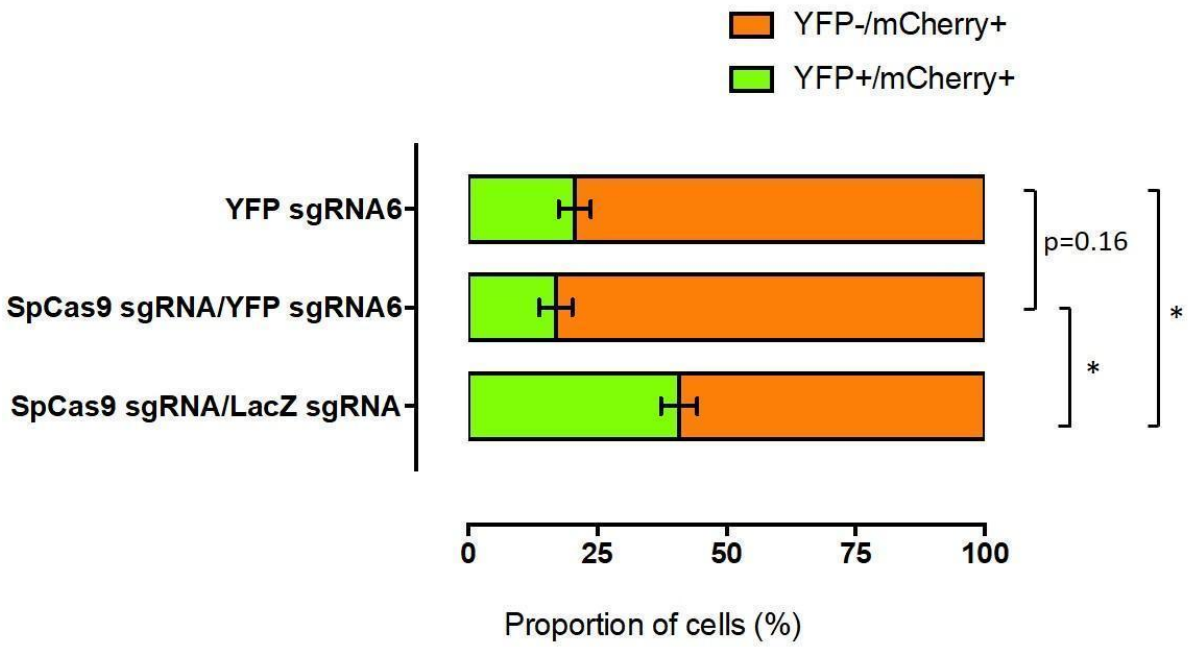

Figure 3.18 Quantification of YFP disruption in the retina (YFP sgRNA6).

Differences were found in YFP expression following AAV2-mediated delivery of SpCas9 sgRNA/YFP sgRNA6 (n=6), YFP sgRNA6 (n=6) or SpCas9 sgRNA/LacZ sgRNA (n=3). Mean ± SEM for 3-5 independent replicates. Representative data are shown for 3-5 independent replicates and expressed as mean ± SEM. Statistical analysis between groups was performed using one-way ANOVA followed by Tukey's multiple comparisons test (*p<0.05).

3.2.6 Kamikaze CRISPR/Cas didn't affect retinal structure or thickness by OCT

To evaluate whether our "kamikaze"-CRISPR/Cas construct would affect retinal structure or retinal thickness, OCT was performed at 8 weeks after intravitreal injection in the Thy1-YFP mouse. The thickness of retinal nerve fiber layer and whole retina was measured manually as illustrated in Figure 3.19 A. OCT analysis suggested that none of the CRISPR/Cas constructs negatively impacted retinal structure, and there were no significant differences in the thickness of the retinal nerve fiber layer or total retinal thickness between viral-injected eyes and the contralateral non-injected control eyes of all three groups (Figure 3.19 B, C).

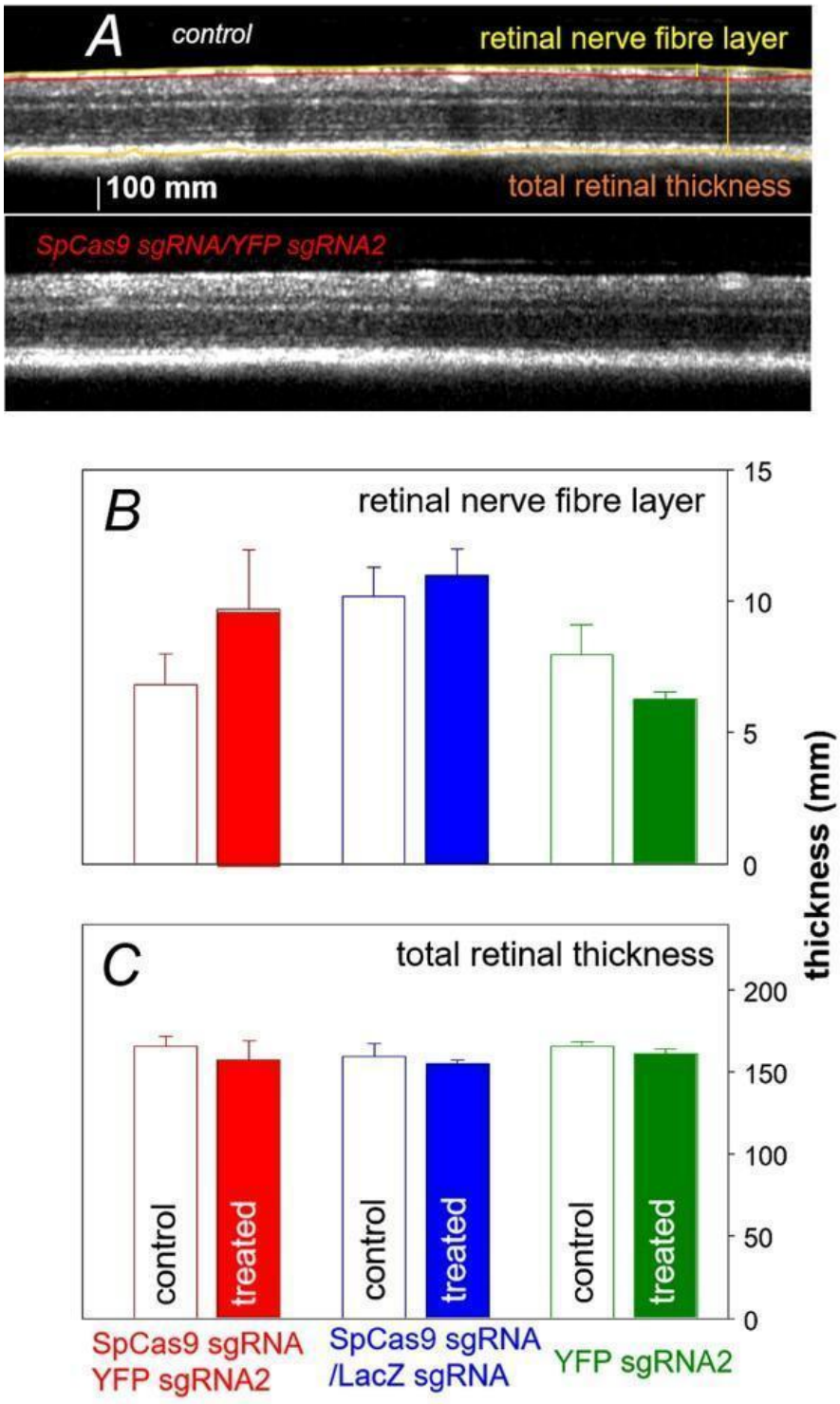

Figure 3.19 Morphological measurement and analysis in mouse retinas following viral injection.

Representative OCT images illustrating measurement of retinal nerve fiber layer thickness and total retinal thickness (A). *Scale bar, 100 mm*. Group average (± SEM) retinal nerve

fiber layer thickness (B) for SpCas9 sgRNA/YFP sgRNA2 treated (filled red, n=4) and their contralateral controls (unfilled red, n=4), SpCas9 sgRNA/LacZ sgRNA treated (filled blue, n=4) and their contralateral controls (unfilled blue, n=4) and YFP sgRNA2 treated (filled green, n=5) and their contralateral controls (unfilled green, n=5). Total retinal thickness (C). Statistical analysis between injected and control eyes was performed using two-tailed Student t-test (*p<0.05).

3.2.7 Functional test of retina following AAV-mediated CRISPR/Cas editing by ERG

To investigate whether our “kamikaze”-CRISPR/Cas constructs would affect retinal function, ERG was performed at 8 weeks after intravitreal injection of viral suspensions in Thy1-YFP mouse. Group averaged waveforms generated from eyes injected with *YFP*-targeting kamikaze-CRISPR/Cas constructs (AAV2-SpCas9 sgRNA/YFP sgRNA2, Figure 3.20 A and B) and non-kamikaze *YFP*-targeting CRISPR/Cas constructs (AAV2-YFP sgRNA2, Figure 3.20 E and F) were lower compared to those from contralateral control eyes, while ERG from *LacZ*-targeting kamikaze-CRISPR/Cas construct (AAV2-SpCas9 sgRNA/LacZ sgRNA, Figure 3.20 C and D) treated eyes weren’t affected. Retinal function was also decreased in AAV2-SpCas9 sgRNA/YFP sgRNA6 and AAV2-YFP sgRNA6-treated mice. Details of ERG assessment for each group are shown in Figure 3.21-23 (YFP sgRNA2) and Figure 3.24-26 (YFP sgRNA6). Data are presented as the mean ± SEM. Statistical analysis between groups was performed using two-tailed Student’s t-test (*p<0.05, **p<0.01, ***p<0.001).

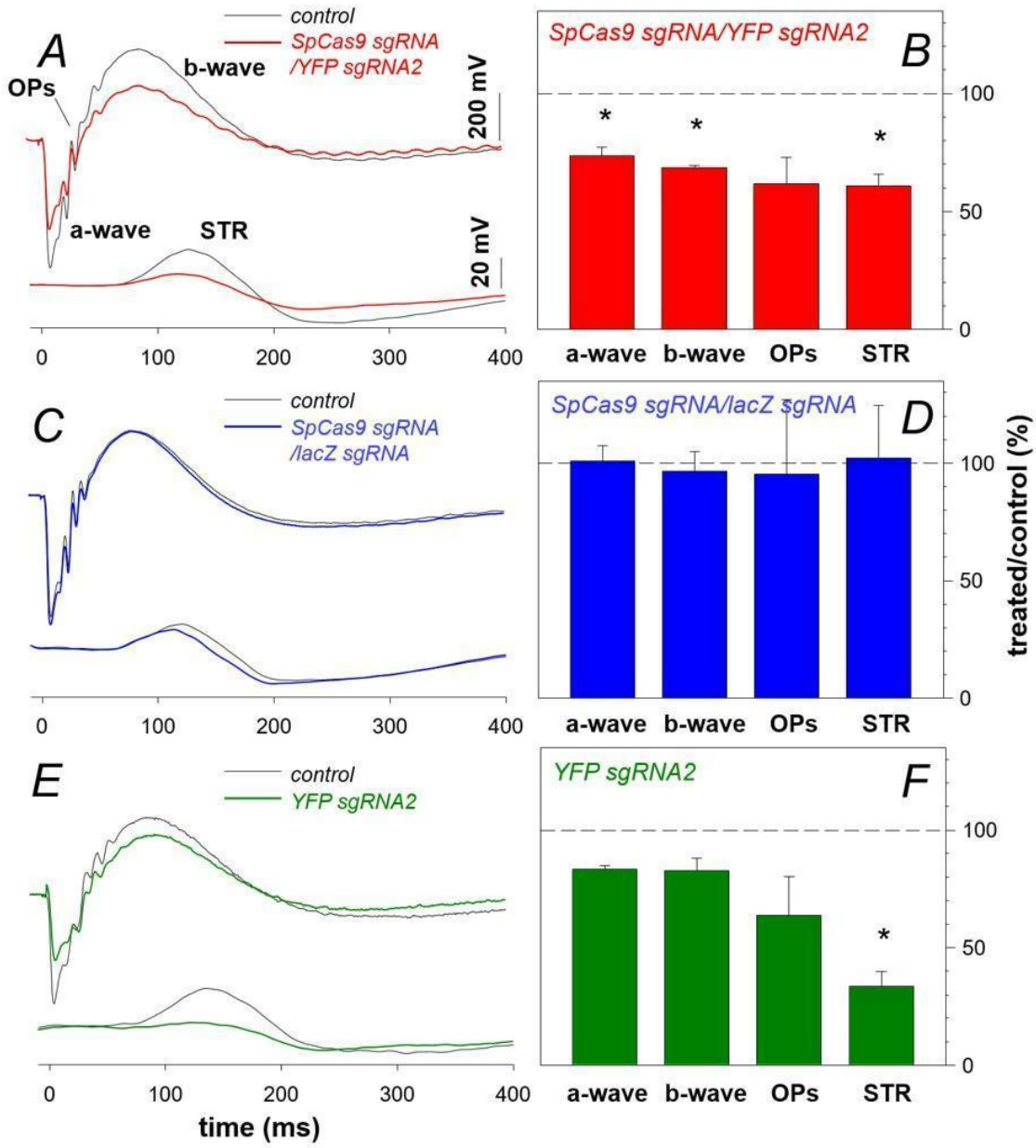

Figure 3.20 Effect of AAV2-mediated CRISPR/Cas administration on retinal function. Averaged ERG waveforms at selected intensities for control (black traces) and SpCas9 sgRNA/YFP sgRNA2 (n=4, red traces; A), SpCas9 sgRNA/LacZ sgRNA (n=4, blue traces; C) and YFP sgRNA2 (n=5, green traces; E) injected eyes. Group average (± SEM) photoreceptoral (a-wave), bipolar cell (b-wave), amacrine cell (oscillatory potentials, OPs) and ganglion cell (scotopic threshold response, STR) amplitude relative to contralateral control eyes (%) for each group (B, D and F).

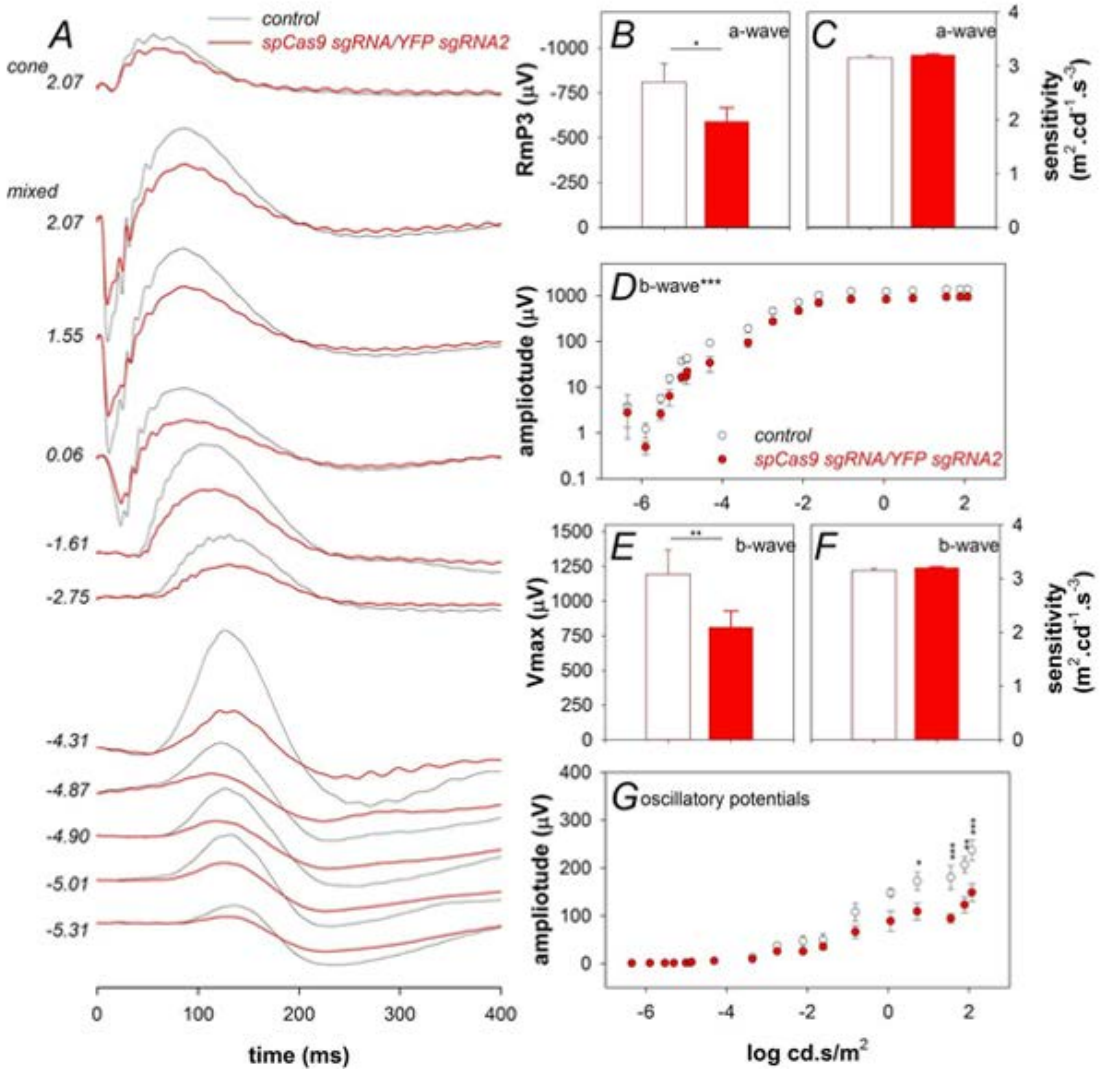

Figure 3.21 SpCas9 sgRNA/YFP sgRNA2 decreased retinal function.

(A) Averaged ERG waveforms at selected intensities for control (n=4, black) and treated eyes (n=4, red). (B) Groups average photoreceptoral (a-wave) saturated amplitude for contralateral control (unfilled) and treated eyes (filled). (C) Photoreceptoral sensitivity to light. (D) Intensity response characteristics across the entire range of intensities. (E) Bipolar cell amplitude. (F) Bipolar cell sensitivity to light. (G) Inner retinal amacrine cell-mediated response (oscillatory potentials).

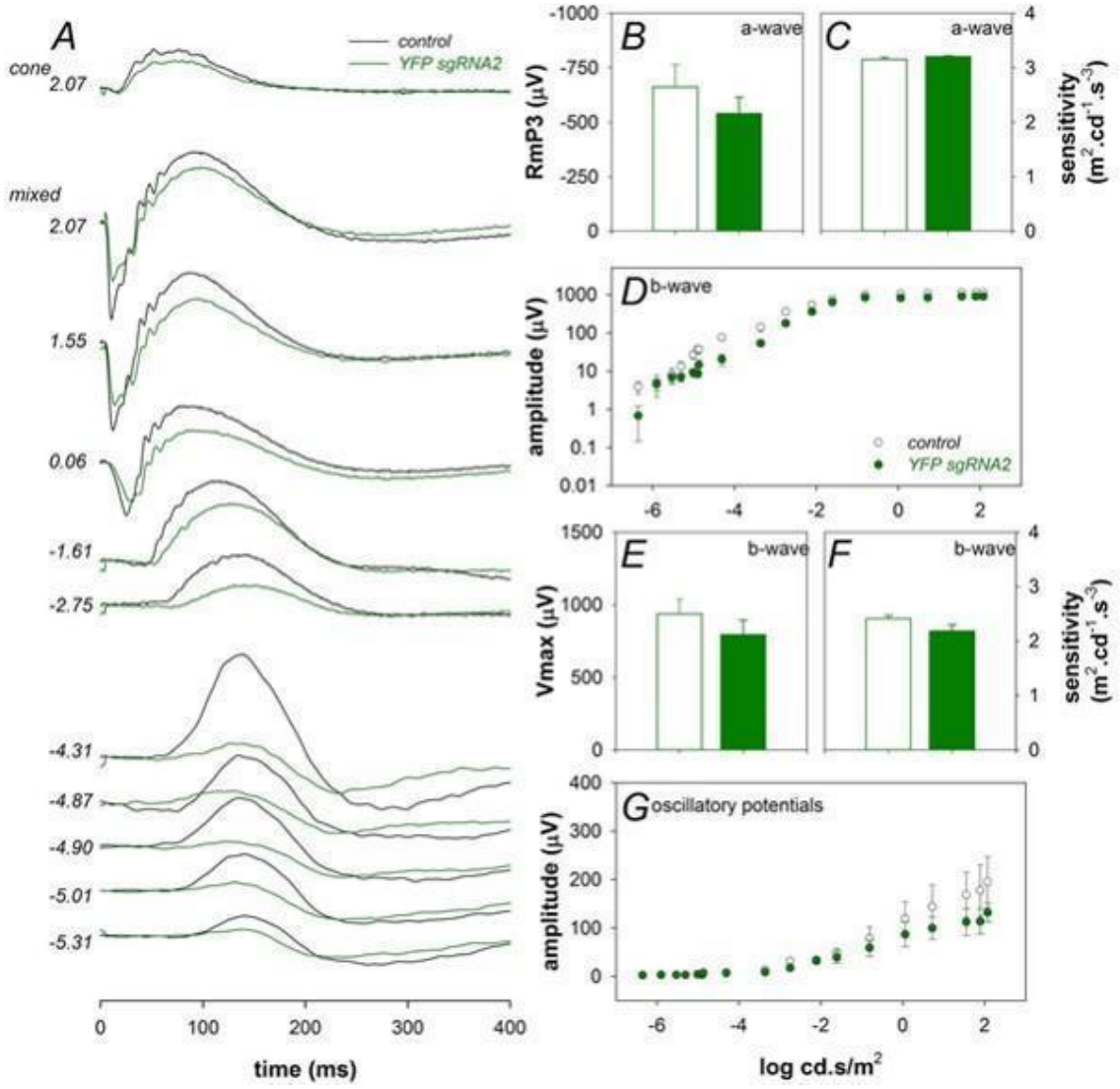

Figure 3.22 YFP sgRNA2 alone affected inner retinal function.

(A) Averaged ERG waveforms at selected intensities for control (n=5, black) and treated eyes (n=5, green). (B) Groups average (±SEM) photoreceptoral (a-wave) saturated amplitude for contralateral control (unfilled) and treated eyes (filled). (C) Photoreceptoral sensitivity to light. (D) Intensity response characteristics across the entire range of intensities. (E) Bipolar cell amplitude. (F) Bipolar cell sensitivity to light. (G) Inner retinal amacrine cell-mediated response (oscillatory potentials).

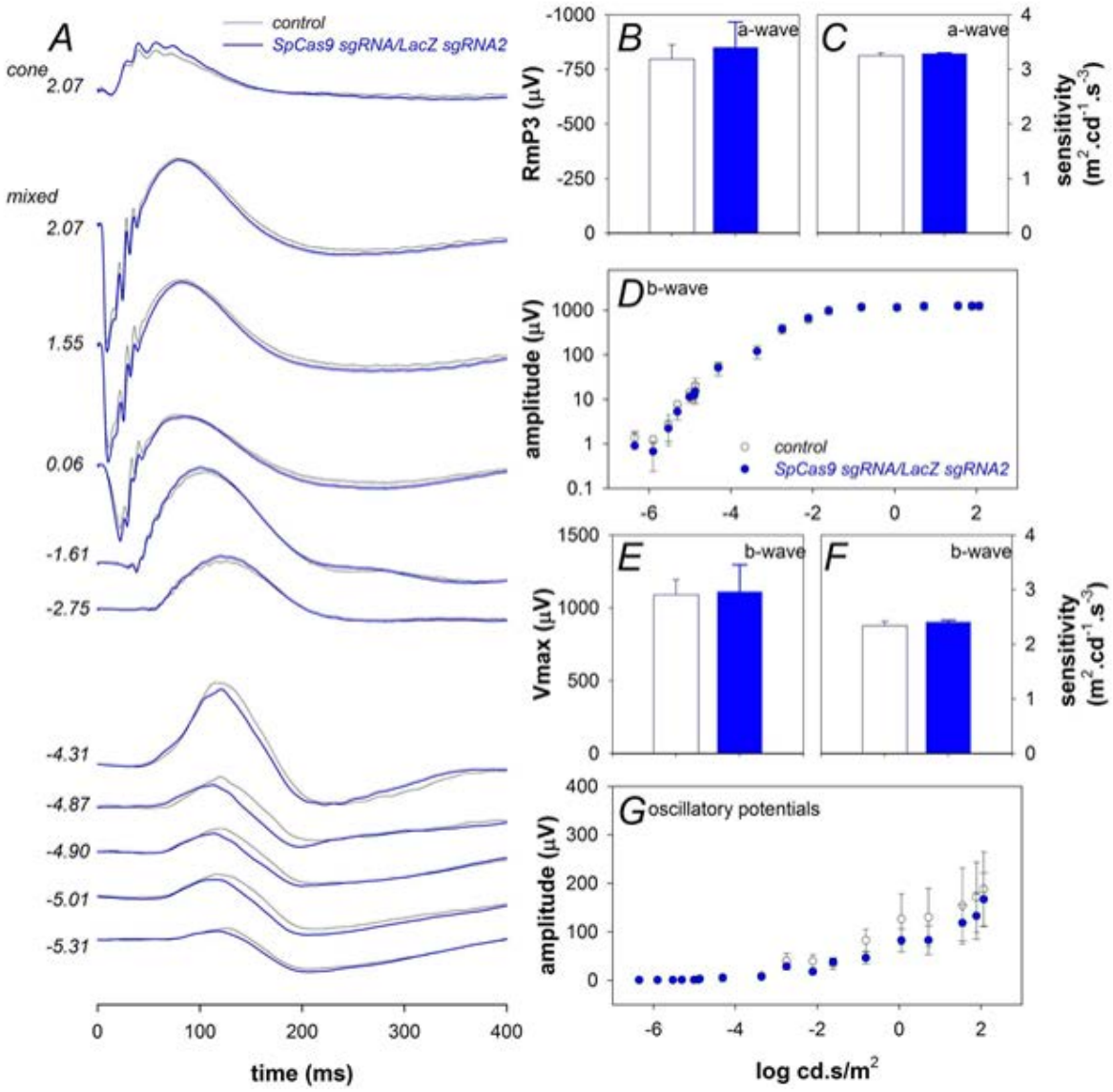

Figure 3.23 SpCas9 sgRNA/LacZ sgRNA did not affect retinal function.

(A) Averaged ERG waveforms at selected intensities for control (n=3, black) and treated eyes (n=3, blue). (B) Groups average (±SEM) photoreceptoral (a-wave) saturated amplitude for contralateral control (unfilled) and treated eyes (filled). (C) Photoreceptoral sensitivity to light. (D) Intensity response characteristics across the entire range of intensities. (E) Bipolar cell amplitude. (F) Bipolar cell sensitivity to light. (G) Inner retinal amacrine cell-mediated response (oscillatory potentials).

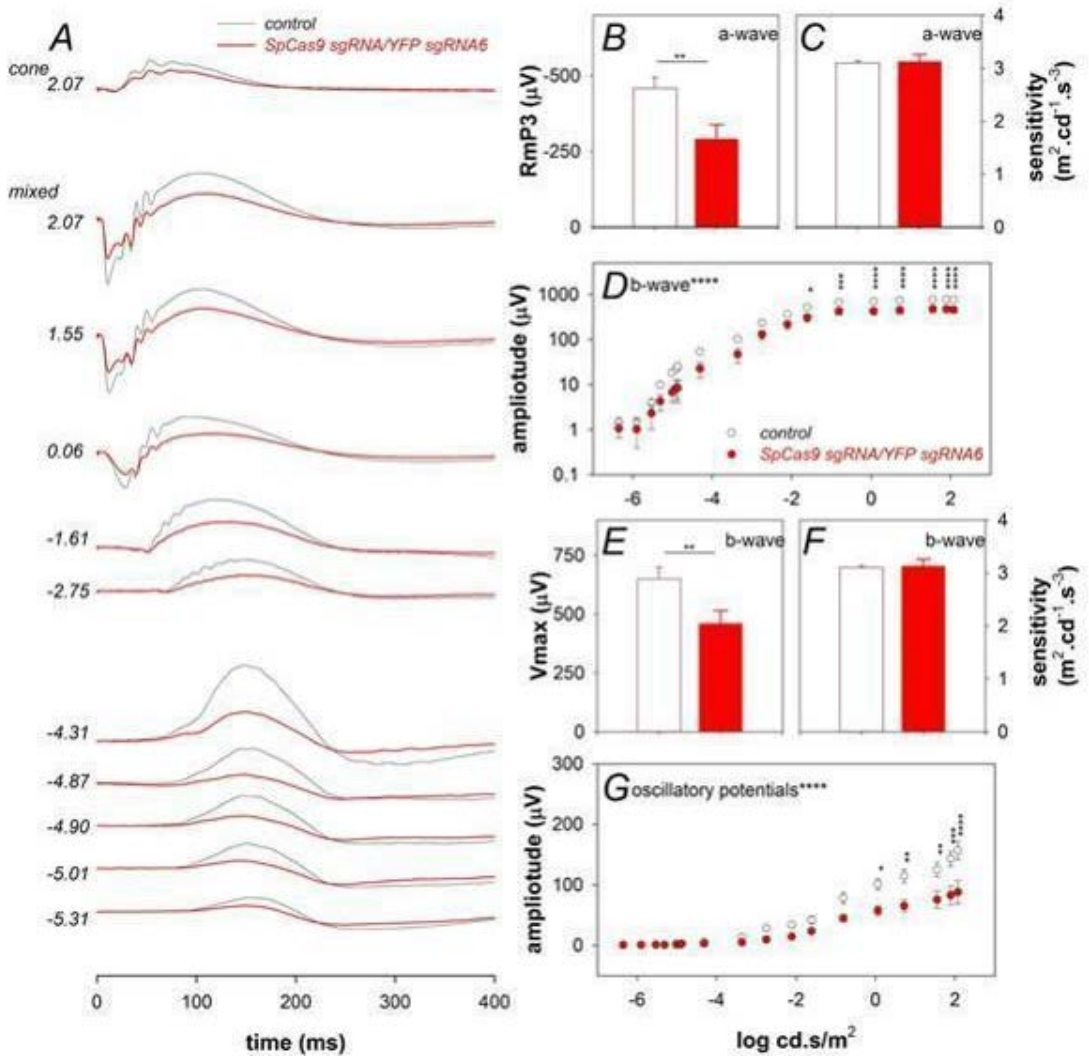

Figure 3.24 SpCas9 sgRNA/YFP sgRNA6 decreased retinal function.

(A) Averaged ERG waveforms at selected intensities for control (n=10, black) and treated eyes (n=10, red). (B) Groups average (±SEM) photoreceptoral (a-wave) saturated amplitude for contralateral control (unfilled) and treated eyes (filled). (C) Photoreceptoral sensitivity to light. (D) Intensity response characteristics across the entire range of intensities. (E) Bipolar cell amplitude. (F) Bipolar cell sensitivity to light. (G) Inner retinal amacrine cell-mediated response (oscillatory potentials). Data are expressed as the mean ± SEM. Statistical analysis between groups was performed using two-tailed Student's t-test. Asterisks denote significance *p<0.05, **p<0.01, ***p<0.001, ****p<0.0001.

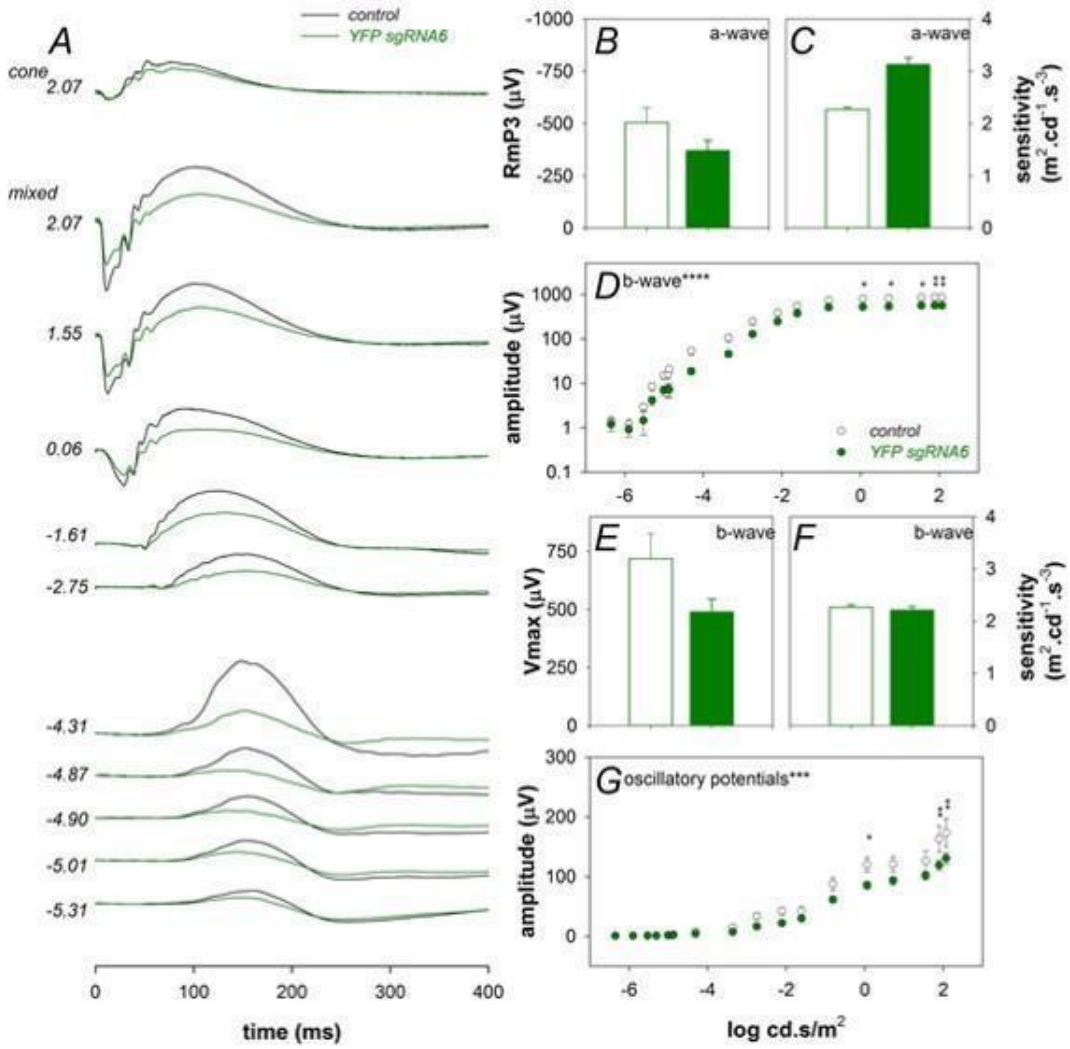

Figure 3.25 YFP sgRNA6 alone affected inner retinal function.

(A) Averaged ERG waveforms at selected intensities for control (n=8, black) and treated eyes (n=8, green). (B) Groups average photoreceptoral (a-wave) saturated amplitude for contralateral control (unfilled) and treated eyes (filled). (C) Photoreceptoral sensitivity to light. (D) Intensity response characteristics across the entire range of intensities. (E) Bipolar cell amplitude. (F) Bipolar cell sensitivity to light. (G) Inner retinal amacrine cell-mediated response (oscillatory potentials). Data are expressed as the mean ± SEM. Statistical analysis between groups was performed using two-tailed Student's t-test. Asterisks denote significance. *p<0.05, **p<0.01.

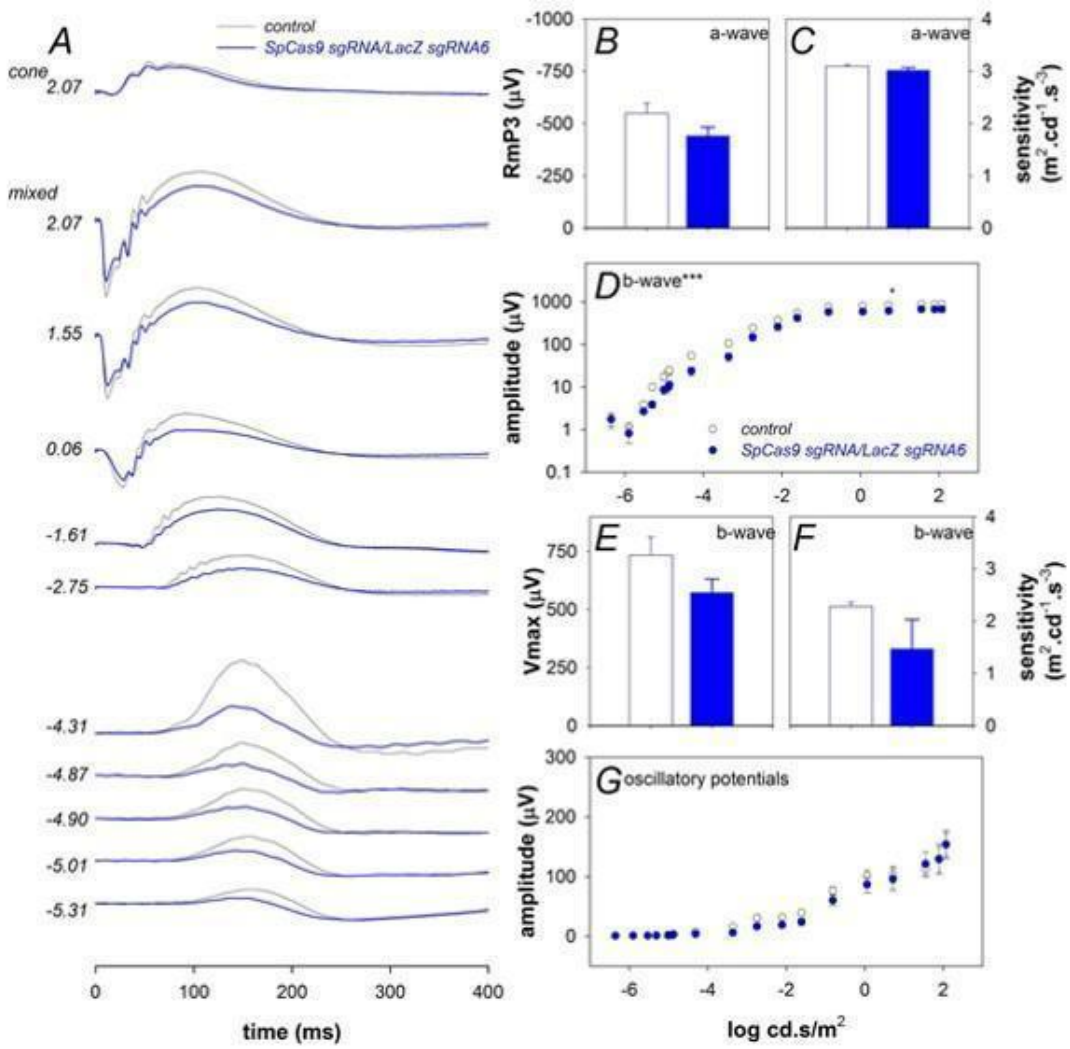

Figure 3.26 SpCas9 sgRNA/LacZ sgRNA did not affect retinal function.

(A) Averaged ERG waveforms at selected intensities for control (n=8, black) and treated eyes (n=8, blue). (B) Groups average photoreceptoral (a-wave) saturated amplitude for contralateral control (unfilled) and treated eyes (filled). (C) Photoreceptoral sensitivity to light. (D) Intensity response characteristics across the entire range of intensities. (E) Bipolar cell amplitude. (F) Bipolar cell sensitivity to light. (G) Inner retinal amacrine cell-mediated response (oscillatory potentials). Data are expressed as the mean ± SEM. Statistical analysis between groups was performed using two-tailed Student's t-test.

3.2.8 Kamikaze CRISPR/Cas didn't aggravate off-target effect *in vivo*

Whole-exome sequencing from two pairs of retina samples (eyes receiving AAV2-SpCas9-YFP sgRNA6 and contralateral control eyes) showed no off-target effect of AAV2-SpCas9 sgRNA-YFP sgRNA6 in the protein-coding region of mouse genome. To be more specific, 303 indel variants were detected in all four retina samples and 120 indels were removed as they were shared between treated retinas and contralateral control retinas. About 79 indels were unique in treated retinas and these were removed due to a match in dbSNP and/or were homozygous. When searching for putative off-target sequences around the remaining indels in the reference genome, we did not find any indels that could be associated with off-target effects of our kamikaze-CRISPR/Cas system.

3.3 Discussion

This study was based on our previous work using AAV2-mediated CRISPR/Cas for gene editing in mouse retina. However, with this viral delivery system, active endonucleases will remain in the retina for an extended period, which may cause deleterious effects including off-target effects or genotoxicity. Ways to reduce off-target cleavage include improved guide-RNA design[33,90], or modification of Cas9 enzymes[91,92], which may reduce editing efficiency and does not address the issue of Cas9 accumulation. In particular, it poses a significant challenge to the clinical application of CRISPR/Cas9 in genetic retinal diseases, as the natural barriers in the retina aggravate accumulation of SpCas9.

Our approach was to employ a self-destructive CRISPR/Cas system that disrupts the CRISPR/Cas enzyme itself after the active protein has been expressed. Our kamikaze-CRISPR/Cas system can significantly reduce SpCas9 expression, without dramatically compromising the efficiency of on-target editing. As *YFP* sequence did not exist endogenously in the mouse genome, we used an alternative method to indirectly test whether our kamikaze CRISPR could reduce potential off-target *in vitro*. Previous studies showed that potential off-target cleavage activity occurred on DNA sequence with a few base pair mismatches in the PAM-distal part of the sgRNA-guiding sequence[127,129]. Our

results are consistent with previous findings that clear CRISPR cleavage existed using sgRNAs bearing a single nucleotide mismatch in both conventional CRISPR and Kamikaze CRISPR, with less editing detected in Kamikaze group. Our results showed that Kamikaze CRISPR could reduce mismatch-related editing therefore reducing potential off-target *in vitro*, probably due to the reduced expression of Cas9.

As a proof of concept study, we used YFP transgenic mice as a robust, easy quantifiable tool to explore this self-destructive CRISPR/Cas editing system. An endogenous ocular disease-specific gene in preclinical *in vivo* study could later be tested with our kamikaze CRISPR/Cas system for broader application. At the start of this project, there were no published papers employing this self-targeting approach to reduce SpCas9 expression. Similar strategies have now been tested by Merienne and colleagues[98]. They demonstrated that progressively inactivating the nuclease using a Cas9 self-inactivating editing system resulted in a lower frequency of off-target cleavage of *HTT* (mutant huntingtin responsible for Huntington's disease) in human iPSCs-derived neurons *in vitro* and in mouse brains via lentiviral-mediated *in vivo* delivery. Two groups[22,99] have also tested similar self-restrictive CRISPR/Cas systems *in vitro*. A recent study described a SaCas9-based self-deleting AAV system in the liver[97]. While these studies have shown the feasibility of a self-limiting CRISPR/Cas system, our study highlights the effectiveness of an AAV-mediated self-destructive CRISPR/Cas system for *in vivo* genome editing in the retina.

We observed a difference between *in vitro* and *in vivo* models in the efficiency of YFP and SpCas9 disruption with our Kamikaze-CRISPR/Cas9 constructs. The reduced efficiency may be due to the difference in promoters and delivery systems used *in vitro* and *in vivo*. A ubiquitous cytomegalovirus (CMV) promoter was used in the *in vitro* test to ensure strong expression of SpCas9 in cells, while MeCP2 promoter was used in the *in vivo* study to achieve neuron-specific expression in the retina. A dual AAV2 vector system was employed to deliver the kamikaze CRISPR/Cas construct into the retina. The expression of the CRISPR/Cas9 machinery requires the receipt of both Cas9 and sgRNA from two

separate viral vectors, which may significantly reduce editing efficiency. Cas9 orthologs such as SaCas9[130] or CjCas9[29] delivered via a single vector system may provide better *in vivo* editing efficiency, but dual-vector systems may still be required for mutation correction as they enable delivery of donor templates and appropriate promoter elements.

An unexpected reduction in retinal function was observed 8 weeks after injection of AAV2-SpCas9 sgRNA/YFP sgRNA2 or AAV2-YFP sRNA2. Interestingly, retinal function was unaffected in mice treated with AAV2-SpCas9 sgRNA/LacZ sgRNA, therefore, deficits in retinal function are not related to the SpCas9 sgRNA construct per se but may be related to either off-target effects of *YFP*-targeting sgRNA or accumulation of non-functional fluorescent proteins resulting from CRISPR/Cas9 editing. To further explore this possibility, we first tested a different YFP sgRNA (sgRNA6 which targets another region of the *YFP* sequence) *in vivo*. However, a significant decrease in retinal function was still present in AAV2-SpCas9 sgRNA/YFP sgRNA6- and AAV2-YFP sgRNA6-treated mice. We then searched the mouse genome for potential off-target sites for two YFP sgRNAs and SpCas9 sgRNA by *in silico* prediction (Cas-OFFinder) and performed WES on the treated mouse retina. No significant candidate genes for the off-target sites were found by *in silico* prediction or by WES. Although off-target analysis through whole-exome sequencing may overlook off-target cleavage in the intron and intergenic region, it is unlikely that the potential off-targets in these regions would cause functional changes in the mouse retina, as the protein-coding areas were not affected. Note that it is difficult to accurately and directly identify off-target *in vivo* using existing off-target detection methods. Most *in vivo* CRISPR studies only applied *in silico or in vitro off-target* discovery methods to partly characterize off-target events. Recently developed *in vivo* off-target detection strategies such as VIVO[88] or DISCOVER-Seq[89] methods could be applied in future *in vivo* studies to provide unbiased and more accurate detection of genome editing off-targets.

We hypothesize that the reduction of retinal function came from accumulation of mutated fluorescent proteins. Although fluorescence proteins such as GFP and YFP have been widely used in neuroscience research[33], accumulation of non-functional proteins resulting

from on-target deletions (indel) may have a deleterious effect on retinal protein homeostasis[34]. This could be confirmed through overexpression of a nonsensical mutant transcript, though this experiment might pose new potential technical issues and is beyond the scope of this work.

Moreover, a recent study also indicated that large on-target deletions could lead to potential genotoxicity[29]. Whether such mechanisms account for the functional deficits observed in our study requires further investigation. Although no retinal toxicity was observed by over-expression of Cas9 enzyme or through delivery of our self-destructive CRISPR/Cas system, this study was conducted over a relatively short period of time (8 weeks). Thus further investigation is required to determine the long-term safety profile, i.e. whether prolonged over-expression of truncated gene products in the retina, as potentially caused by our self-destructive CRISPR/Cas system, are deleterious.

It is also noted that we did not expect the kamikaze CRISPR/Cas system alone to completely address the issue of CRISPR safety or the off-target effects. Combining our novel kamikaze strategy with shortened expression of Cas9 together with a high-fidelity Cas9 as well as through improved guide RNA design will be required to further reduce off-target cleavage and improve the overall long-term safety in retinal gene editing.

As a proof of concept, we tested this self-targeting system in YFP transgenic mice using the most commonly studied SpCas9. However, a similar strategy could be applied to other Cas orthologs such as SaCas9[97] or CjCas9, providing a useful tool for genome editing in the retina.

In summary, we describe and characterize a self-destructive “kamikaze” CRISPR/Cas system for *in vivo* genome editing in the retina. This self-destructive kamikaze CRISPR/Cas system can effectively reduce the expression of SpCas9 in the mouse retina, without substantially sacrificing on-target editing efficiency. Therefore, our AAV2-mediated self-destructive CRISPR/Cas may be a useful and versatile tool for genome editing in the retina.

4 COMPARISON OF CRISPR/CAS ENDONUCLEASE GENE-EDITING EFFICIENCY OF RETINAL CELLS *IN VIVO*

4.1 Introduction

CRISPR/Cas has opened up the prospect of direct gene correction therapy for some inherited retinal disease. Our previous studies[20,57] demonstrated AAV-mediated *in vivo* delivery of retinal cells using SpCas9. However, a dual vector system is required to package both SpCas9 and sgRNA. The limitation of dual vector delivery system has been fully discussed in our self-targeting CRISPR study.

As more CRISPR/Cas endonucleases are discovered, such as Cas12a, SaCas9 and CjCas9, which differs in their editing efficacy, packageability and PAM requirement, it may be possible to use a single vector to package both the Cas endonuclease and its sgRNA. Apart from SpCas9, minimal studies have tested the *in vivo* gene-editing efficiency of SaCas9[28,97,130,131] and Cas12a[31132]. Eunji et al.[29] reported efficient *in vivo* gene editing in mouse muscle cells or RPE cells using an all-in-one AAV-delivered CjCas9 and sgRNA. Taeyoung Koo et al. tested the *in vivo* editing of CjCas9 in a Duchenne muscular dystrophy animal model[133]. To date, it is not clear which of these are most efficacious for gene editing *in vivo*. Would single vector CRISPR/Cas systems work better than the dual vector system in the retina? For the same dual vector system, which of the currently available Cas endonucleases is the most efficient in editing the retina?

To answer these questions, we sought to compare the CRISPR/Cas endonuclease activity in retinal cells, using CMV-Cre::Rosa26-YFP mouse as our model. To approach this, we first designed 1~3 guide RNAs targeting *YFP* for each Cas endonuclease (Figure 4.1) and tested them in an engineered YFP-expressing HEK cell line to select the best-performing guide RNA. For the same clinical application consideration as mentioned previously, we used AAV vectors to deliver CRISPR/Cas into mouse retina. The differences compared with the first study is that we hypothesized that we could deliver CRISPR/Cas to the

deeper layer of retinal via intravitreal injection using a AAV2-based variant AAV7m8. We used AAV7m8 to package CRISPR/Cas constructs using a single or dual vector delivery system (Figure 4.2) and injected them intravitreally into mouse eyes. We then validated CRISPR/Cas gene-editing efficiency by checking the knockout of YFP in retinal cells using FACS.

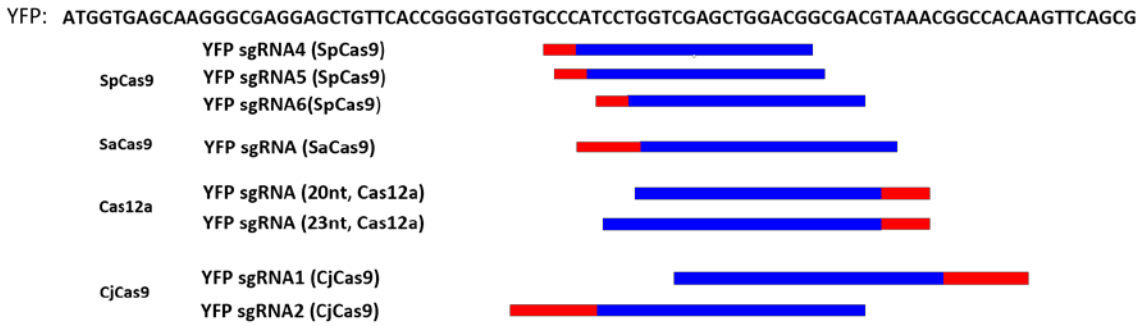

Figure 4.1 *YFP*-targeting sequence for sgRNA design.

YFP-targeting sgRNAs were designed (three sgRNAs for SpCas9, one sgRNA for SaCas9, two sgRNAs for Cas12a and 2 for CjCas9). PAM sequence (red)

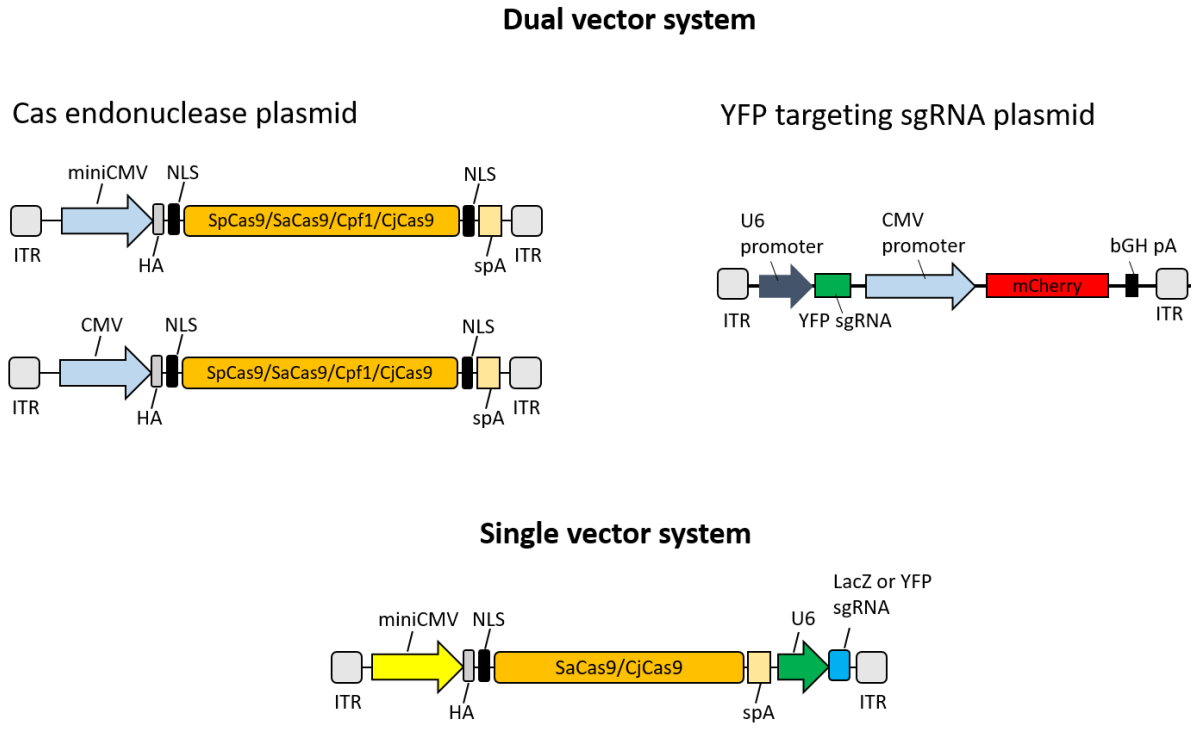

Figure 4.2 Schematic graph for dual and single vector system.

For dual vector system plasmid, Cas endonuclease was driven by miniCMV or CMV promoter (only miniCMV promoter driven plasmid were packaged into AAV for *in vivo* test), sgRNA was driven by U6 promoter with mCherry under the control of CMV promoter to identify vector transfection. Considering the loading capacity of AAV, for the single vector system, an all-in-one plasmid with SaCas9/CjCas9 was designed with Cas endonuclease driven by miniCMV and sgRNA driven by U6 promoter (Only single SaCas9 plasmid was successfully cloned and tested in the following experiment). For Cas12a, we used the Cas endonuclease from *Acidaminococcus* (originally called AsCpf1). Hemagglutinin (HA) tag was fused to the C-terminus of Cas endonuclease in the vector, so Cas protein expression could be detected using an antibody recognizing HA tag by western blot.

4.2 Results

4.2.1 sgRNA selection by *in vitro* validation

YFP-targeting sgRNA plasmids and LacZ sgRNA control for each different Cas endonuclease were generated as follows: For SpCas9, YFP sgRNA4, 5, 6; for Cas12a, YFP sgRNA 20nt and 23nt; for CjCas9, YFP sgRNA1 and 2 (details for plasmid name and cloning method are provided in Appendix 1). To test the editing efficacy for YFP disruption and select the most effective sgRNA for each Cas endonuclease, original Cas endonuclease plasmid (Appendix 1, Table 8.1 and Appendix 2, Table 8.11) driven by CMV promoter and sgRNA plasmid were co-transfected in HEK293A-YFP cells. Cells were collected at day 10.

4.2.1.1 Fluorescence microscopy images

Ten days after transfection, the fluorescence microscopy image (Figure 4.3) showed different degrees of reduction of YFP expression in HEK293-YFP cells co-transfected with Cas endonuclease and respective *YFP*-targeting sgRNA compared with LacZ sgRNA control. A marked reduction of YFP expression was found with all three YFP sgRNAs in the SpCas9-treated group, followed by Cas12a and SaCas9 (dual and single), while the

reduction in CjCas9 group seemed less obvious. Robust expression of mCherry were found in all cells except those transfected with single SaCas9 plasmid as no mCherry cassette was inserted into the single vector due to AAV capacity consideration.

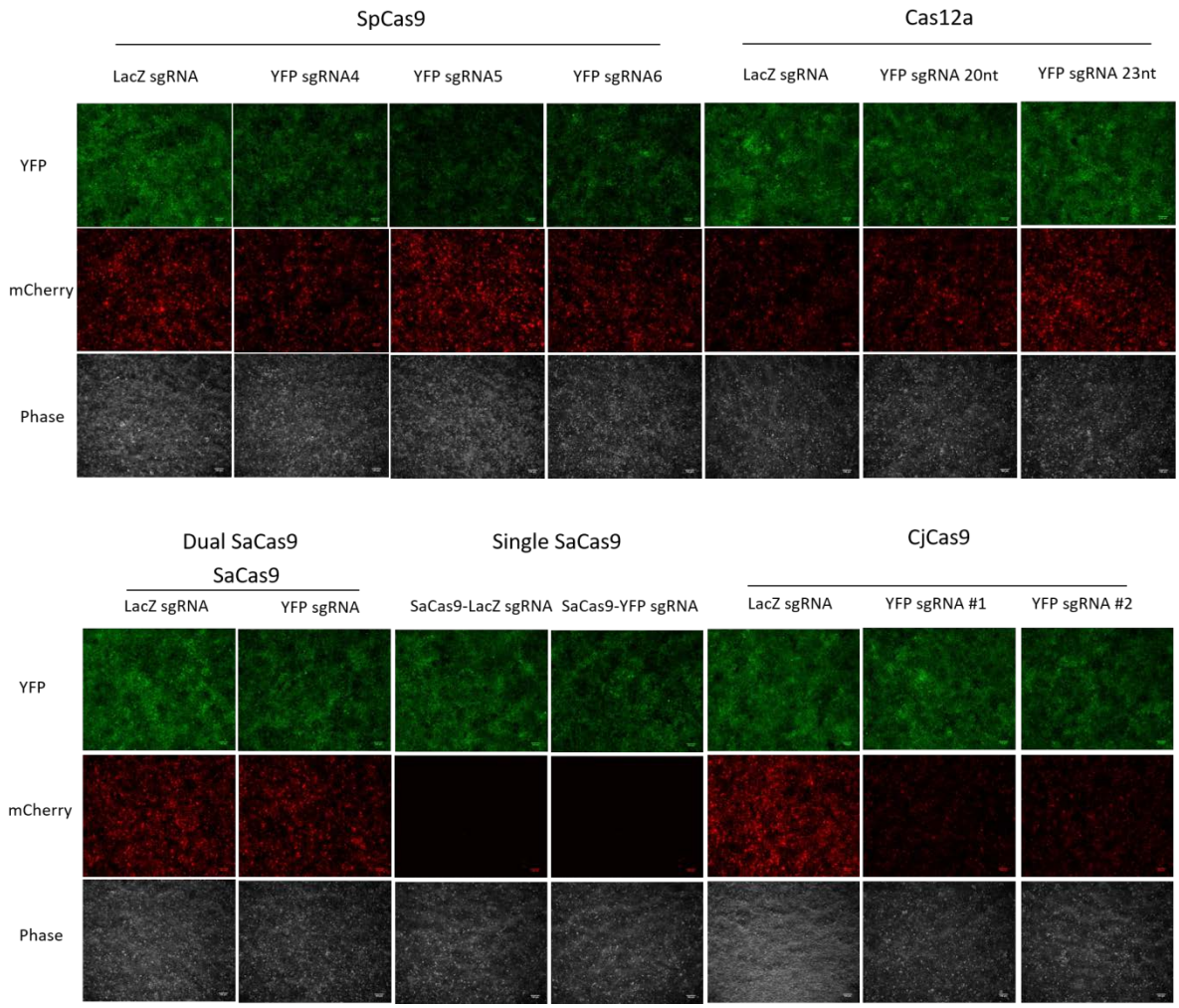

Figure 4.3 Fluorescence microscopy image.

Representative images of YFP expression in cells transfected with different CRISPR/Cas constructs. *Scale bar:100 μm.*

4.2.1.2 T7E1 assay

The T7E1 assay revealed that most of our designed sgRNAs targeted *YFP* effectively, with the exception of YFP sgRNA1 for CjCas9 (Figure 4.4). Expected cut products were found at around 565 bp and 290bp.

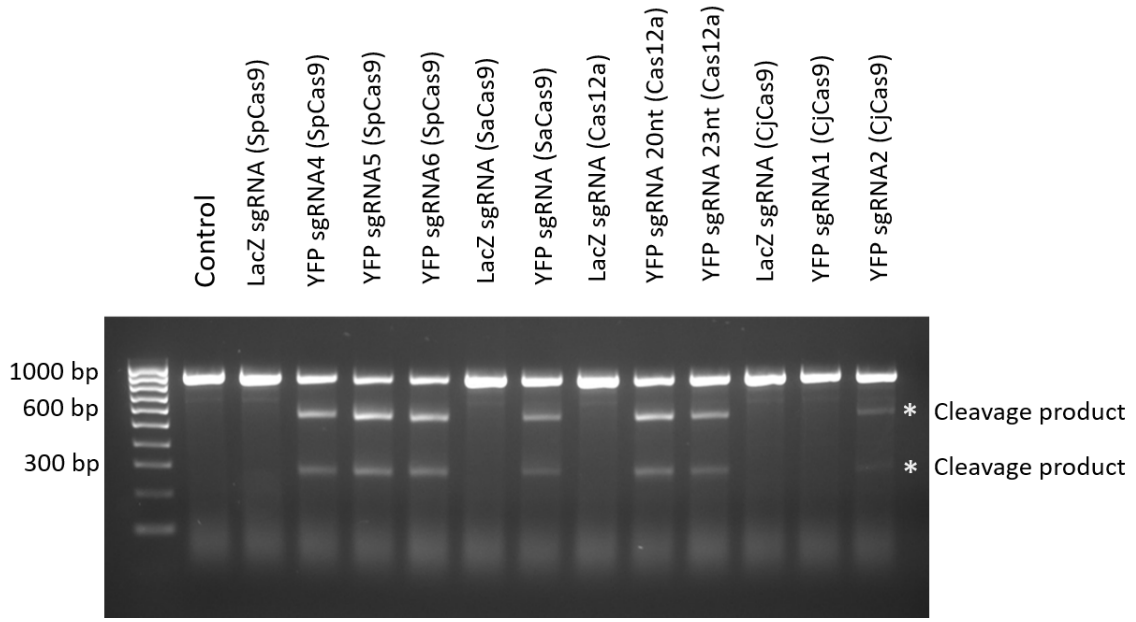

Figure 4.4 T7E1 assay to detect cleavage efficiency for *YFP*.

Expected cleavage products by T7E1 were detected in 2% TAE gel.

4.2.1.3 Flow cytometric analysis

The YFP disruption efficacy for each different CRISPR/Cas construct was further quantified through flow cytometric analysis (Figure 4.5). To be more specific, compared with HEK293A-YFP cells as control, the percentage of YFP-expressing cells was significantly reduced in cells transfected with SpCas9 and its *YFP*-targeting sgRNAs YFP sgRNA4 (26.0±2.9%), YFP sgRNA5 (11.5±1.3%), YFP sgRNA6 (14.7±2.9%); Cas12a and its *YFP*-targeting sgRNAs YFP sgRNA 20nt (33.6±4.9%), 23nt sgRNA (55.0±5.0%); CjCas9 and it *YFP*-targeting sgRNAs YFP sgRNA2 (69.5±3.1%); Dual vector SaCas9 (57.3±3.2%) and Single SaCas9 (57.0±2.0%). There was no significant reduction of YFP expression in cells transfected with CjCas9 and YFP sgRNA1 compared with control. The most effective *YFP*-targeting sgRNA for each Cas endonuclease was therefore selected for subsequent *in vivo* test.

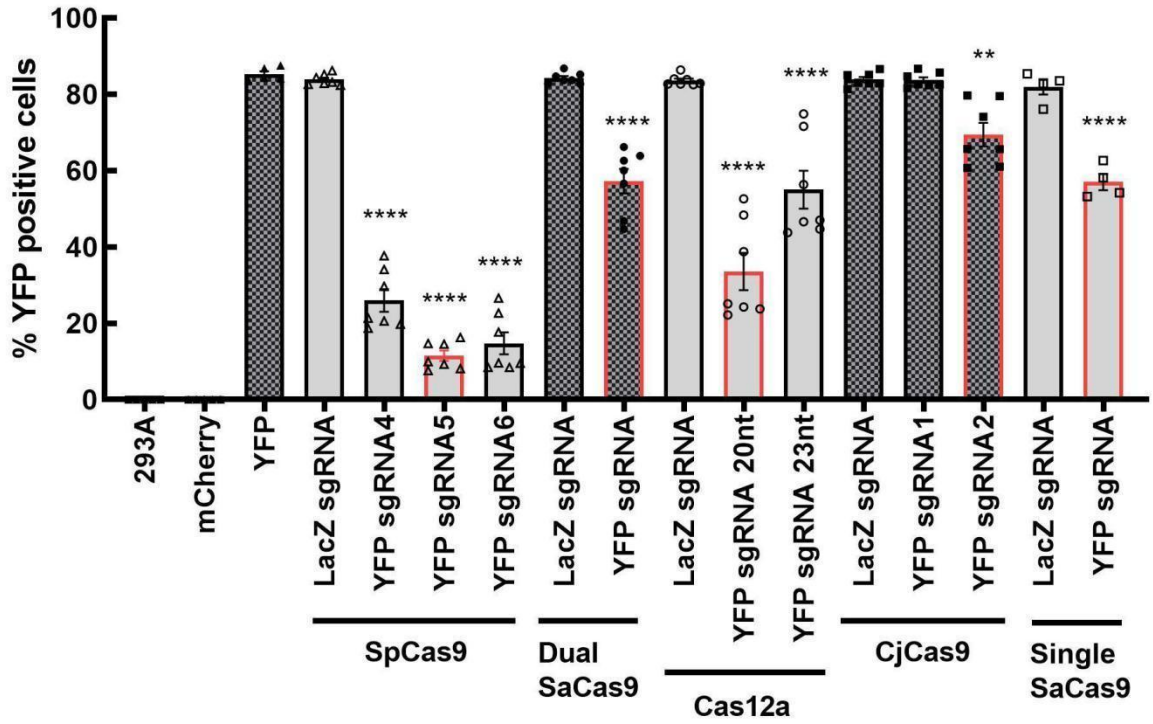

Figure 4.5 Flow cytometry analysis for sgRNA selection.

Data are represented as mean ± SEM for 4-7 independent replicates. Statistical analysis between groups was performed using one-way ANOVA followed by multiple comparisons test (****$p < 0.0001$, compared with control using HEK293A-YFP cells without transfection). HEK293A cells and HEK293A-mCherry cell without YFP expression were also included as negative control. Columns with red border line illustrated the best-performing sgRNAs for each CRISPR/Cas.

4.2.2 Cas endonuclease construct cloning and validation

The original Cas endonuclease-expressing plasmids were not all in AAV2 ITR-containing plasmids (details for Cas endonuclease plasmid cloning are listed in Appendix 1). In order to validate Cas protein expression in cloned AAV2-Cas endonuclease plasmids, HEK293A cells were transfected with SpCas9, SaCas9, Cas12a driven by miniCMV promoter, two CjCas9 plasmids driven by miniCMV and CMV. The expression of different Cas protein was detected with HA tag antibody except miniCMV-CjCas9 (Figure 4.6).

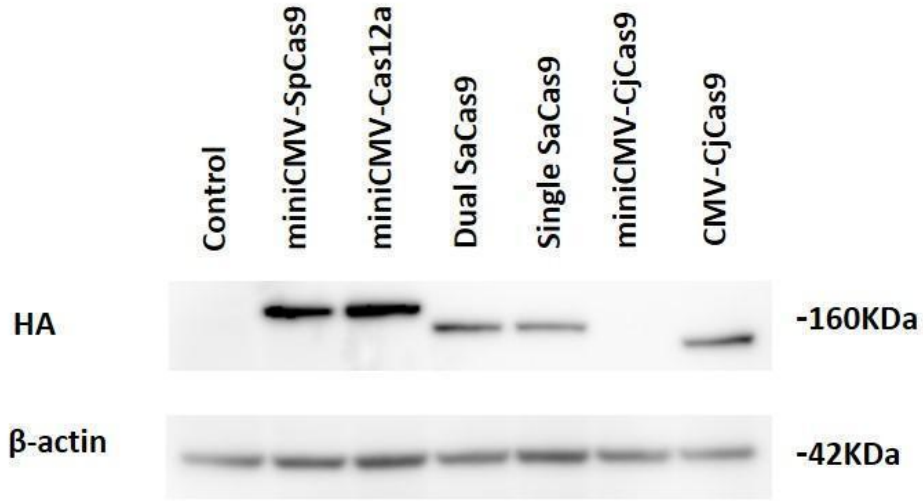

Figure 4.6 *In vitro* validation of different Cas endonucleases by western blot.

Representative western blot of Cas protein expression in HEK293A cells treated with AAV-Cas plasmids two days after transfection. CjCas9 expression was not detectable in cells transfected with miniCMV-CjCas9 plasmid by western blot.

4.2.3 *In vivo* AAV7m8 delivery of CRISPR/Cas in the mouse retina

Both eyes of CMV-Cre::Rosa26-YFP mouse received intravitreal co-injection of 1 µL dual-viral suspension ($2.5x10^9$ vg AAV7m8-Cas endonuclease and $2.5x10^9$ vg AAV7m8-YFP sgRNA) for dual vector system or 1 µL dual-viral suspension ($2.5x10^9$ vg AAV7m8-Single SaCas9 and $2.5x10^9$ vg AAV7m8-mCherry) for single SaCas9 group. Sole AAV7m8-mCherry-treated eyes were included as control. Specific animal groups and numbers are listed in Appendix 4 (Table 8.21). AAV7m8 penetration and distribution were assessed on frozen sections and retinal whole-mount of the CMV-Cre::Rosa26-YFP mouse eye 5 months after intravitreal injection. Fluorescence images taken by Slide Scanner revealed AAV7m8, indicated by mCherry expression, was visible throughout the retina, including Ganglion Cell Layer (GCL), Inner Nuclear Layer (INL) and even some part of the ONL, with major expression within INL (Figure 4.7, 4.8). Robust AAV7m8 transductions in the retina with variation in penetration among individual animals were found (Figure 4.8). Retinal whole-mount images from different AAV7m8-CRISPR/Cas-treated groups showed mCherry positive cells distributed widely across the retina, with higher expression in two

or three quadrants (Figure 4.9). YFP expression could be found in all the layers throughout the retina and no obvious difference could be detected among AAV7m8-CRISPR/Cas-treated mice and control mice.

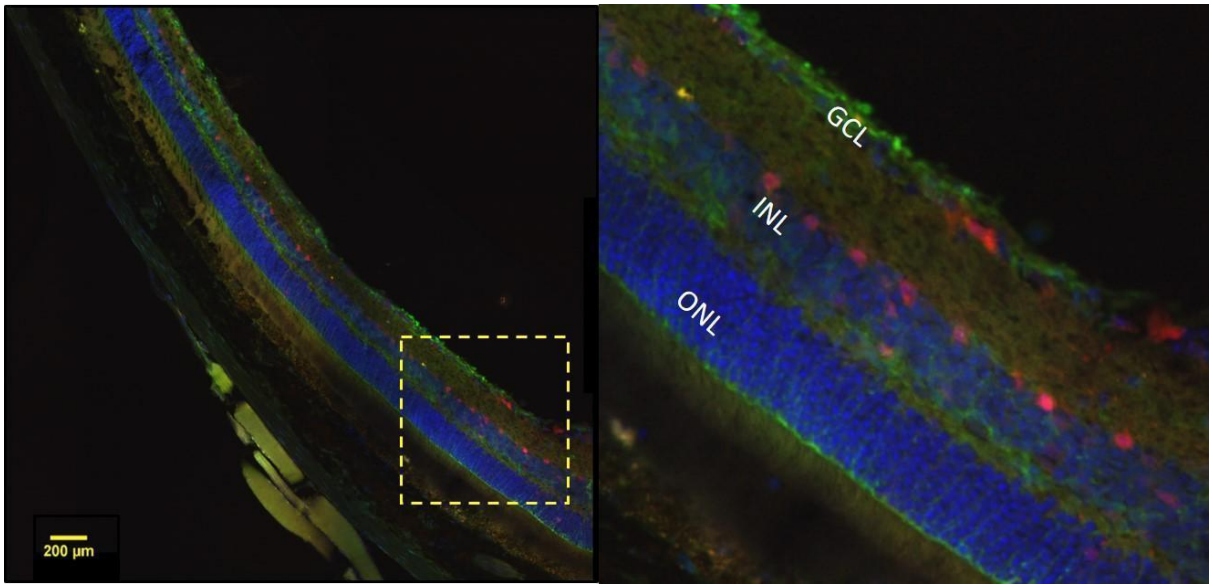

Figure 4.7 Representative cross section image from retina co-transduced with AAV7m8-miniCMV-CjCas9 and its selected YFP sgRNA.

Mouse was sacrificed and images were taken 5 months after intravitreal injection (mouse ID: 81). *Scale bar: 200 µm*. Images were taken by a Zeiss spinning disk confocal microscope.

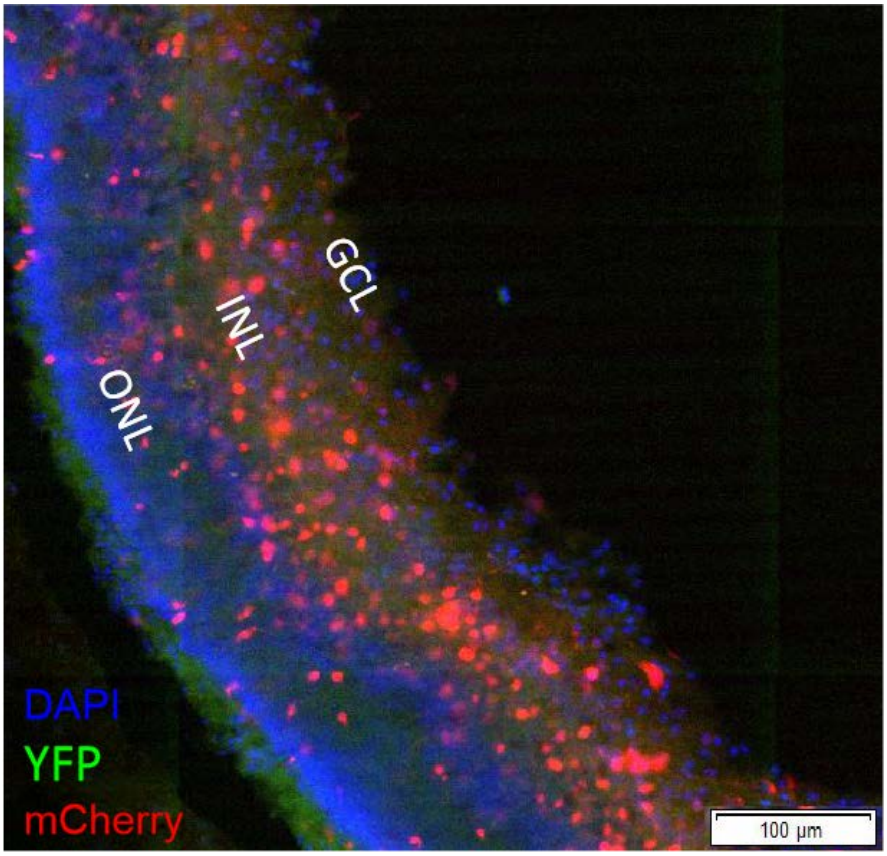

Figure 4.8 Representative cross section image from another mouse receiving AAV7m8-miniCMV-CjCas9 and its selected YFP sgRNA.

Mouse ID: 183. Strong mCherry expression was in all the layers of retina; however, the layers of retina could not be clearly identified as the slice of retina cryosection was thicker. *Scale bar: 200 µm*. Images were taken by Olympus Slide Scanner.

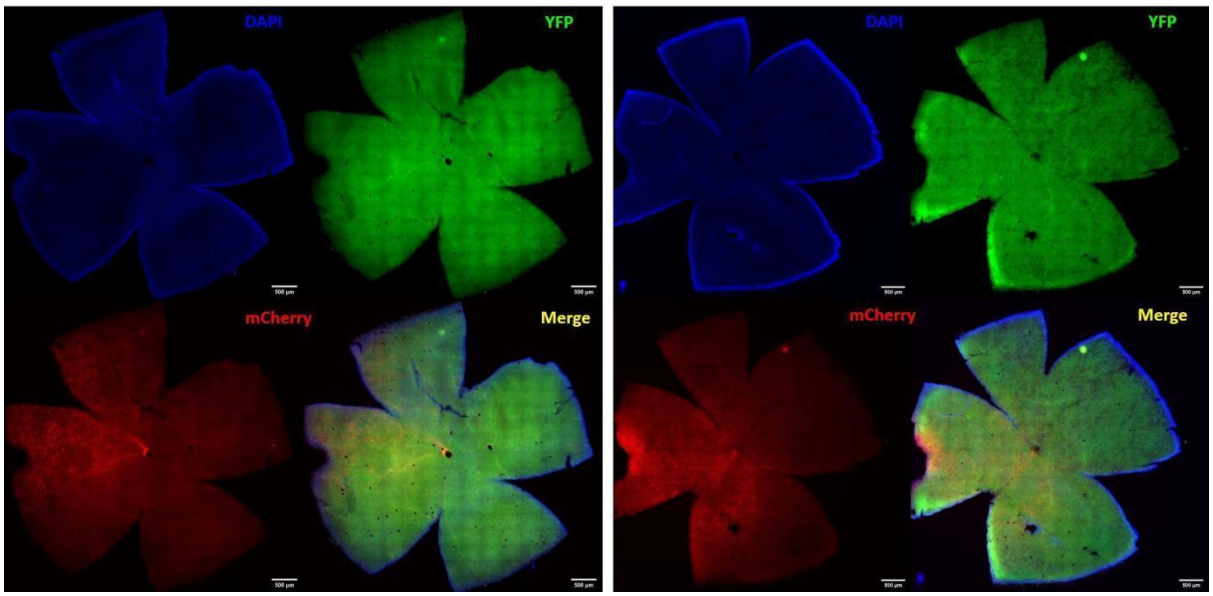

Figure 4.9 Representative retinal whole-mount images from two mouse eyes receiving different AAV7m8-CRISPR/Cas.

Left panel : AAV7m9-CMV-CjCas9, mouse ID 29, right eye; Right panel: AAV7m8-miniCMV-CjCas9, mouse ID 76, right eye. *Scale bar: 500 µm*. Images were taken by Olympus Slide Scanner.

4.2.4 Comparison of *in vivo* YFP knockout in the mouse retina by FACS

To evaluate and compare the YFP knockout *in vivo* in different AAV7m8-CRISPR/Cas-treated eyes, the percentage of YFP disruption among mCherry positive retinal cells was quantified by FACS. The FACS plots of the pre-gating for single live cells are shown in Figure 4.10. Representative FACS plots in Figure 4.11 illustrated the difference in YFP disruption in retinal cells receiving control or SpCas9. Eyes with severe surgical complications such as cataract or retinal detachment or those with very low mCherry expression by FACS were excluded from the final FACS analysis. Dissociated retinal cells prepared from one retina were presented as one dot in the plot (Figure 4.12 and 4.13). Slight to medium differences in AAV7m8 transfection in different CRISPR/Cas treatment groups were observed (Figure 4.12), and the lowest percentage of mCherry positive cells

was in miniCMV-CjCas9-treated retinas (28.6±3.4%). Retinas receiving SpCas9 (SP), Single SaCas9 (SSA), or Dual SaCas9 (DSA) had a relatively high proportion of mCherry expression (50.0±4.6%, 52.0±4.3%, 57.7±3.3%, respectively), similar to the mCherry control (51.4±7.0%). Lower variation within the group was seen in Cas12a (35.1±10.7%) and two CjCas9 treatment groups (miniCMV-CjCas9: 28.6±3.4%, CMV-CjCas9: 34.0±4.8%). SpCas9 had the highest knockout efficiency of YFP among all the Cas endonucleases (18.9±2.9%), followed by Single SaCas9 (9.8±2.6%), Dual SaCas9 (8.4±3.4%) and Cas12a (5.4±2.0%), while CjCas9 (both miniCMV-CjCas9 and CMV-CjCas9) showed no disruption of YFP expression. Other Cas endonucleases (SaCas9 and Cas12a) had limited YFP knockout effect with variation among individuals. There were significant differences in YFP knockout between the SpCas9- and Single SaCas9-treated groups compared with control (Figure 4.13).

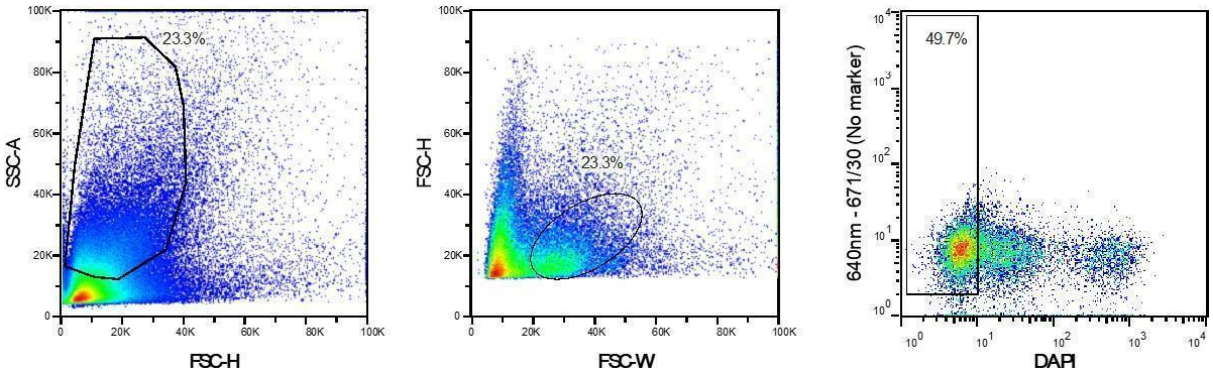

Figure 4.10 Representative FACS plot showing pre-gating based on scatter and live/dead staining by DAPI.

Single cells from dissociated retina were gated on forward scatter (FSC-H)/side scatter (SSC-A) plot and live cells were further gated on DAPI plot.

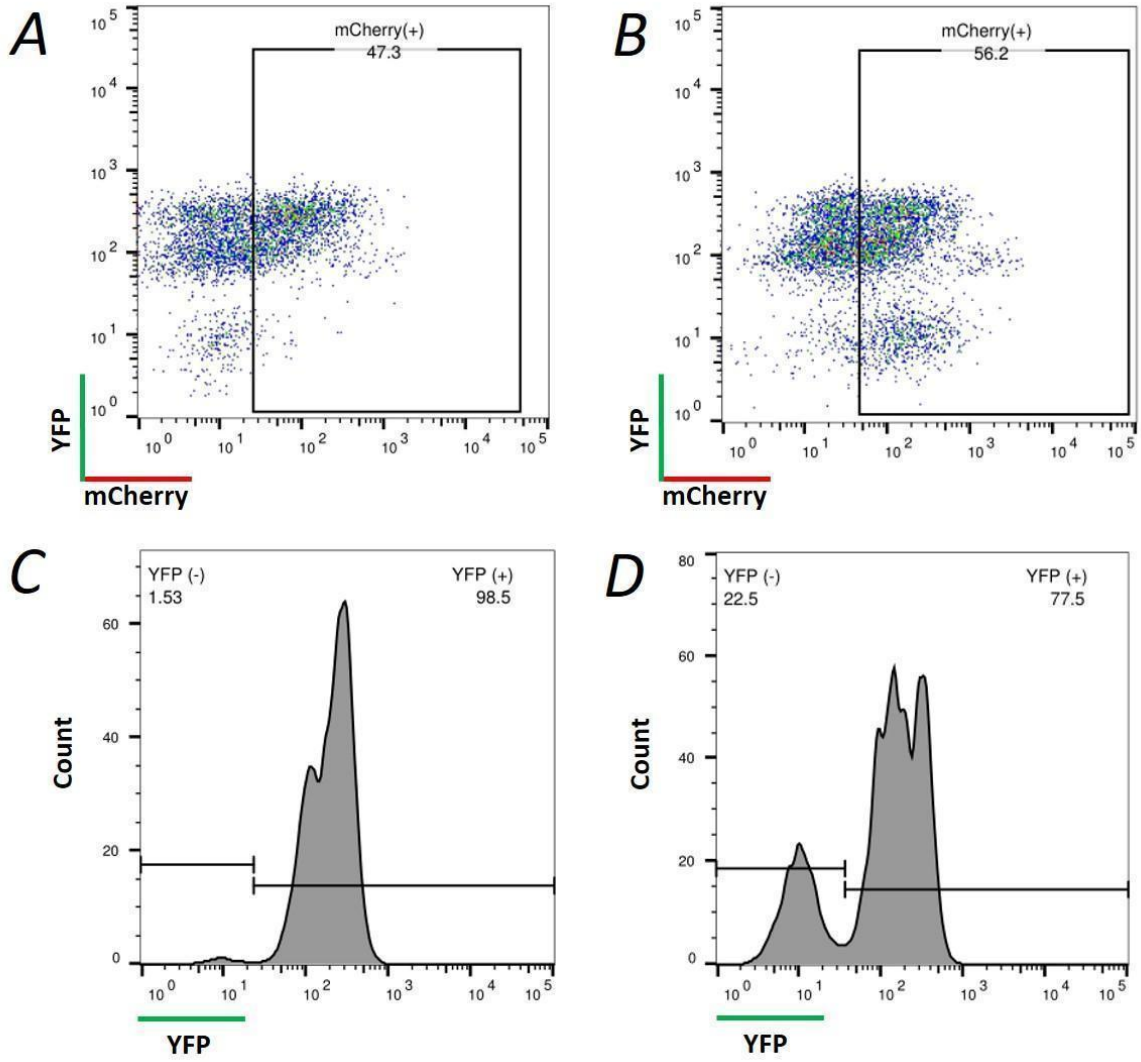

Figure 4.11 Representative FACS plots of dissociated retinal cells receiving AAV7m8.

AAV7m8-mCherry control (A, C) or AAV7m8-SpCas9 / AAV7m8-YFP sgRNA (B, D). The histograms in the lower panels (C, D) were based on mCherry gating. Dissociated cells from one retina were used in each group.

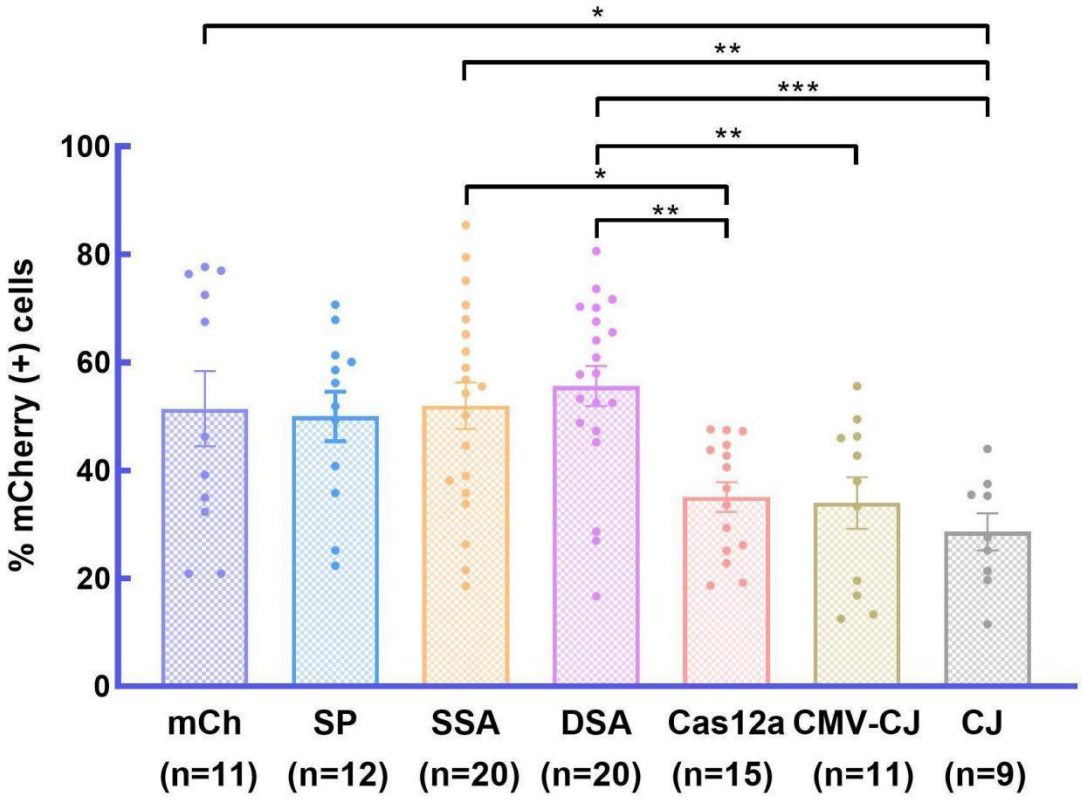

Figure 4.12 mCherry expression indicating AAV7m8 transduction in the retina by FACS.

mCh: mCherry, SP: SpCas9, SSA: Single SaCas9, DSA: Dual SaCas9, CMV-CJ: CMV-CjCas9, CJ: CjCas9. Data are presented as mean ± SEM for 9-20 independent samples in each group. Statistical analysis between groups was performed using one-way ANOVA followed by multiple comparisons test. n=number of injected eyes. * $p<0.05$, ** $p<0.01$, *** $p<0.001$.

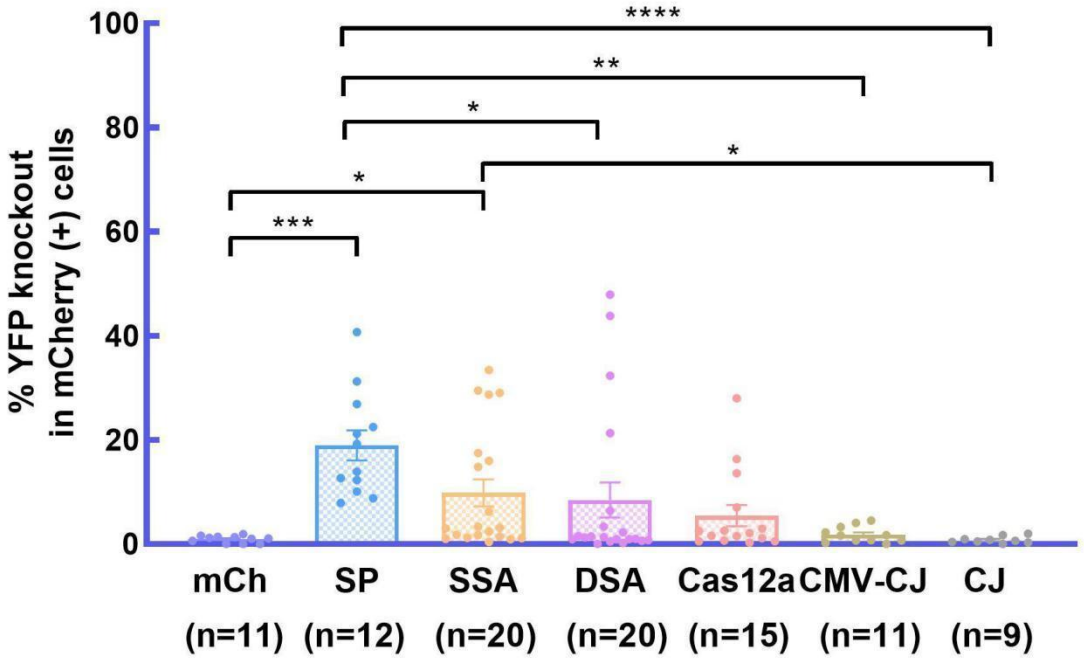

Figure 4.13 YFP knockout in mCherry positive cells by FACS.

mCh: mCherry, SP: SpCas9, SSA: Single SaCas9, DSA: Dual SaCas9, CMV-CJ: CMV-CjCas9, CJ: CjCas9. Data are presented as mean ± SEM for 9-20 independent samples in each group. Non-parametric one-way ANOVA - the Kruskal-Wallis test was applied as data in two groups (Cas12a and Dual SaCas9) didn't pass the D'Agostino & Pearson normality test. n=number of injected eyes. * p<0.05, ** p<0.01, *** p<0.001.

4.3 Discussion

AAV2-mediated gene delivery via intravitreal injection results in transduction mainly in the inner retinal layer, due to the barrier of the inner limiting membrane. Injected subretinally, AAV2 vectors primarily infect the outer layers of the retina, including photoreceptors and the RPE. Intravitreal injection has been an established clinical practice for many years, with few surgical complications, while subretinal injection is a more challenging procedure with confined diffusion within the injection bubble. AAV7m8 is an AAV2-based variant with a novel capsid that enables higher penetration in the retina[134–136] and other tissues such as the inner ear[137]. As the degeneration of RPE and photoreceptors are involved in most inherited retinal diseases, it is imperative to explore a minimally invasive, safer and reproducible delivery method to bring CRISPR/Cas constructs to the outer layer of the retina. Our study shows that AAV7m8-mediated CRISPR/Cas has good pan-retinal transduction, with higher expression in two or three quadrants, which might be due to injection error. We noted cataract, inflammation, and retinal detachment as complications of the injection. For FACS analysis, we excluded the eyes with severe surgical complications and those with very limited viral infection.

Previous studies show that the target sequence of guide RNAs affects targeting efficiency of CRISPR/Cas system. Crucial as it is to ensure a fair comparison between these currently available CRISPR/Cas systems, it is rather difficult to design a study to fully exclude the influence of sequence variation with different PAMs for different Cas endonucleases. We took several steps to ensure a relatively fair comparison of editing efficiency between different CRISPR/Cas systems. First, we checked the *YFP* gene for all the potential PAM sites for each Cas endonuclease and then designed sgRNA targeting *YFP* within the similar region. Furthermore, we designed many sgRNAs for each CRISPR/Cas systems targeting the similar region of *YFP* and chose the most effective one for each system for *in vivo* comparison. Also, we ensured that the expression of each endonuclease was being driven by the same ubiquitous promoter (CMV for *in vitro* sgRNA

selection, miniCMV for *in vivo*) and allowed for the same viral delivery method. The only exception was CjCas9, which had poor expression via western blot, so we added an extra CjCas9 driven by a stronger promoter CMV. Still, CjCas9 barely demonstrated knockout YFP by FACS analysis *in vivo*. When I started this project, there was no human-codon optimized version of CjCas9, which may explain the difference in our editing efficiency results to other groups[29]. Moreover, there is a tradeoff between aiming to target the same region of the *YFP* gene versus each sgRNA having similar efficacy.

We found differences in gene knockout efficiency between *in vitro* and *in vivo* modes. For the *in vitro* study, SpCas9 outperforms Cas12a, followed by SaCas9 and CjCas9. For the *in vivo* test, SpCas9 is still the best-performing Cas endonuclease among all, without a clear trend among the other Cas orthologs. Initially, we hypothesized that single SaCas9 might have competitive or even higher editing efficiency compared to dual SpCas9, but we didn't observe that in our *in vivo* test. Among all the other tested groups, the overall editing efficiency of single SaCas9 was second best; however, the conclusion is not firm as the variation was unexpectedly high in each injected eye. One limitation of this study is that due to time and funding constraints, we did not directly sequence the sorted cells to further investigate the actual on-target efficacy between each group or check the ones with exceedingly high editing efficiency. More work is required to explain the variation in knockout efficiency among individual mice within the same group and draw a more solid conclusion.

In summary, we compared four currently available CRISPR/Cas systems for *in vivo* gene editing in the retina and found SpCas9 has the highest editing efficiency overall.

5 A GENOME-WIDE CRISPR/CAS9 SCREEN TO IDENTIFY NOVEL THERAPEUTIC TARGETS FOR UVEAL MELANOMA

5.1 Introduction

Uveal melanoma (UM) is the most common primary malignant ocular tumor in adults involving the choroid (80%), the ciliary body (15%) or the iris (5%) (Collectively referred to as the uvea or uveal tract, the pigmented middle layer of the eye). Up to 50% of UM patients develop metastasis, mostly in the liver, indicating a poor survival and high mortality rate.

As a rare subtype of melanoma, UM has unique features compared with Skin Cutaneous Melanoma (SKCM), including risk factors, genetics, treatment strategies and prognosis. Weak correlation has been found with sun exposure and the onset of UM[138]. The most common melanoma-related mutations, such as *BRAF*, *NRAS* and *NF1*[139], were not closely related to UM. Over 80% of UM, however, is associated with *GNAQ* and *GNA11* mutations[140,141]. Other genes including *BAP1*[142,143], *CYSLTR2*[144,145], *SF3B1*[146–148], *EIF1AX*[148,149] have been reported to be related to UM. Treatment for UM includes enucleation and radiation and other methods, such as immunotherapy or chemotherapy[150]. Targeted therapy, such as anti-PD1 treatment used in SKCM, has limited activity in UM[151]. Other chemotherapeutics including dacarbazine have also had disappointing results for treating UM[152–154].

A comprehensive analysis of 4,999 UM patients revealed that the survival rate had not changed over a period of 40 years in the USA[155]. It is crucial that we uncover more novel therapeutic targets to treat this commonly fatal yet understudied cancer.

Just as CRISPR/Cas can be applied to target a single gene, it is also possible to interrogate every possible gene in the genome. Thus, this powerful genome-scale CRISPR/Cas screening approach has been developed by several researchers[109–111,156] for functional genetic study in various fields. Oligonucleotide synthesis technology allows for

the production of a large-scale pooled library that is faster and more affordable than an arrayed library. The advantage of Lentivirus DNA integrating into the host genome is that it enables stable, permanent and heritable genetic perturbation. Thus pooled Lentiviral CRISPR library is a powerful tool to study cancer genetics and biology.

Depending on the purpose of the CRISPR library, there are three main types: CRISPR knockout library, CRISPRi (CRISPR-based interference) library and CRISPRa (CRISPR gene activation) library. Pooled screening can be further divided into negative selection screen and positive selection screen, both of which have been tested by Shalem et al.[156] A negative-selection screen approach, as applied in our UM screen study, can be used to identify genes that are essential to cell viability as the cells with important genes that are knocked out will die with these related guide RNAs depleted from the population. By identifying the missing guide RNAs, it is possible to determine which genes are important for the growth and proliferation of specific cells. A positive screen has been applied to identify drug-resistant genes. An example of a positive screen is identifying genes resistant to vemurafenib in a human melanoma cell line A375. The workflow of Lentiviral CRISPR library screen is shown in Figure 5.1.

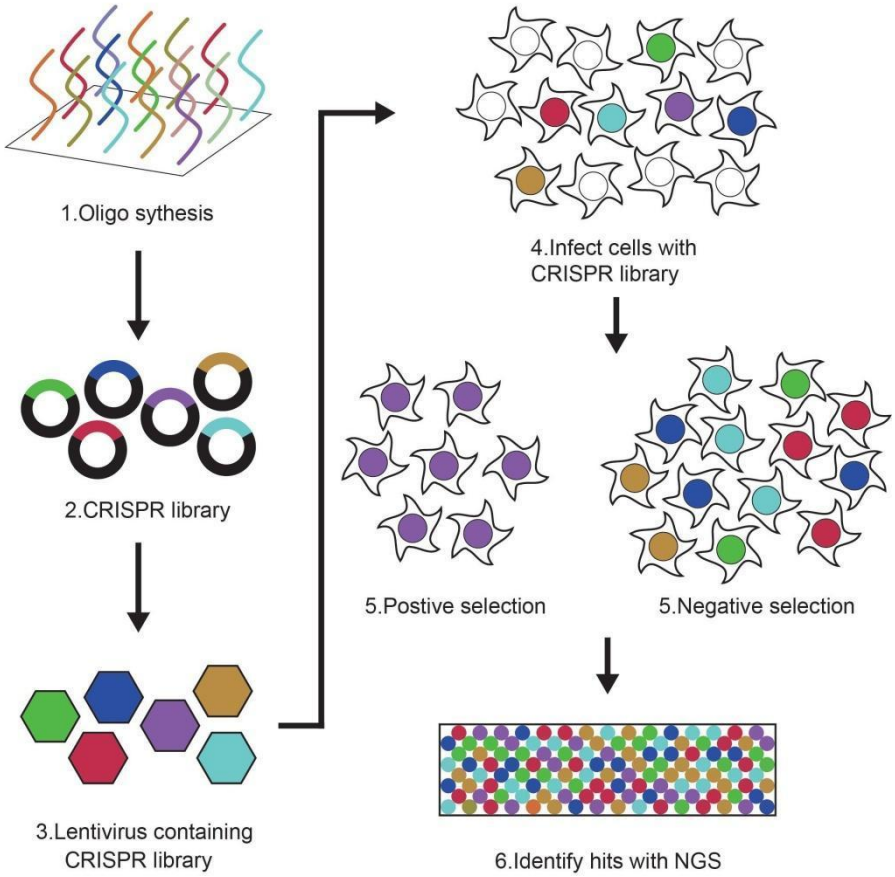

Figure 5.1 Workflow of Lentiviral CRISPR library screen.

To date, this genome-wide CRISPR/Cas9 knockout screen has been used to identify novel gene targets for different cancers, such as bladder cancer[157], colorectal cancer[158], breast cancer[159], liver tumor[160,161], acute myeloid leukemia[162,163] and glioblastoma[164]. We sought to identify genes that are essential for UM using this leading genetic approach.

5.2 Results

5.2.1 Quality control for uveal melanoma screening

Standard quality control was carried out to determine base quality within reads. The quality-trimmed Fastq files from two different conditions, Passage 0 (P0) and Passage 12 (P12) from UM (OCM1) cell lines were mapped to the Human_GeCKO v2_Library[109] using MAGeCK. The mapping summary for all samples is listed in Table 5.1 with Gini index and read count distribution are shown in Figure 5.2.

Table 5.1 Quality control and summary OCM-1 screen samples

	Sample ID	Reads	Mapped	Percentage	Total sgRNA	Zero Counts	Gini Index
1	UMP0_1	387529989	306261122	0.79	119461	286	0.06
2	UMP0_2	427247327	311118165	0.73	119461	276	0.06
3	UMP0_3	359356334	286941293	0.80	119461	69	0.06
4	UMP12_1	416965737	322517953	0.77	119461	6309	0.17
5	UMP12_2	679106595	524070831	0.77	119461	3320	0.12
6	UMP12_3	417905201	309265060	0.74	119461	8800	0.21

The Gini Index of the read count distribution indicates more evenness of the count distribution. Three biological replicates for P0 are listed as UMP0_1, UMP0_2, UMP0_3, and P12 as UMP12_1, UMP12_2, UMP12_3.

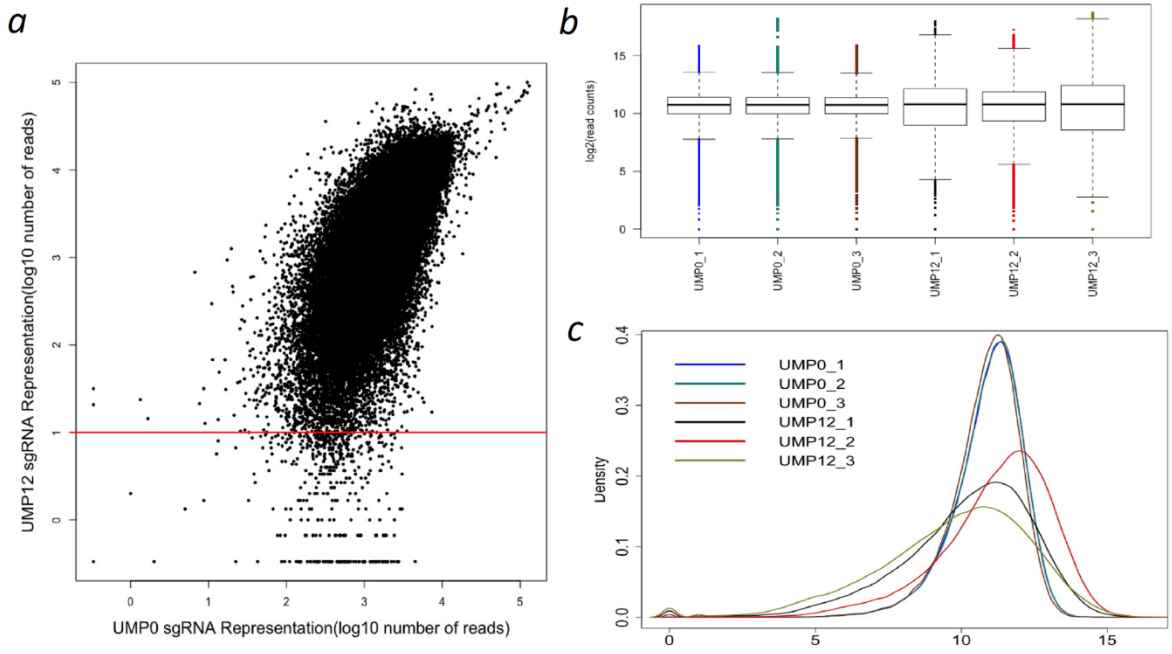

Figure 5.2 Plots showing sgRNA distribution in OCM-1 P0 and P12.

a) Scatterplot showing distribution of sgRNA read count in UMP0 and UMP12. b) Boxplot showing the distributions of sgRNA frequencies of all the samples. c) Distribution plot between biological replicates at two different time points with normalized read count.

5.2.2 15 genes were identified by CRISPR/Cas9 screen analysis in UM *in vitro*

The read count data were further accessed and sgRNAs with less than 100 read counts were calculated in P0 and P12. We found 0.45% reads in P0 had less than 100 read counts whereas 3.9% reads in P12 had less than 100 read counts. The number of sgRNAs with read counts less than 10 in P12 compared to P0 and only 0.16% sgRNAs were identified (Figure 5.2 a). From the initial screening, the sgRNAs with less than 100 read counts in P12 and more than 100 read counts in P0 were identified as potential candidate genes. Fifty-six genes (Table 5.2) were identified with low expression in three or more sgRNAs in P12 and therefore considered as possible hits.

Table 5.2 List of genes with three or more sgRNA missing in UMP12 compared with UMP0

Gene	Number of missing sgRNA	Gene	Number of missing sgRNA
CDIPT	4	*PHAX*	3
DUX2	4	*POLG2*	3
GOLGA8B	4	*POLR2I*	3
hsa-mir-3929	4	*PRPF40A*	3
OR5AR1	4	*PSMA3*	3
RPL35A	4	*RAD9A*	3
CIT	3	*RBM8A*	3
CLPB	3	*RPL13*	3
COPA	3	*RPL21*	3
CWC22	3	*RPL23*	3
DDX56	3	*RPL8*	3
DHX33	3	*RPS27*	3
EIF2S1	3	*S100A10*	3
EIF6	3	*SART3*	3
GAPDH	3	*SCAF11*	3
H2AFZ	3	*SLC25A3*	3
hsa-mir-4459	3	*SNRPD3*	3
hsa-mir-566	3	*SNRPF*	3
hsa-mir-619	3	*SON*	3
hsa-mir-663a	3	*SOX10*	3
hsa-mir-8078	3	*SRA1*	3
LONP1	3	*SRSF1*	3
MAD2L1	3	*SYNCRIP*	3
MED14	3	*UBL5*	3

MEF2C	3	*VARS2*	3
MESP1	3	*WDR43*	3
MRPS10	3	*WDR70*	3
OGDH	3	*WDR74*	3

Furthermore, we used CRISPRAnalyzeR, a multiple algorithm implemented online platform, to identify significant hits. From our analysis in negative selection, we found 48 significant genes for OCM-1 using MAGeCK (adjusted *p* value<0.05) (Figure 5.3a), 25 significant genes using sgRSEA (adjusted *p* value<0.05) (Figure 5.3b), 77 significant genes using DESeq2 (adjusted *p* value<0.001) (Figure 5.3c) and 2164 significant genes using EdgeR (adjusted *p* value<0.05) (Figure 5.3d).

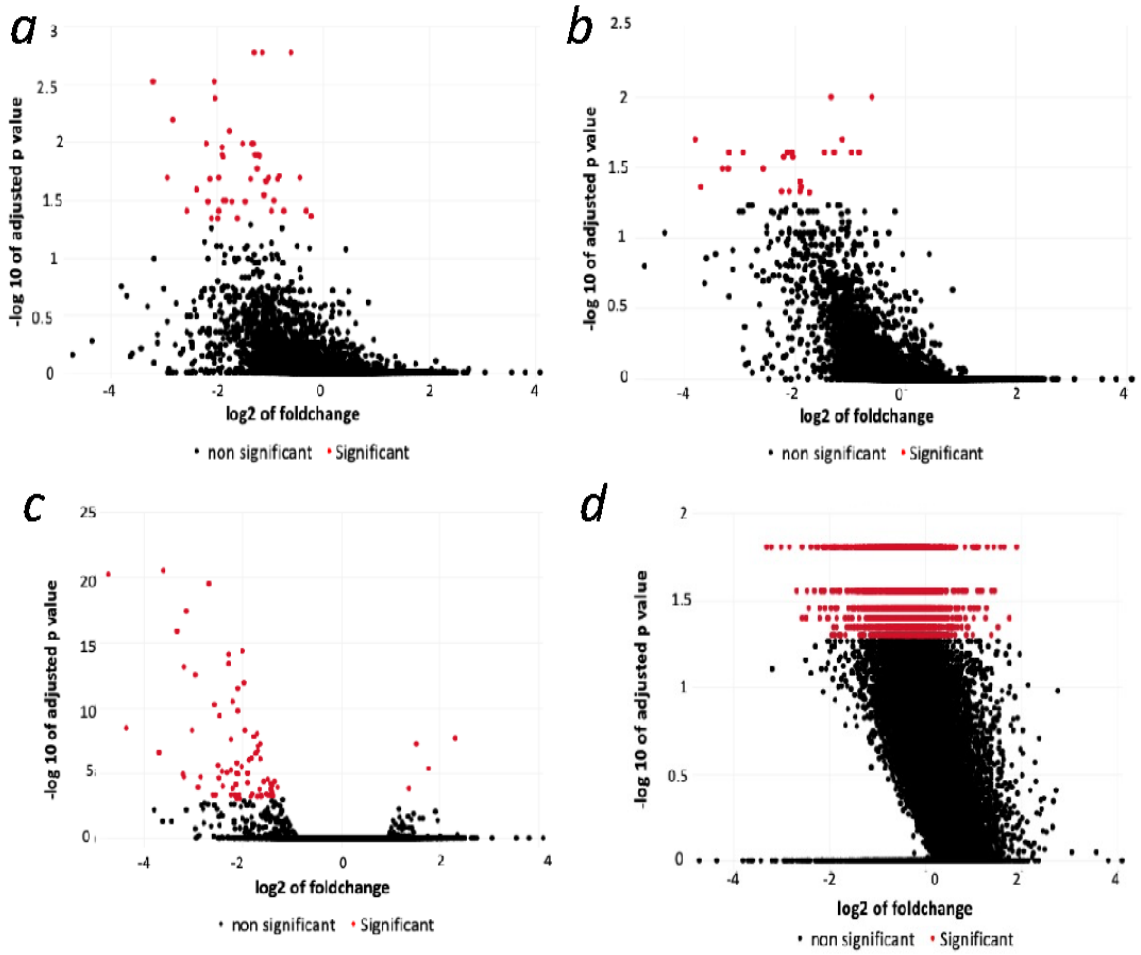

Figure 5.3 Scatterplot showing significant genes using MAGeCK (a), sgRSEA (b), DESeq2 (c), and EdgeR (d).

Gene overlap between different algorithms was identified (Figure 5.4a). Finally, we selected 15 candidate genes that had lower expression in P12 compared with P0 by identifying the overlap of genes using MAGeCK and DESeq2 (Figure 5.4b), as listed in Table 5.3.

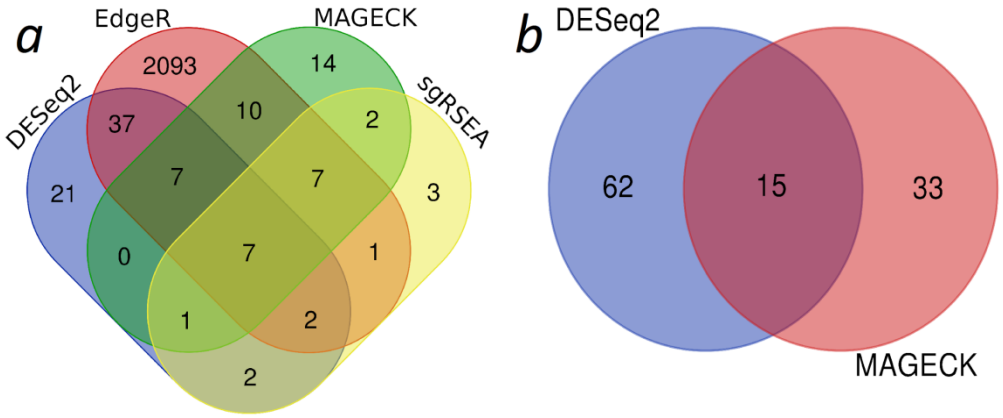

Figure 5.4 Venn diagram showing the overlap of genes between the different algorithms.

The overlap of genes between four different algorithms: DESeq2, EdgeR, MAGECK and sgRSEA (a); the overlap of genes with final selected algorithms MAGeCK and DESeq2.

Table 5.3 List of final gene subset select based on MAGeCK and DESeq2 algorithms

Genes	Total sgRNA in P0 and P12	Number of sgRNA with low expression in P12
WASH1	6	6
SLC3A2	6	6
ABT1	6	6
NDUFB10	6	6
RPL35	6	5
COQ2	6	6
LSM11	6	6
KATNB1	6	6
UBL5	6	6
MRPL22	6	4
HIST2H4A	6	6
HTRA2	6	6
SPDYE5	4	4
CCNA2	6	6
POLR3K	6	6

5.2.3 Major pathways identified by functional enrichment analysis using g:Profiler

A final selected subset of genes was used for the functional analysis and significant gene ontology pathways were identified using g:Profiler. The detailed pathways interactions are shown in Figure 5.5. Major pathways with the most intersects were as follows: metabolic process, cellular process, primary metabolic process, cellular metabolic process, biological process and organic substance metabolic process.

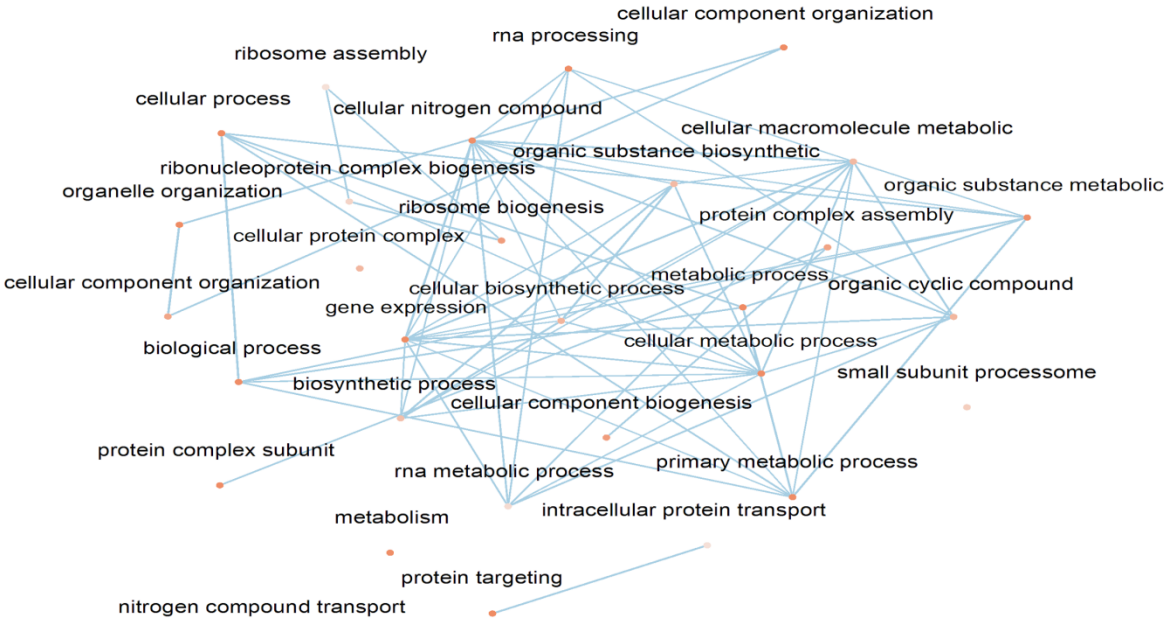

Figure 5.5 Pathway analysis showing statistically significant pathways using gProfiler.

5.2.4 Different expression levels of each candidate gene on different cancer stages and its effect on uveal melanoma patient survival

To check the gene expression level at different cancer stages, we assessed the tumor subgroup expression on our hit candidates by using the online portal ULCAN[120]. Based on genomic data from the Cancer Genome Atlas (TCGA) datasets[165], we found that all the other 14 genes have relatively fair expression on the UM genomic dataset as shown in Figure 5.6, whereas *WASH1* gene expression was not detected. Heatmap (Figure 5.7) confirmed the difference in expression level with our selected genes. *RPL35*, *SLC3A*,

UBL5 and *NDUFB10* have relatively higher expression in UM patients, while *SPDYE5*, *LSM11* and *CCNA2* have lower expression. Noted that gene expression level in normal controls is not provided in this heat map using ULCAN.

To evaluate whether these genes are related to UM prognosis, we further checked the effect of gene expression level on UM patient survival. Survival analysis revealed that the expression level of three genes (*COQ2*, *MRPL22* and *POLR3K*) is associated with UM patient survival (Figure 5.8). Interestingly, the expression level of three different genes (*SLC3A2*, *ABT1* and *RPL35*) was correlated with SKCM patient survival (Figure 5.9).

Pan-cancer analysis for individual genes was also performed using ULCAN. Overall, the differences in gene expression among 33 TCGA tumors were not remarkable. Notably, *SPDYE5* had the highest expression in acute myeloid leukemia (AML) among all the TCGA tumors; the expression of *SLC3A2* seemed higher in UM compared with other tumors in TCGA datasets (Figure 5.10). Moreover, expression of *SLC3A2* was higher in different cancers compared with normal control samples in each cancer type (Figure 5.11).

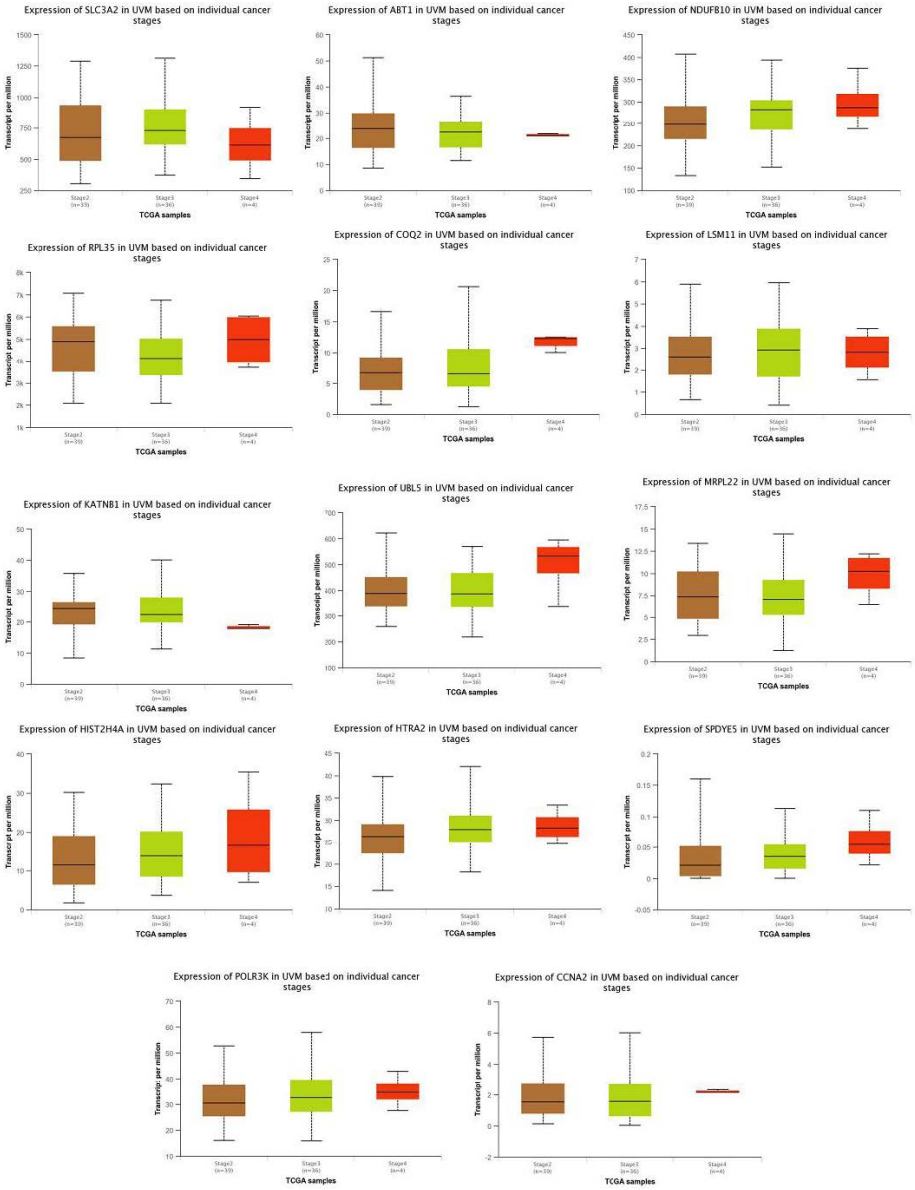

Figure 5.6 Expression level of final selected gene in TCGA datasets.

Gene expressions were recorded in different cancer stages in uveal melanoma based on tpm (transcript per million) values.

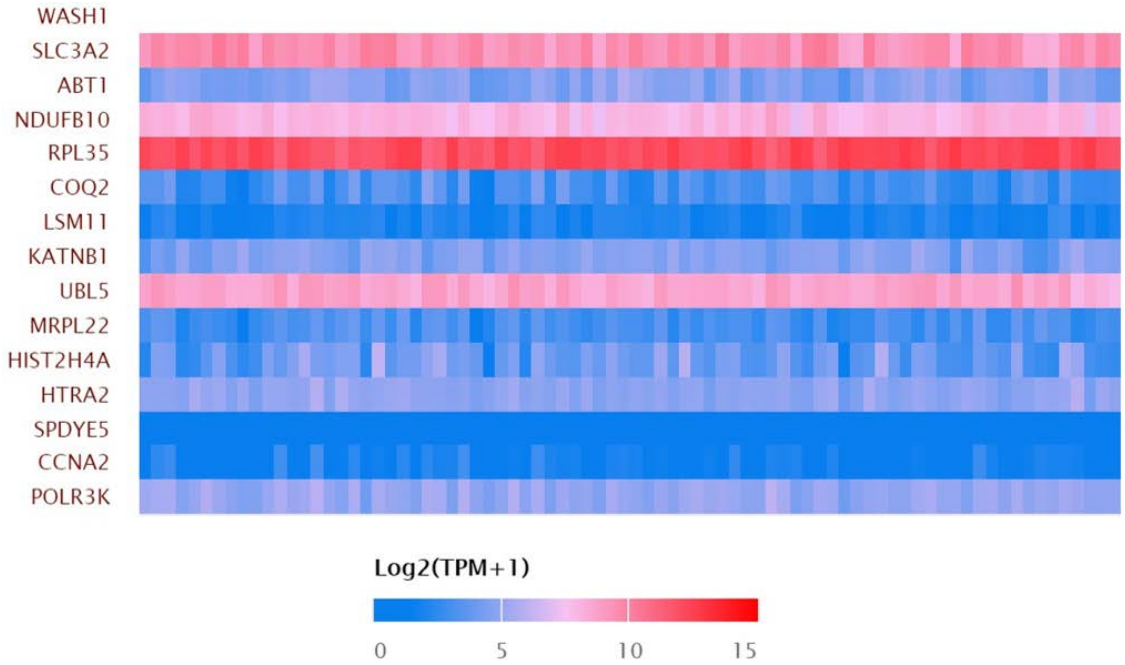

Figure 5.7 Heatmap showing expression pattern of selected genes in uveal melanoma.

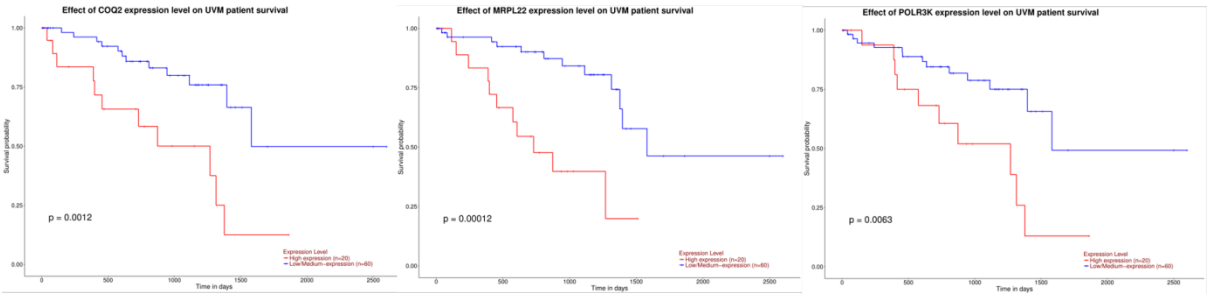

Figure 5.8 Expression level of selected genes that are significantly associated with UM patient survival (*p*<0.05).

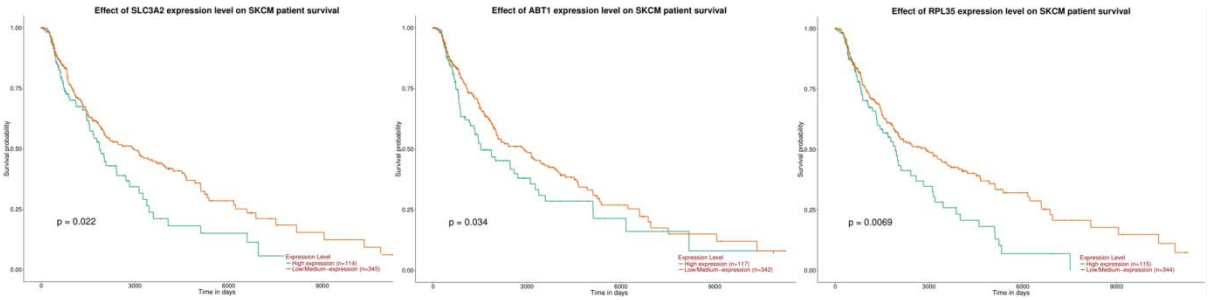

Figure 5.9 Expression level of selected genes that are significantly associated with SKCM patient survival (*p*<0.05).

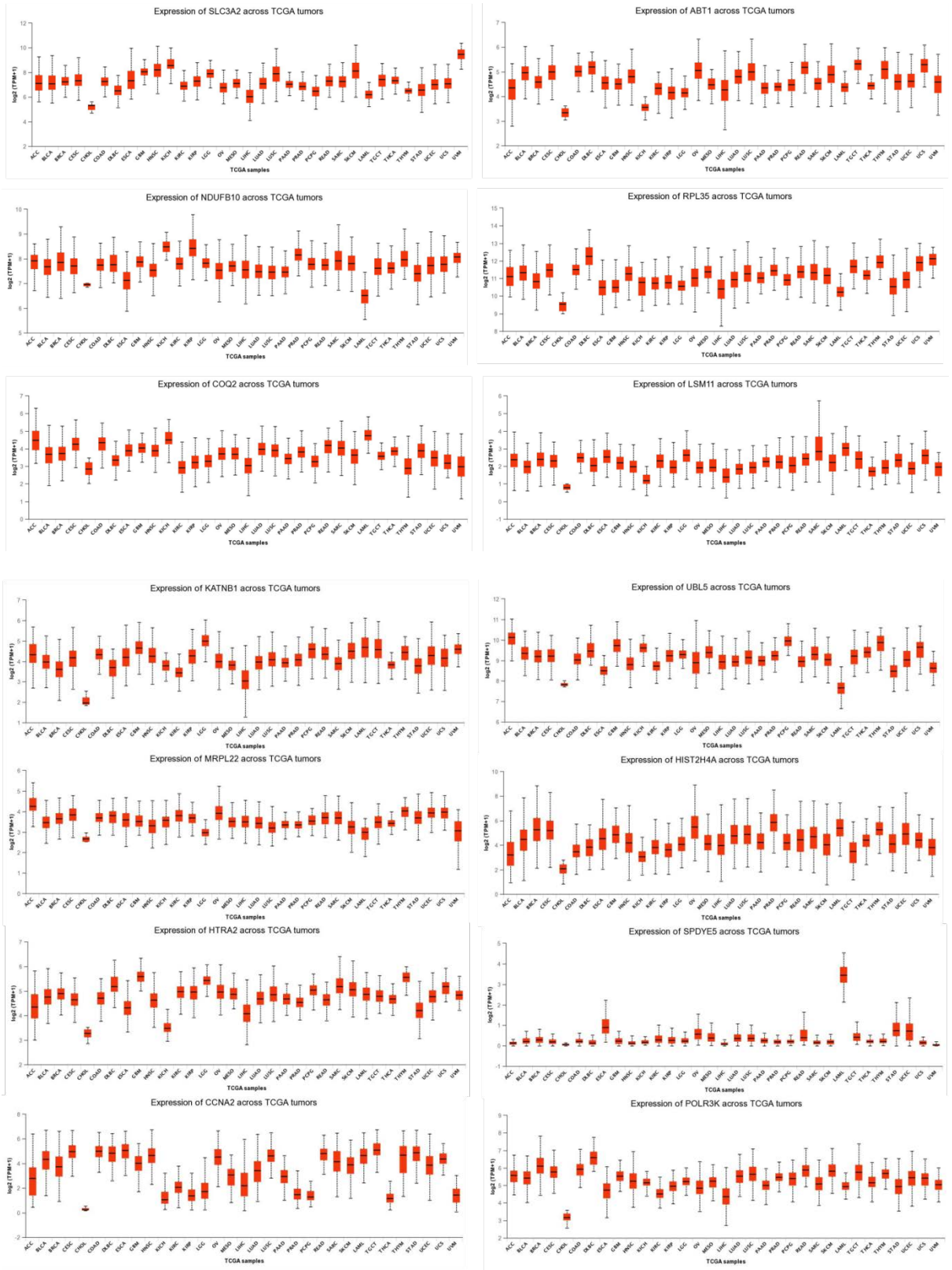

Figure 5.10 Expression level of selected gene in different TCGA tumors.

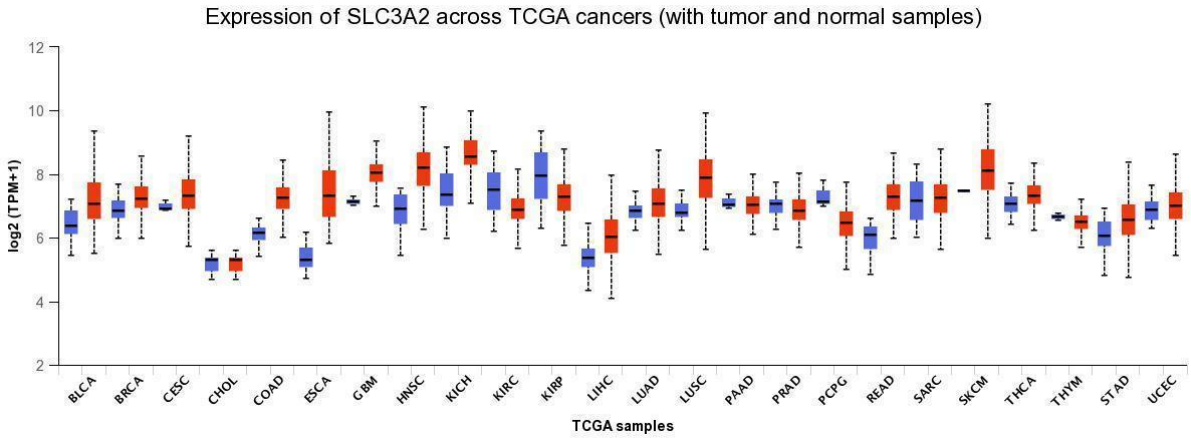

Figure 5.11 Comparison of SLC3A2 expression in different TCGA tumors with normal controls.

The comparison of SLC3A2 expression between uveal melanoma and normal control samples was not provided in this analysis. The tumor types types included in the analysis are adrenocortical carcinoma (ACC), bladder urothelial carcinoma (BLCA), cervical squamous cell carcinoma and endocervical adenocarcinoma (CESC), cholangiocarcinoma (CHOL), colon adenocarcinoma (COAD), lymphoid neoplasm diffuse large B-cell lymphoma (DLBC), esophageal carcinoma (ESCA), glioblastoma multiforme (GBM), head and neck squamous cell carcinoma (HNSC), kidney chromophobe (KICH), kidney renal clear cell carcinoma (KIRP), brain lower grade glioma (LGG), ovarian serous cystadenocarcinoma (OV), mesothelioma (MESO), liver hepatocellular carcinoma (LIHC), Lung adenocarcinoma (LUAD), lung squamous cell carcinoma (LUSC), pancreatic adenocarcinoma (PAAD), prostate adenocarcinoma (PRAD), pheochromocytoma and paraganglioma (PCPG), rectum adenocarcinoma (READ), sarcoma (SARC), skin cutaneous melanoma (SKCM), acute myeloid leukemia (LAML), testicular germ cell tumors (TGCT), thyroid carcinoma (THCA), thymoma (THYM), stomach adenocarcinoma (STAD), uterine corpus endometrial carcinoma (UCEC), uterine carcinosarcoma (UCS), uveal melanoma (UVM).

5.3 Discussion

UM is a relatively rare but deadly ocular cancer. As UM and SKCM are biologically distinct, treatments effective for the latter may have limited or minimal activity in UM. Also, for UM patients at an advanced stage, there is no standard treatment. Even timely enucleation cannot prevent fatal metastases from developing. Compared with SKCM, UM is under-studied. For example, UALCAN, the online tool that we used to evaluate gene expression in UM, only included UM data this March. Less information, e.g. patient ethnicity, was provided compared to other TCGA cancers. It is imperative that we investigate UM to find new therapeutic targets.

Other methods such as Genome-wide association studies (GWASs) have been used to study cancer biology. In the past few years, GWASs have identified thousands of genetic variants that might be associated with common diseases or traits. Whether these variants could lead to therapeutic applications needs to be further assessed with functional genetic tests.

Advances in functional genetic fields have facilitated the study of disease-related genes. Genomic perturbation tools, especially CRISPR, open new possibilities for analyzing how genetic variants affect phenotypes. The genome-wide CRISPR knockout screen has been reported to perform better with minimal off-target effects and experimental consistency compared with knockdown approaches[156]. So far, a handful of genes, including *MSH2*[157], *TRPS1*[166], *ENL*[167], *DCPS*[168], *NF2*, *CUL3*, *TADA2B*, and *TADA1*[156] have been found to be novel targets for various cancer types using this leading genetic approach.

In our primary screen, we found 56 possible hits that lost three or more sgRNAs during selection. We then applied different algorithms for data analysis and identified 15 overlapped genes that were considered to be potentially essential for growth and proliferation of UM with two most commonly used algorithms. Major pathways including metabolic process, cellular process were found to be closely associated with these genes. Shared gene information in GeneCards[169] and previous studies indicated that most of

these genes were related with the biological process of cancer cells, including mitochondrial activity, endoplasmic reticulum docking, pre-mRNA splicing or cell proliferation. Whether these genes are directly associated with uveal melanoma biology or with cancer progress is yet to be uncovered. The expression level of three genes, *COQ2*, *MRPL22* and *POLR3K*, are associated with UM patient survival.

Out of these 15 genes, one promising target gene *SLC3A2* (Solute carrier family 3 member 2) (also known as *CD98hc*) is a transmembrane protein and exists as a heavy chain of heterodimer with a large neutral amino acid transporter L-type amino acid transporter 1 (*LAT1* or *SLC7A5*) in cells[170,171]. SLC3A2 overexpression widely occurs in different cancer cells such as skin squamous cell carcinoma[170], gastric cancer[172] and osteosarcoma[173]. Overexpression of *SLC3A2* in various cancers was also confirmed by our analysis using TCGA data in that the expression of *SLC3A2* was higher in cancer compared with normal controls in each cancer type. Overexpression of *SLC3A2* in UM has not been reported to date. Interestingly, through analysis based on TCGA data, we found that the overall expression level of *SLC3A2* is higher in UM than in other tumors. Although no conclusion can be drawn in the pan-cancer view, we could see the trend of expression among different cancer types. One hypothesis of *SLC3A2* overexpression in UM is that it could be mediated in part with hippo pathway effectors YAP. A previous study showed that transcriptional co-activators *YAP* and *TAZ* could promote cell growth through *SLC7A5* (*LAT1*) [174]. Over 80% of UM is associated with mutations in the *GNAQ* and *GNA11* oncogenes, encoding heterotrimeric Gαq family members[140,141]. Feng et al.[175] found that Gαq stimulates *YAP* and promotes the *YAP*-dependent growth of UM cells. Therefore, *SLC7A5* might be a potential therapeutic target in UM. This hypothesis, however, was been further validated in our study.

Another possible target gene *COQ2* (Coenzyme Q2, Polyprenyl transferase) encodes for the biosynthesis of *COQ* (ubiquinone), an electron and proton carrier in the mitochondrial respiratory chain and a lipid-soluble antioxidant[176]. The deficiency in coenzyme Q_{10} related

to the *COQ2* gene was associated with retinopathy in some patients[177]; homozygous mutation visual dysfunction trait related to rod-cone retinopathy was also observed[178].

RPL35 and *POLR3K* are differentially expressed in the MCF-7 and MDA-MB-231 breast tumor cell lines and are associated with the Translation- and Transcription-related molecular pathways[179]. No previous findings have shown any link between these two genes and UM, and it is interesting to confirm whether these genes play a vital role in UM growth and proliferation.

CCNA2 (CyclinA2) is a highly conserved member of the cyclin family and functions as a regulator in the cell cycle[180]. *CCNA2* is identified as a prognosis biomarker for estrogen-positive breast cancer and tamoxifen resistance[181]. Diseases associated with *CCNA2* include Retinoblastoma, the most common eye cancer in children. Whether this gene is directly associated with UM, the most common form of intraocular cancer in adults, needs to be validated in future studies.

These 15 selected genes are located in different chromosomes, including chromosome 1, 2, 3, 4, 5, 6, 7, 9, 11, 16 and 19. Most of them are protein-coding genes, playing an important role in many biological processes, including cellular metabolism, biosynthetic and protein transportation.

Due to time constraints, our screening results are preliminary *in vitro* study. It is necessary to take further downstream steps: a secondary focused screening, with gene-by-gene knockout screen via cell viability assay in uveal melanoma cells to exclude false positive results based on these bioinformatics analysis, followed by confirmation of phenotypic changes such as protein level change, and moreover preferably *in vivo* screening in a UM animal model could be performed to validate our identification of these novel therapeutic targets.

Nonetheless, we have identified some novel genes essential for the proliferation and growth of UM via *in vitro* “genome-wide CRISPR/Cas9 screen”. Our work provides new insights to the molecular mechanisms of UM and reveal new therapeutic targets for this

devastating disease and will probably lead to more translational studies for the treatment of uveal melanoma.

6 GENERAL DISCUSSION AND CONCLUSIONS

Inherited retinal diseases are disabling disorders of visual function that affect millions of people worldwide. Despite the development of next-generation sequencing that helps identify more genetic variants associated with inherited retinal degeneration, there remains no effective treatment for the majority of these genetic disorders.

Advances in genome editing techniques, in particular, the recent advances in CRISPR/Cas technology, has renewed excitement in ocular gene-based therapy for inherited retinal diseases. A handful of preclinical animal studies have shown the feasibility and efficacy of CRISPR/Cas-based treatment in retinal degenerative diseases including retinitis pigmentosa, LCA, AMD etc. More exciting news is the recent commencement of a phase 1/2 clinical trial employing AAV mediated CRISPR/Cas to treat LCA patients (ClinicalTrials.gov; identifier: NCT03872479), the first ever somatic genome editing trial in humans. With its great power of CRISPR/Cas gene editing to directly and permanently correct the genome, comes with great concerns and challenges, and as such the principal issues in the clinical consideration of somatic gene editing need to be fully addressed, which includes improving *in vivo* gene editing efficiency and efficacy, eliminating off-target effects etc.

Although previous studies have shown the efficiency of CRISPR/Cas gene editing in the retina using electroporation[19,21,51,72], this approach is not applicable in a clinical setting. Our group demonstrated the first *in vivo* use of CRISPR/Cas9 in the adult retina using AAV2 delivery[20]. With the encouraging results of the high efficiency of genome editing in the retina via AAV2 delivery in previous study, the central aim of this thesis is to validate the feasibility and efficacy of a “clinic-ready” AAV-mediated CRISPR/Cas gene editing in the retina.

Safe delivery of CRISPR/Cas endonucleases remains one of the major barriers to the widespread application of *in vivo* genome editing. Potentially deleterious effects of prolonged over-expression of CRISPR/Cas endonuclease, including elevated off-target

cleavage and cellular immune responses, remain important safety hurdles to clinical application. Therefore the first aim of this thesis was to validate a self-destructing CRISPR/Cas system with reduced expression of Cas endonuclease to reduce off-target and immune response or cellular toxicity in the retina. The first part of this thesis demonstrated that similar efficiency in *YFP*-gene perturbation between a conventional and a kamikaze-CRISPR/Cas system: AAV2-mediated delivery of YFP/SpCas9-targeting CRISPR/Cas significantly reduced the number of YFP fluorescent cells among mCherry-expressing cells (~85.5% reduction compared to LacZ/SpCas9-targeting CRISPR/Cas) in the transfected retina of Thy1-YFP transgenic mice.

The main limitation of this body of work was lack of accurate *in vivo* off-target detection method. No significant candidate genes for the off-target sites were found by whole-exome sequencing in the treated mouse retina, which indicated that the reduction of retinal function might not arise from off-target effect from YFP sgRNAs or SpCas9 sgRNA. However, WES is unable to accurately detect *in vivo* off-target cleavages. Recently developed *in vivo* off-target detection strategies such as VIVO[88] or DISCOVER-Seq[89] methods could be applied in future *in vivo* studies to provide unbiased and more accurate detection of genome editing off-targets.

We found differences between *in vitro* and *in vivo* models, especially in SpCas9 sgRNA/YFP sgRNA6 construct (% YFP reduction *in vitro*: 93.5% vs *in vivo*: 49.5%) and YFP sgRNA6 construct (% YFP reduction *in vitro*: 91.4% vs *in vivo*: 58.3%). This difference may be due to the fact that a dual AAV2 vector system was employed to deliver the kamikaze-CRISPR/Cas constructs *in vivo*. In this case, it may be necessary to conduct studies on CRISPR-based editing efficiency via a single viral vector system employing smaller Cas9 orthologs such as SaCas9 or CjCas9 and compare these different Cas endonucleases. With the expanding repertoire of CRISPR/Cas endonucleases, such as Cas12a, SaCas9 and CjCas9, a single viral vector system employing these Cas9 orthologs may provide better *in vivo* editing efficiency. It is, however, not clear which of these are most efficacious for retinal editing *in vivo*. Neither do we know whether a single

delivery of a certain CRISPR/Cas system would outperform the dual delivery system package using the same Cas endonucleases and sgRNA. To answer this question, the second aim of this thesis was to compare the CRISPR/Cas endonuclease activity in retinal cells *in vivo*.

To test CRISPR/Cas editing efficiency in the whole retina instead of the inner retina in the first study, we used a different fluorescent transgenic mice model, CMV-Cre::Rosa26-YFP transgenic mice, with YFP expression in the whole retina under a ubiquitous promoter. To achieve high transduction in the whole retina, an AAV2-based variant AAV7m8, was used for *in vivo* delivery through intravitreal injection. High AAV7m8 penetration in the retinas was observed, which is consistent with other studies using AAV7m8 for gene delivery. As intravitreal injection is a technically easier, less invasive, safer and more reproducible procedure compared with subretinal injection, transgenes or CRISPR constructs delivered with AAV7m8 could have great potential in addressing inherited retinal diseases involving photoreceptors or RPE. While the difference in transduction efficiency among different species, e.g. rodent versus non-human primate, should be further tested and compared, AAV7m8 might be a great tool for gene delivery with robust transduction in the retina.

We tested and compared the gene-editing efficiency of currently available Cas endonucleases both *in vitro* and *in vivo*. We found a great difference in genome-editing efficiency *in vitro* versus *in vivo*. The overall efficiency of YFP disruption in engineered YFP-expressing HEK293A cells in almost all designed *YFP*-targeting sgRNAs co-delivered with respective Cas endonuclease is high, with SpCas9 and Cas12a better than SaCas9 and CjCas9. For the *in vivo* test, SpCas9 was the best-performing Cas endonuclease among all those we tested. However, the difference in editing efficiency among other Cas endonuclease via single or dual vector delivery was not as notable as in the *in vitro* test, with unexpected variation in individual animals within the same group.

We have taken the following steps to ensure a relatively fair comparison for editing efficiency between different CRISPR/Cas systems. Firstly, we checked the *YFP* gene for all the potential PAM sites for each Cas endonuclease and then designed sgRNA targeting

YFP within the similar region. Also, we ensured that the expression of each endonuclease was being driven by the same ubiquitous promoter (miniCMV) and allowed for the same viral delivery method. The only exception is CjCas9, which had poor expression via western blot, so we added an extra CjCas9 driven by a stronger promoter CMV. Nonetheless, CjCas9 showed minimal knockout of YFP by FACS analysis *in vivo*. When I started this project, there was no human-codon optimized version of CjCas9, which may explain the difference in editing efficiency compared to another group[29]. Moreover, there is a tradeoff between aiming to target the same region of the *YFP* gene for a fair comparison versus each sgRNA having similar efficacy.

One limitation of this part is that we didn't directly sequence the sorted cells to further investigate the indels between each group or check the ones with exceedingly high editing efficiency. In order to explain the variation in knockout efficiency among individual mice within the same group and draw a more solid conclusion, more work might be needed in the future.

As the central aim of this thesis is the optimization and validation of a "clinic ready" CRISPR/Cas system, it would be particularly interesting and exciting to find a novel therapeutic target in human eye diseases for which we could apply this therapy in the future. For this purpose, the last part of this thesis illustrated the feasibility of employing GeCKO screening strategy to identify potential therapeutic targets for a human ocular cancer, uveal melanoma. The preliminary *in vitro* findings revealed 56 possible hits that lost three or more sgRNAs during selection, with 15 overlapped genes identified as potential essential genes for the growth and proliferation of UM. Major pathways including metabolic process and cellular process were found to closely interact with these identified genes.

The limitation of this part is that our screening results are preliminary *in vitro* results due to time constraints. It is necessary to take further downstream steps: gene-by-gene knockout screen via cell viability assay and preferably an *in vivo* screening in a UM animal model could be conducted to further validate these novel therapeutic targets.

Conclusions

In summary, this thesis has demonstrated a novel self-destructive kamikaze-CRISPR/Cas system, which can effectively reduce the expression of SpCas9 in the mouse retina, without substantially sacrificing on-target editing efficiency. Also, the results of this thesis illustrated that SpCas9 achieved the highest knockout efficacy among all Cas endonucleases *in vivo*, and AAV2 based variant AAV7m8-mediated delivery of CRISPR/Cas constructs achieved effective transduction and deeper penetration in the adult mouse retina. Furthermore, using an *in vitro* GeCKO screen method, the last part of this thesis identified 15 novel genes that appear to underpin the proliferation and growth of UM.

Taken together, this thesis provides original, useful additional knowledge and new insight for the *in vivo* application of CRISPR/Cas gene editing in the retina. We expect our findings will lead to more translational research “from bench to bedside” that eventually contribute to the development of “clinic ready” CRISPR/Cas-based genome editing to treat devastating ocular diseases.

7 REFERENCES

1. Neveling, K. *et al.* Next-generation genetic testing for retinitis pigmentosa. *Hum. Mutat.* 33, 963–972 (2012).
2. Ratnapriya, R. & Swaroop, A. Genetic architecture of retinal and macular degenerative diseases: the promise and challenges of next-generation sequencing. *Genome Med.* 5, 84 (2013).
3. Bainbridge, J. W. B. *et al.* Long-term effect of gene therapy on Leber's congenital amaurosis. *N. Engl. J. Med.* 372, 1887–1897 (2015).
4. Jacobson, S. G. *et al.* Improvement and decline in vision with gene therapy in childhood blindness. *N. Engl. J. Med.* 372, 1920–1926 (2015).
5. Lee, J. H. *et al.* Gene therapy for visual loss: Opportunities and concerns. *Prog. Retin. Eye Res.* 68, 31–53 (2019).
6. Le Meur, G. *et al.* Safety and Long-Term Efficacy of AAV4 Gene Therapy in Patients with RPE65 Leber Congenital Amaurosis. *Mol. Ther.* 26, 256–268 (2018).
7. Maguire, A. M. *et al.* Safety and efficacy of gene transfer for Leber's congenital amaurosis. *N. Engl. J. Med.* 358, 2240–2248 (2008).
8. Maguire, A. M. *et al.* Age-dependent effects of RPE65 gene therapy for Leber's congenital amaurosis: a phase 1 dose-escalation trial. *Lancet* 374, 1597–1605 (2009).
9. Barrangou, R. *et al.* CRISPR provides acquired resistance against viruses in prokaryotes. *Science* 315, 1709–1712 (2007).
10. Garneau, J. E. *et al.* The CRISPR/Cas bacterial immune system cleaves bacteriophage and plasmid DNA. *Nature* 468, 67–71 (2010).
11. Mali, P. *et al.* RNA-guided human genome engineering via Cas9. *Science* 339, 823–826 (2013).
12. Cong, L. *et al.* Multiplex genome engineering using CRISPR/Cas systems. *Science* 339, 819–823 (2013).
13. Makarova, K. S. *et al.* An updated evolutionary classification of CRISPR-Cas systems.

Nat. Rev. Microbiol. 13, 722–736 (2015).

14. Zetsche, B. *et al.* Cpf1 is a single RNA-guided endonuclease of a class 2 CRISPR-Cas system. *Cell* 163, 759–771 (2015).
15. Makarova, K. S., Zhang, F. & Koonin, E. V. SnapShot: Class 1 CRISPR-Cas Systems. *Cell* 168, 946–946.e1 (2017).
16. Makarova, K. S., Zhang, F. & Koonin, E. V. SnapShot: Class 2 CRISPR-Cas Systems. *Cell* vol. 168 328–328.e1 (2017).
17. Mali, P., Esvelt, K. M. & Church, G. M. Cas9 as a versatile tool for engineering biology. *Nat. Methods* 10, 957–963 (2013).
18. Jinek, M. *et al.* A programmable dual-RNA-guided DNA endonuclease in adaptive bacterial immunity. *Science* 337, 816–821 (2012).
19. Bakondi, B. *et al.* In Vivo CRISPR/Cas9 Gene Editing Corrects Retinal Dystrophy in the S334ter-3 Rat Model of Autosomal Dominant Retinitis Pigmentosa. *Mol. Ther.* 24, 556–563 (2016).
20. Hung, S. S. C. *et al.* AAV-Mediated CRISPR/Cas Gene Editing of Retinal Cells In Vivo. *Invest. Ophthalmol. Vis. Sci.* 57, 3470–3476 (2016).
21. Latella, M. C. *et al.* In vivo Editing of the Human Mutant Rhodopsin Gene by Electroporation of Plasmid-based CRISPR/Cas9 in the Mouse Retina. *Mol. Ther. Nucleic Acids* 5, e389 (2016).
22. Ruan, G.-X. *et al.* CRISPR/Cas9-Mediated Genome Editing as a Therapeutic Approach for Leber Congenital Amaurosis 10. *Mol. Ther.* 25, 331–341 (2017).
23. Yu, W. *et al.* Nrl knockdown by AAV-delivered CRISPR/Cas9 prevents retinal degeneration in mice. *Nat. Commun.* 8, 14716 (2017).
24. Huang, X. *et al.* Genome editing abrogates angiogenesis in vivo. *Nat. Commun.* 8, 112 (2017).
25. Jain, A. *et al.* CRISPR-Cas9-based treatment of myocilin-associated glaucoma. *Proc. Natl. Acad. Sci. U. S. A.* 114, 11199–11204 (2017).
26. Tsai, Y.-T. *et al.* Clustered Regularly Interspaced Short Palindromic Repeats-Based

Genome Surgery for the Treatment of Autosomal Dominant Retinitis Pigmentosa. *Ophthalmology* 125, 1421–1430 (2018).

27. Li, F. *et al.* Title Page Efficacy and dynamics of self-targeting CRISPR/Cas constructs for gene editing in the retina. doi:10.1101/243683.
28. Maeder, M. L. *et al.* Development of a gene-editing approach to restore vision loss in Leber congenital amaurosis type 10. *Nat. Med.* 25, 229–233 (2019).
29. Kim, E. *et al.* In vivo genome editing with a small Cas9 orthologue derived from Campylobacter jejuni. *Nat. Commun.* 8, 14500 (2017).
30. Jo, D. H. *et al.* Long-Term Effects of In Vivo Genome Editing in the Mouse Retina Using Campylobacter jejuni Cas9 Expressed via Adeno-Associated Virus. *Mol. Ther.* 27, 130–136 (2019).
31. Koo, T. *et al.* CRISPR-LbCpf1 prevents choroidal neovascularization in a mouse model of age-related macular degeneration. *Nat. Commun.* 9, 1855 (2018).
32. Xia, C.-H. *et al.* Essential function of NHE8 in mouse retina demonstrated by AAV-mediated CRISPR/Cas9 knockdown. *Exp. Eye Res.* 176, 29–39 (2018).
33. Ran, F. A. *et al.* Double nicking by RNA-guided CRISPR Cas9 for enhanced genome editing specificity. *Cell* 154, 1380–1389 (2013).
34. Giannelli, S. G. *et al.* Cas9/sgRNA selective targeting of the P23H Rhodopsin mutant allele for treating retinitis pigmentosa by intravitreal AAV9.PHP.B-based delivery. *Hum. Mol. Genet.* 27, 761–779 (2018).
35. Qi, L. S. *et al.* Repurposing CRISPR as an RNA-guided platform for sequence-specific control of gene expression. *Cell* 152, 1173–1183 (2013).
36. Ma, H. *et al.* Multiplexed labeling of genomic loci with dCas9 and engineered sgRNAs using CRISPRainbow. *Nat. Biotechnol.* 34, 528–530 (2016).
37. Komor, A. C., Kim, Y. B., Packer, M. S., Zuris, J. A. & Liu, D. R. Programmable editing of a target base in genomic DNA without double-stranded DNA cleavage. *Nature* 533, 420–424 (2016).
38. Gaudelli, N. M. *et al.* Programmable base editing of A•T to G•C in genomic DNA

without DNA cleavage. *Nature* 551, 464–471 (2017).

39. Chadwick, A. C., Wang, X. & Musunuru, K. In Vivo Base Editing of PCSK9 (Proprotein Convertase Subtilisin/Kexin Type 9) as a Therapeutic Alternative to Genome Editing. *Arterioscler. Thromb. Vasc. Biol.* 37, 1741–1747 (2017).
40. Yeh, W.-H., Chiang, H., Rees, H. A., Edge, A. S. B. & Liu, D. R. In vivo base editing of post-mitotic sensory cells. *Nat. Commun.* 9, 2184 (2018).
41. Carreras, A. *et al.* In vivo genome and base editing of a human PCSK9 knock-in hypercholesterolemic mouse model. *BMC Biol.* 17, 4 (2019).
42. Doudna, J. A. & Charpentier, E. The new frontier of genome engineering with CRISPR-Cas9. *Science* 346, 1258096 (2014).
43. Hsu, P. D., Lander, E. S. & Zhang, F. Development and applications of CRISPR-Cas9 for genome engineering. *Cell* (2014).
44. Kim, K. *et al.* Genome surgery using Cas9 ribonucleoproteins for the treatment of age-related macular degeneration. *Genome Res.* 27, 419–426 (2017).
45. Holmgaard, A. *et al.* In Vivo Knockout of the Vegfa Gene by Lentiviral Delivery of CRISPR/Cas9 in Mouse Retinal Pigment Epithelium Cells. *Mol. Ther. Nucleic Acids* 9, 89–99 (2017).
46. Swiech, L. *et al.* In vivo interrogation of gene function in the mammalian brain using CRISPR-Cas9. *Nat. Biotechnol.* 33, 102–106 (2015).
47. Cheng, R. *et al.* Efficient gene editing in adult mouse livers via adenoviral delivery of CRISPR/Cas9. *FEBS Lett.* 588, 3954–3958 (2014).
48. Nishiyama, J., Mikuni, T. & Yasuda, R. Virus-Mediated Genome Editing via Homology-Directed Repair in Mitotic and Postmitotic Cells in Mammalian Brain. *Neuron* 96, 755–768.e5 (2017).
49. Suzuki, K. *et al.* In vivo genome editing via CRISPR/Cas9 mediated homology-independent targeted integration. *Nature* 540, 144–149 (2016).
50. Cai, Y. *et al.* In vivo genome editing rescues photoreceptor degeneration via a Cas9/RecA-mediated homology-directed repair pathway. *Science Advances* vol. 5

eaav3335 (2019).

51. Li, P. *et al.* Allele-Specific CRISPR-Cas9 Genome Editing of the Single-Base P23H Mutation for Rhodopsin-Associated Dominant Retinitis Pigmentosa. *CRISPR J* 1, 55–64 (2018).
52. Home - ClinicalTrials.gov. https://clinicaltrials.gov/.
53. Biffi, A. Gene therapy as a curative option for beta-thalassemia. *N. Engl. J. Med.* (2018).
54. Home - ClinicalTrials.gov. https://clinicaltrials.gov/.
55. Vannucci, L., Lai, M., Chiuppesi, F., Ceccherini-Nelli, L. & Pistello, M. Viral vectors: a look back and ahead on gene transfer technology. *New Microbiol.* 36, 1–22 (2013).
56. Wang, D., Tai, P. W. L. & Gao, G. Adeno-associated virus vector as a platform for gene therapy delivery. *Nat. Rev. Drug Discov.* 18, 358–378 (2019).
57. Li, F. *et al.* Utility of self-destructing CRISPR/Cas constructs for targeted gene editing in the retina. *Hum. Gene Ther.* (2019) doi:10.1089/hum.2019.021.
58. Ding, Q. *et al.* Permanent alteration of PCSK9 with in vivo CRISPR-Cas9 genome editing. *Circ. Res.* 115, 488–492 (2014).
59. Wang, X., Raghavan, A., Chen, T. & Qiao, L. CRISPR-Cas9 Targeting of PCSK9 in Human Hepatocytes In Vivo—Brief Report. *, and vascular biology* (2016).
60. Wang, D. *et al.* Adenovirus-Mediated Somatic Genome Editing of Pten by CRISPR/Cas9 in Mouse Liver in Spite of Cas9-Specific Immune Responses. *Hum. Gene Ther.* 26, 432–442 (2015).
61. Stephens, C. J., Kashentseva, E., Everett, W., Kaliberova, L. & Curiel, D. T. Targeted in vivo knock-in of human alpha-1-antitrypsin cDNA using adenoviral delivery of CRISPR/Cas9. *Gene Ther.* 25, 139–156 (2018).
62. Maddalo, D. *et al.* In vivo engineering of oncogenic chromosomal rearrangements with the CRISPR/Cas9 system. *Nature* 516, 423–427 (2014).
63. Chiou, S.-H. *et al.* Pancreatic cancer modeling using retrograde viral vector delivery and in vivo CRISPR/Cas9-mediated somatic genome editing. *Genes Dev.* 29, 1576–

1585 (2015).

64. Yin, H. *et al.* Non-viral vectors for gene-based therapy. *Nat. Rev. Genet.* 15, 541–555 (2014).
65. Putnam, D. Polymers for gene delivery across length scales. *Nat. Mater.* 5, 439–451 (2006).
66. Zuris, J. A. *et al.* Cationic lipid-mediated delivery of proteins enables efficient protein-based genome editing in vitro and in vivo. *Nat. Biotechnol.* 33, 73–80 (2015).
67. Gao, X. *et al.* Treatment of autosomal dominant hearing loss by in vivo delivery of genome editing agents. *Nature* 553, 217–221 (2018).
68. Yuan, L. *et al.* CRISPR/Cas9-mediated GJA8 knockout in rabbits recapitulates human congenital cataracts. *Sci. Rep.* 6, 22024 (2016).
69. Yuan, L. *et al.* CRISPR/Cas9-Mediated Mutation of αA-Crystallin Gene Induces Congenital Cataracts in Rabbits. *Invest. Ophthalmol. Vis. Sci.* 58, BIO34–BIO41 (2017).
70. Yeo, J. H. *et al.* Development of a Pde6b Gene Knockout Rat Model for Studies of Degenerative Retinal Diseases. *Invest. Ophthalmol. Vis. Sci.* 60, 1519–1526 (2019).
71. Dong, F. *et al.* A Mouse Model of Schnyder Corneal Dystrophy with the N100S Point Mutation. *Sci. Rep.* 8, 10219 (2018).
72. Wang, S., Sengel, C., Emerson, M. M. & Cepko, C. L. A gene regulatory network controls the binary fate decision of rod and bipolar cells in the vertebrate retina. *Dev. Cell* 30, 513–527 (2014).
73. Campla, C. K. *et al.* Targeted deletion of an NRL- and CRX-regulated alternative promoter specifically silences FERM and PDZ domain containing 1 (Frmpd1) in rod photoreceptors. *Hum. Mol. Genet.* 28, 804–817 (2019).
74. Dias, M. F. *et al.* Molecular genetics and emerging therapies for retinitis pigmentosa: Basic research and clinical perspectives. *Prog. Retin. Eye Res.* 63, 107–131 (2018).
75. den Hollander, A. I. *et al.* Mutations in the CEP290 (NPHP6) gene are a frequent cause of Leber congenital amaurosis. *Am. J. Hum. Genet.* 79, 556–561 (2006).

76. Perrault, I. *et al.* Spectrum of NPHP6/CEP290 mutations in Leber congenital amaurosis and delineation of the associated phenotype. *Hum. Mutat.* 28, 416 (2007).
77. Vallespin, E. *et al.* Frequency of CEP290 c.2991_1655A>G mutation in 175 Spanish families affected with Leber congenital amaurosis and early-onset retinitis pigmentosa. *Mol. Vis.* 13, 2160–2162 (2007).
78. Zhang, W., Li, L., Su, Q., Gao, G. & Khanna, H. Gene Therapy Using a miniCEP290 Fragment Delays Photoreceptor Degeneration in a Mouse Model of Leber Congenital Amaurosis. *Hum. Gene Ther.* 29, 42–50 (2018).
79. Collin, R. W. *et al.* Antisense Oligonucleotide (AON)-based Therapy for Leber Congenital Amaurosis Caused by a Frequent Mutation in CEP290. *Mol. Ther. Nucleic Acids* 1, e14 (2012).
80. Gerard, X. *et al.* AON-mediated Exon Skipping Restores Ciliation in Fibroblasts Harboring the Common Leber Congenital Amaurosis CEP290 Mutation. *Mol. Ther. Nucleic Acids* 1, e29 (2012).
81. Geller, A. M. & Sieving, P. A. Assessment of foveal cone photoreceptors in Stargardt's macular dystrophy using a small dot detection task. *Vision Res.* 33, 1509–1524 (1993).
82. Geller, A. M., Sieving, P. A. & Green, D. G. Effect on grating identification of sampling with degenerate arrays. *J. Opt. Soc. Am. A* 9, 472–477 (1992).
83. Erke, M. G. *et al.* Prevalence of age-related macular degeneration in elderly Caucasians: the Tromsø Eye Study. *Ophthalmology* 119, 1737–1743 (2012).
84. Kawasaki, R. *et al.* The prevalence of age-related macular degeneration in Asians: a systematic review and meta-analysis. *Ophthalmology* 117, 921–927 (2010).
85. Wong, W. L. *et al.* Global prevalence of age-related macular degeneration and disease burden projection for 2020 and 2040: a systematic review and meta-analysis. *Lancet Glob Health* 2, e106–16 (2014).
86. Tamm, E. R. Myocilin and glaucoma: facts and ideas. *Prog. Retin. Eye Res.* 21, 395–428 (2002).

87. Tsai, S. Q. *et al.* CIRCLE-seq: a highly sensitive in vitro screen for genome-wide CRISPR-Cas9 nuclease off-targets. *Nat. Methods* 14, 607–614 (2017).
88. Akcakaya, P. *et al.* In vivo CRISPR editing with no detectable genome-wide off-target mutations. *Nature* 561, 416–419 (2018).
89. Wienert, B. *et al.* Unbiased detection of CRISPR off-targets in vivo using DISCOVER-Seq. *Science* 364, 286–289 (2019).
90. Moreno-Mateos, M. A. *et al.* CRISPRscan: designing highly efficient sgRNAs for CRISPR-Cas9 targeting in vivo. *Nat. Methods* 12, 982–988 (2015).
91. Kleinstiver, B. P. *et al.* High-fidelity CRISPR-Cas9 nucleases with no detectable genome-wide off-target effects. *Nature* 529, 490–495 (2016).
92. Slaymaker, I. M. *et al.* Rationally engineered Cas9 nucleases with improved specificity. *Science* 351, 84–88 (2016).
93. Davis, K. M., Pattanayak, V., Thompson, D. B., Zuris, J. A. & Liu, D. R. Small molecule-triggered Cas9 protein with improved genome-editing specificity. *Nat. Chem. Biol.* 11, 316–318 (2015).
94. Dow, L. E. *et al.* Inducible in vivo genome editing with CRISPR-Cas9. *Nat. Biotechnol.* 33, 390–394 (2015).
95. Hemphill, J., Borchardt, E. K., Brown, K., Asokan, A. & Deiters, A. Optical Control of CRISPR/Cas9 Gene Editing. *J. Am. Chem. Soc.* 137, 5642–5645 (2015).
96. Nuñez, J. K., Harrington, L. B. & Doudna, J. A. Chemical and Biophysical Modulation of Cas9 for Tunable Genome Engineering. *ACS Chem. Biol.* 11, 681–688 (2016).
97. Li, A. *et al.* A Self-Deleting AAV-CRISPR System for In Vivo Genome Editing. *Mol Ther Methods Clin Dev* 12, 111–122 (2019).
98. Merienne, N. *et al.* The Self-Inactivating KamiCas9 System for the Editing of CNS Disease Genes. *Cell Rep.* 20, 2980–2991 (2017).
99. Chen, Y. *et al.* A Self-restricted CRISPR System to Reduce Off-target Effects. *Mol. Ther.* 24, 1508–1510 (2016).
100. Srivastava, M. *et al.* An inhibitor of nonhomologous end-joining abrogates double-

strand break repair and impedes cancer progression. *Cell* 151, 1474–1487 (2012).

101. Kohout, T. A. *et al.* Augmentation of cardiac contractility mediated by the human beta(3)-adrenergic receptor overexpressed in the hearts of transgenic mice. *Circulation* 104, 2485–2491 (2001).

102. Song, J. *et al.* RS-1 enhances CRISPR/Cas9- and TALEN-mediated knock-in efficiency. *Nat. Commun.* 7, 10548 (2016).

103. Canny, M. D. *et al.* Inhibition of 53BP1 favors homology-dependent DNA repair and increases CRISPR-Cas9 genome-editing efficiency. *Nat. Biotechnol.* 36, 95–102 (2018).

104. Villiger, L. *et al.* Treatment of a metabolic liver disease by in vivo genome base editing in adult mice. *Nat. Med.* 24, 1519–1525 (2018).

105. Hung, S. S. *et al.* Methods for In Vivo CRISPR/Cas Editing of the Adult Murine Retina. *Methods Mol. Biol.* 1715, 113–133 (2018).

106. Bui, B. V. & Fortune, B. Ganglion cell contributions to the rat full-field electroretinogram. *The Journal of Physiology* vol. 555 153–173 (2004).

107. Liu, H.-H. *et al.* Chronic ocular hypertension induced by circumlimbal suture in rats. *Invest. Ophthalmol. Vis. Sci.* 56, 2811–2820 (2015).

108. Livak, K. J. & Schmittgen, T. D. Analysis of Relative Gene Expression Data Using Real-Time Quantitative PCR and the 2−ΔΔCT Method. *Methods* vol. 25 402–408 (2001).

109. Sanjana, N. E., Shalem, O. & Zhang, F. Improved vectors and genome-wide libraries for CRISPR screening. *Nat. Methods* 11, 783–784 (2014).

110. Wang, T., Wei, J. J., Sabatini, D. M. & Lander, E. S. Genetic screens in human cells using the CRISPR-Cas9 system. *Science* 343, 80–84 (2014).

111. Joung, J. *et al.* Genome-scale CRISPR-Cas9 knockout and transcriptional activation screening. *Nat. Protoc.* 12, 828–863 (2017).

112. Winter, J. *et al.* CRISPRAnalyzeR: Interactive analysis, annotation and documentation of pooled CRISPR screens. doi:10.1101/109967.

113. Love, M. I., Huber, W. & Anders, S. Moderated estimation of fold change and dispersion for RNA-seq data with DESeq2. *Genome Biol.* 15, 550 (2014).
114. Li, W. *et al.* MAGeCK enables robust identification of essential genes from genome-scale CRISPR/Cas9 knockout screens. *Genome Biol.* 15, 554 (2014).
115. Robinson, M. D., McCarthy, D. J. & Smyth, G. K. edgeR: a Bioconductor package for differential expression analysis of digital gene expression data. *Bioinformatics* 26, 139–140 (2010).
116. Hart, A. Mann-Whitney test is not just a test of medians: differences in spread can be important. *BMJ* vol. 323 391–393 (2001).
117. Yu, J., Silva, J. & Califano, A. ScreenBEAM: a novel meta-analysis algorithm for functional genomics screens via Bayesian hierarchical modeling. *Bioinformatics* 32, 260–267 (2016).
118. Hart, T. & Moffat, J. BAGEL: a computational framework for identifying essential genes from pooled library screens. *BMC Bioinformatics* vol. 17 (2016).
119. Kolde, R., Laur, S., Adler, P. & Vilo, J. Robust rank aggregation for gene list integration and meta-analysis. *Bioinformatics* vol. 28 573–580 (2012).
120. Chandrashekar, D. S. *et al.* UALCAN: A Portal for Facilitating Tumor Subgroup Gene Expression and Survival Analyses. *Neoplasia* 19, 649–658 (2017).
121. Reimand, J., Kull, M., Peterson, H., Hansen, J. & Vilo, J. g:Profiler—a web-based toolset for functional profiling of gene lists from large-scale experiments. *Nucleic Acids Research* vol. 35 W193–W200 (2007).
122. Raudvere, U. *et al.* g:Profiler: a web server for functional enrichment analysis and conversions of gene lists (2019 update). *Nucleic Acids Research* vol. 47 W191–W198 (2019).
123. Shannon, P. *et al.* Cytoscape: a software environment for integrated models of biomolecular interaction networks. *Genome Res.* 13, 2498–2504 (2003).
124. Isserlin, R., Merico, D., Voisin, V. & Bader, G. D. Enrichment Map - a Cytoscape app to visualize and explore OMICs pathway enrichment results. *F1000Res.* 3, 141 (2014).

125. Reimand, J. *et al.* Pathway enrichment analysis and visualization of omics data using g:Profiler, GSEA, Cytoscape and EnrichmentMap. *Nature Protocols* vol. 14 482–517 (2019).
126. Katoh, K., Rozewicki, J. & Yamada, K. D. MAFFT online service: multiple sequence alignment, interactive sequence choice and visualization. *Brief. Bioinform.* (2017) doi:10.1093/bib/bbx108.
127. Hsu, P. D. *et al.* DNA targeting specificity of RNA-guided Cas9 nucleases. *Nat. Biotechnol.* 31, 827–832 (2013).
128. Fu, Y., Sander, J. D., Reyon, D., Cascio, V. M. & Joung, J. K. Improving CRISPR-Cas nuclease specificity using truncated guide RNAs. *Nat. Biotechnol.* 32, 279–284 (2014).
129. Cho, S. W. *et al.* Analysis of off-target effects of CRISPR/Cas-derived RNA-guided endonucleases and nickases. *Genome Res.* 24, 132–141 (2014).
130. Ran, F. A. *et al.* In vivo genome editing using Staphylococcus aureus Cas9. *Nature* 520, 186–191 (2015).
131. Nelson, C. E. *et al.* In vivo genome editing improves muscle function in a mouse model of Duchenne muscular dystrophy. *Science* 351, 403–407 (2016).
132. Park, H. M. *et al.* Extension of the crRNA enhances Cpf1 gene editing in vitro and in vivo. *Nat. Commun.* 9, 3313 (2018).
133. Masubuchi, N., Shidoh, Y., Kondo, S., Takatoh, J. & Hanaoka, K. Subcellular Localization of Dystrophin Isoforms in Cardiomyocytes and Phenotypic Analysis of Dystrophin-deficient Mice Reveal Cardiac Myopathy is Predominantly Caused by a Deficiency in Full-length Dystrophin. *Experimental Animals* vol. 62 211–217 (2013).
134. Khabou, H. *et al.* Insight into the mechanisms of enhanced retinal transduction by the engineered AAV2 capsid variant -7m8. *Biotechnol. Bioeng.* 113, 2712–2724 (2016).
135. 5. In Vivo Directed Evolution of a Novel Adeno-Associated Virus for Therapeutic Outer Retinal Gene Delivery from the Vitreous. *Molecular Therapy* vol. 21 S2 (2013).
136. Dalkara, D. *et al.* In vivo-directed evolution of a new adeno-associated virus for

therapeutic outer retinal gene delivery from the vitreous. *Sci. Transl. Med.* 5, 189ra76 (2013).

137. Isgrig, K. *et al.* AAV2.7m8 is a powerful viral vector for inner ear gene therapy. *Nat. Commun.* 10, 427 (2019).

138. Singh, A. D., Rennie, I. G., Seregard, S., Giblin, M. & McKenzie, J. Sunlight exposure and pathogenesis of uveal melanoma. *Surv. Ophthalmol.* 49, 419–428 (2004).

139. Cancer Genome Atlas Network. Genomic Classification of Cutaneous Melanoma. *Cell* 161, 1681–1696 (2015).

140. Van Raamsdonk, C. D. *et al.* Frequent somatic mutations of GNAQ in uveal melanoma and blue naevi. *Nature* 457, 599–602 (2009).

141. Van Raamsdonk, C. D. *et al.* Mutations in GNA11 in uveal melanoma. *N. Engl. J. Med.* 363, 2191–2199 (2010).

142. Harbour, J. W. *et al.* Frequent mutation of BAP1 in metastasizing uveal melanomas. *Science* 330, 1410–1413 (2010).

143. Bononi, A. *et al.* BAP1 regulates IP3R3-mediated Ca flux to mitochondria suppressing cell transformation. *Nature* 546, 549–553 (2017).

144. Moore, A. R. *et al.* Recurrent activating mutations of G-protein-coupled receptor CYSLTR2 in uveal melanoma. *Nat. Genet.* 48, 675–680 (2016).

145. Uveal Melanomas Harbor Recurrent Activating Mutations in CYSLTR2. *Cancer Discovery* vol. 6 573–573 (2016).

146. Alsafadi, S. *et al.* Cancer-associated SF3B1 mutations affect alternative splicing by promoting alternative branchpoint usage. *Nat. Commun.* 7, 10615 (2016).

147. Furney, S. J. *et al.* SF3B1 mutations are associated with alternative splicing in uveal melanoma. *Cancer Discov.* 3, 1122–1129 (2013).

148. Martin, M. *et al.* Exome sequencing identifies recurrent somatic mutations in EIF1AX and SF3B1 in uveal melanoma with disomy 3. *Nat. Genet.* 45, 933–936 (2013).

149. Robertson, A. G. *et al.* Integrative Analysis Identifies Four Molecular and Clinical Subsets in Uveal Melanoma. *Cancer Cell* 33, 151 (2018).

150. Nathan, P. *et al.* Uveal Melanoma UK National Guidelines. *Eur. J. Cancer* 51, 2404–2412 (2015).

151. Algazi, A. P. *et al.* Clinical outcomes in metastatic uveal melanoma treated with PD-1 and PD-L1 antibodies. *Cancer* 122, 3344–3353 (2016).

152. Dummer, R. *et al.* Cutaneous melanoma: ESMO Clinical Practice Guidelines for diagnosis, treatment and follow-up. *Ann. Oncol.* 26 Suppl 5, v126–32 (2015).

153. Carvajal, R. D. *et al.* Effect of selumetinib vs chemotherapy on progression-free survival in uveal melanoma: a randomized clinical trial. *JAMA* 311, 2397–2405 (2014).

154. Robert, C. *et al.* Selumetinib plus dacarbazine versus placebo plus dacarbazine as first-line treatment for BRAF-mutant metastatic melanoma: a phase 2 double-blind randomised study. *Lancet Oncol.* 14, 733–740 (2013).

155. Aronow, M. E., Topham, A. K. & Singh, A. D. Uveal Melanoma: 5-Year Update on Incidence, Treatment, and Survival (SEER 1973-2013). *Ocul Oncol Pathol* 4, 145–151 (2018).

156. Shalem, O. *et al.* Genome-scale CRISPR-Cas9 knockout screening in human cells. *Science* 343, 84–87 (2014).

157. Goodspeed, A., Jean, A. & Costello, J. C. A Whole-genome CRISPR Screen Identifies a Role of MSH2 in Cisplatin-mediated Cell Death in Muscle-invasive Bladder Cancer. *Eur. Urol.* 75, 242–250 (2019).

158. Yau, E. H. *et al.* Genome-Wide CRISPR Screen for Essential Cell Growth Mediators in Mutant KRAS Colorectal Cancers. *Cancer Res.* 77, 6330–6339 (2017).

159. Korkmaz, G. *et al.* A CRISPR-Cas9 screen identifies essential CTCF anchor sites for estrogen receptor-driven breast cancer cell proliferation. *Nucleic Acids Res.* (2019) doi:10.1093/nar/gkz675.

160. Song, C.-Q. *et al.* Genome-Wide CRISPR Screen Identifies Regulators of Mitogen-Activated Protein Kinase as Suppressors of Liver Tumors in Mice. *Gastroenterology* 152, 1161–1173.e1 (2017).

161. Sun, W. *et al.* Genome-wide CRISPR screen reveals SGOL1 as a druggable target

of sorafenib-treated hepatocellular carcinoma. *Lab. Invest.* 98, 734–744 (2018).

162. Tzelepis, K. *et al.* A CRISPR Dropout Screen Identifies Genetic Vulnerabilities and Therapeutic Targets in Acute Myeloid Leukemia. *Cell Rep.* 17, 1193–1205 (2016).

163. Mercier, F. *et al.* A genome-wide, in vivo dropout CRISPR screen in acute myeloid leukemia. *Experimental Hematology* vol. 53 S78–S79 (2017).

164. Chow, R. D. *et al.* AAV-mediated direct in vivo CRISPR screen identifies functional suppressors in glioblastoma. *Nat. Neurosci.* 20, 1329–1341 (2017).

165. Cancer Genome Atlas Research Network *et al.* The Cancer Genome Atlas Pan-Cancer analysis project. *Nat. Genet.* 45, 1113–1120 (2013).

166. Elster, D. *et al.* TRPS1 shapes YAP/TEAD-dependent transcription in breast cancer cells. *Nat. Commun.* 9, 3115 (2018).

167. Erb, M. A. *et al.* Transcription control by the ENL YEATS domain in acute leukaemia. *Nature* 543, 270–274 (2017).

168. Yamauchi, T. *et al.* Genome-wide CRISPR-Cas9 Screen Identifies Leukemia-Specific Dependence on a Pre-mRNA Metabolic Pathway Regulated by DCPS. *Cancer Cell* 33, 386–400.e5 (2018).

169. GeneCards Human Gene Database. GeneCards - Human Genes | Gene Database | Gene Search. https://www.genecards.org/.

170. Estrach, S. *et al.* CD98hc (SLC3A2) loss protects against ras-driven tumorigenesis by modulating integrin-mediated mechanotransduction. *Cancer Res.* 74, 6878–6889 (2014).

171. Lee, Y. *et al.* Cryo-EM structure of the human L-type amino acid transporter 1 in complex with glycoprotein CD98hc. *Nat. Struct. Mol. Biol.* 26, 510–517 (2019).

172. Wang, S. *et al.* SLC3A2, antigen of mAb 3G9, promotes migration and invasion by upregulating of mucins in gastric cancer. *Oncotarget* 8, 88586–88598 (2017).

173. Zhu, B. *et al.* SLC3A2 is upregulated in human osteosarcoma and promotes tumor growth through the PI3K/Akt signaling pathway. *Oncol. Rep.* 37, 2575–2582 (2017).

174. Hansen, C. G., Ng, Y. L. D., Lam, W.-L. M., Plouffe, S. W. & Guan, K.-L. The Hippo

pathway effectors YAP and TAZ promote cell growth by modulating amino acid signaling to mTORC1. *Cell Res.* 25, 1299–1313 (2015).

175. Feng, X. *et al.* Hippo-independent activation of YAP by the GNAQ uveal melanoma oncogene through a trio-regulated rho GTPase signaling circuitry. *Cancer Cell* 25, 831–845 (2014).

176. Forsman, U., Sjöberg, M., Turunen, M. & Sindelar, P. J. 4-Nitrobenzoate inhibits coenzyme Q biosynthesis in mammalian cell cultures. *Nat. Chem. Biol.* 6, 515–517 (2010).

177. Desbats, M. A. *et al.* The COQ2 genotype predicts the severity of coenzyme Q10 deficiency. *Hum. Mol. Genet.* 25, 4256–4265 (2016).

178. Schottlaender, L. V., Houlden, H. & Multiple-System Atrophy (MSA) Brain Bank Collaboration. Mutant COQ2 in multiple-system atrophy. *The New England journal of medicine* vol. 371 81 (2014).

179. Satih, S. *et al.* Gene Expression Profiling of Breast Cancer Cell Lines in Response to Soy Isoflavones Using a Pangenomic Microarray Approach. *OMICS* 14, 231–238 (2010).

180. O'Leary, N. A. *et al.* Reference sequence (RefSeq) database at NCBI: current status, taxonomic expansion, and functional annotation. *Nucleic Acids Res.* 44, D733–45 (2016).

181. Gao, T. *et al.* CCNA2 is a prognostic biomarker for ER+ breast cancer and tamoxifen resistance. *PLoS One* 9, e91771 (2014).

8 Appendixes

Appendix 1 Plasmid cloning and primers

Table 8.1 List of plasmid cloning by restriction enzyme digest method

Plasmid name	vector	insert	Enzyme
pX551-CMV-SpCas9	pX551	pX601-AAV-CMV::NLS-SaCas9-NLS-3xHA-bGHpA;U6::BsaI-sgRNA	AgeI/XbaI
pX551-miniCMV-SaCas9	pX551-miniCMV-SpCas9	pX601-AAV-CMV::NLS-SaCas9-NLS-3xHA-bGHpA;U6::BsaI-sgRNA	AgeI/EcoRI
pX551-CMV-CjCas9	pX551-miniCMV-CjCas9	pX551-CMV-SpCas9	AgeI/XbaI
pX552-CMV-mCherry	AAV-U6-sgRNA-hSyn-mCherry	pX552-CMV-GFP	ApaI/KpnI
pX552-CMV-mCherry-SpCas9 sgRNA4	pX552-CMV-mCherry	pX552-SpCas9 sgRNA4-LacZ sgRNA-mCherry	MluI

Table 8.2 List of plasmid cloning by PCR

Plasmid name	Vector (enzymes)	Insert PCR template	Primers for PCR
pX551-miniCMV-Cas12a (AsCpf1)	pX551-miniCMV-SpCas9 (AgeI/EcoRI)	pY010 (pcDNA3.1-hAsCpf1)	Kozak Cas12a AgeI F; AsCpf1 EcoRI R
pX552-CMV-GFP	pX552 (ApaI/KpnI)	pHpa-trs-KS-luci	CMV-ApaI F; CMV-KpnI R
pX552-hsyn1 -mCherry-Cas9 sgRNA4 -YFP sgRNA2	pX552-YFP sgRNA2-mCherry (MluI)	pX552-CMV-GFP -SpCas9 sgRNA4	MluI-U6promoter fwd primer; SpCas9 sgRNA scaffold-MluI reverse primer
pX552-hsyn1 -mCherry-Cas9 sgRNA4 -YFP sgRNA6	pX552-hsyn1-mCherry -YFP sgRNA6 (MluI)	pX552-CMV-GFP -SpCas9 sgRNA4	MluI-U6promoter fwd primer; SpCas9 sgRNA scaffold-MluI reverse primer
pX552-hsyn1 -mCherry-Cas9 sgRNA4 -LacZ sgRNA	pX552-LacZ sgRNA-mCherry (MluI)	pX552-CMV-GFP -SpCas9 sgRNA4	MluI-U6promoter fwd primer; SpCas9 sgRNA scaffold-MluI reverse primer

Table 8.3 List of plasmid cloning by oligo annealing

Plasmid name	Vector (enzymes)	Insert (oligo annealing)	
		Top oligo	Bottom oligo
pX551-miniCMV -SpCas9	pX551-CMV-SpCas9 (AgeI/XbaI)	miniCMV-XbaI/AgeI F	miniCMV-XbaI/AgeI R
pX552-CMV-GFP -SpCas9 sgRNA1	pX552-CMV-GFP (SapI)	SpCas9 gRNA1 top	SpCas9 gRNA1 Btm
pX552-CMV-GFP -SpCas9 sgRNA2	pX552-CMV-GFP (SapI)	SpCas9 gRNA2 top	SpCas9 gRNA2 Btm
pX552-CMV-GFP -SpCas9 sgRNA3	pX552-CMV-GFP (SapI)	SpCas9 gRNA3 top	SpCas9 gRNA3 Btm
pX552-CMV-GFP	pX552-CMV-GFP	SpCas9 gRNA4 top	SpCas9 gRNA4 Btm

-SpCas9 sgRNA4	(SapI)		
pX552-hsyn1-mCherry-YFP sgRNA6	pX552-hsyn-mCherry (SapI)	YFP sgRNA6 top (SpCas9)	YFP sgRNA6 btm (SpCas9)
pX552-CMV-mCherry -YFP sgRNA4 (SpCas9)	pX552-CMV-mCherry (SapI)	YFP sgRNA4 top (SpCas9)	YFP sgRNA4 btm (SpCas9)
pX552-CMV-mCherry -YFP sgRNA5 (SpCas9)	pX552-CMV-mCherry (SapI)	YFP sgRNA5 top (SpCas9)	YFP sgRNA5 btm (SpCas9)
pX552-CMV-mCherry -YFP sgRNA6 (SpCas9)	pX552-CMV-mCherry (SapI)	YFP sgRNA6 btm (SpCas9)	YFP sgRNA6 btm (SpCas9)
pX552-CMV-mCherry -LacZ sgRNA (SpCas9)	pX552-CMV-mCherry (SapI)	LacZ sgRNA1 top (SpCas9)	LacZ sgRNA1 btm (SpCas9)
pX552-CMV-mCherry -YFP sgRNA 20nt (Cas12a)	pX552-CMV-mCherry -U6-Cas12a scaffold (SapI)	YFP sgRNA 20nt top (Cas12a)	YFP sgRNA 20nt btm (Cas12a)
pX552-CMV-mCherry -YFP sgRNA 23nt (Cas12a)	pX552-CMV-mCherry -U6-Cas12a scaffold (SapI)	YFP sgRNA 23nt top (Cas12a)	YFP sgRNA 23nt btm (Cas12a)
pX552-CMV-mCherry -LacZ sgRNA 20nt (Cas12a)	pX552-CMV-mCherry -U6-Cas12a scaffold (SapI)	LacZ sgRNA 20nt top (Cas12a)	LacZ sgRNA 20nt top (Cas12a)
pX552-CMV-mCherry-LacZ sgRNA 23nt (Cas12a)	pX552-CMV-mCherry -U6-Cas12a scaffold	LacZ sgRNA 23nt top (Cas12a)	LacZ sgRNA 23nt btm (Cas12a)
pX552-CMV-mCherry -YFP sgRNA (SaCas9)	pX552-CMV-mCherry -U6-SaCas9 scaffold (SapI)	YFP sgRNA (SapI) top (SaCas9)	YFP sgRNA (SapI) btm (SaCas9)
pX552-CMV-mCherry -LacZ sgRNA (SaCas9)	pX552-CMV-mCherry -U6-SaCas9 scaffold (SapI)	LacZ sgRNA (SapI) top (SaCas9)	LacZ sgRNA (SapI) btm (SaCas9)
pX552-CMV-mCherry -YFP sgRNA1 (CjCas9)	pX552-CMV-mCherry -U6-CjCas9 scaffold (SapI)	YFP sgRNA1 top (CjCas9)	YFP sgRNA1 btm (CjCas9)
pX552-CMV-mCherry -YFP sgRNA2 (CjCas9)	pX552-CMV-mCherry -U6-CjCas9 scaffold (SapI)	YFP sgRNA2 top (CjCas9)	YFP sgRNA2 btm (CjCas9)
pX552-CMV-mCherry -LacZ sgRNA (CjCas9)	pX552-CMV-mCherry -U6-CjCas9 scaffold (SapI)	LacZ sgRNA top (CjCas9)	LacZ sgRNA btm (CjCas9)
pX601-miniCMV-SaCas9-bGHpA-U6-sgRNA (SapI)	pX601-U6-SaCas9 sgRNA scaffold (SapI) (AgeI/XbaI)	miniCMV-XbaI/AgeI F	miniCMV-XbaI/AgeI R
pX601-miniCMV-SaCas9-SpA-sgRNA scaffold (SapI)	pX601-miniCMV -SaCas9-bGHpA-U6 -sgRNA(SapI) (EcoRI/MluI)	SpA F	SpA R
pX601-miniCMV-SaCas9-U6-YFP sgRNA	pX601-miniCMV -SaCas9-SpA-sgRNA scaffold (SapI)	YFP sgRNA (SapI) top (SaCas9)	YFP sgRNA (SapI) btm (SaCas9)
pX601-miniCMV-SaCas9-U6-LacZ sgRNA	pX601-miniCMV -SaCas9-SpA-sgRNA scaffold (SapI)	LacZ sgRNA (SapI) top (SaCas9)	LacZ sgRNA (SapI) btm (SaCas9)
pX552-CMV-mCherry -YFP sgRNA6 M20-M2	pX552-CMV-mCherry (SapI)	M20~M2FWD	M20~M2REV

pX552-CMV-mCherry-SpCas9 sgRNA4-YFP sgRNA6 M20-M2	pX552-CMV-mCherry -SpCas9 sgRNA4 (SapI)	M20~M2FWD	M20~M2REV

Table 8.4 List of plasmid cloning by gBlocks

Plasmid name	vector	Insert (gBlock)	Enzyme
pX552-CMV-mCherry-U6-Cas12a scaffold	pX552-CMV-mCherry	gB1	MluI/ApaI
pX552-CMV-mCherry-U6-SaCas9 scaffold	pX552-CMV-mCherry	gB2	MluI/ApaI
pX552-CMV-mCherry-U6-CjCas9 scaffold	pX552-CMV-mCherry	gB3	MluI/ApaI
pX601-U6-SaCas9 sgRNA scaffold (SapI)	pX601-AAV-CMV::NLS-SaCas9-NLS-3xHA -bGHpA;U6::BsaI-sgRNA	gB2	KpnI/NotI

Table 8.5 Primers for PCR, qPCR and for sequencing

Primer name	Sequence	Purpose
Kozak Cas12a AgeI F	CGCACCGGTgccaccATGACACAGTTCGAGGGCTT	cloning
AsCpf1 EcoRI R	CGCGAATTCTTAGGCATAGTCGGGGACAT	cloning
CMV-ApaI F	GCGGGGCCCCGTTACATAACTTACGGTAAATGGC	cloning
CMV-KpnI R	GCGGGTACCTCTGACGGTTCACTAAACGAGC	cloning
miniCMV_CjCas9 FWD	ACGATGTTCCAGATTACGCTTCGCCGAAGAAAAAGCGCAA	cloning
miniCMV_CjCas9 REV	AAAGATCTTTTATTGAATTCTTAGCTGGCCTCCACCTTTC	cloning
MluI-U6promoter fwd primer	agcACGCGTgagggcctatttcccatgat	sequencing
SpCas9 sgRNA scaffold-MluI reverse primer	gctACGCGTAAAAAAAgcaccgactcggt	sequencing
U6 primer for sequencing the gRNA	GAGGGCCTATTTCCCATGATTCC	sequencing
EYFP Seq-REV	GAAGTCGTGCTGCTTCATGTGG	sequencing
miniCMV seq primer	GTACGGTGGGAGGCCTATATAA	sequencing
CMV forward seq primer	CGCAAATGGGCGGTAGGCGTG	sequencing
SpCas9 FWD	TACGCTTCGCCGAAGAAAAAGC	qPCR
SpCas9 REV	GTGTTGCCCAGCACCTTGAATT	qPCR
mCherry FWD	CCGACATCCCCGACTACTTGAA	qPCR
mCherry REV	TGTAGATGAACTCGCCGTCCTG	qPCR
pX551-FWD	CCGAAGAGGTCGTGAAGAAG	qPCR
pX551-REV	GCCTTATCCAGTTCGCTCAG	qPCR
AAV-ITR FW	GGAACCCCTAGTGATGGAGTT	qPCR
AAV-ITR REV	CGGCCTCAGTGAGCGA	qPCR
pX552-FWD	TGTGGAAAGGACGAAACACC	qPCR
pX552-REV	TGGTCCTAAAACCCACTTGC	qPCR
CMV Seq-FWD	CGCAAATGGGCGGTAGGCGTG	T7E1 PCR
EYFP SURVEYOR REV	CTGGTAGCTCAGGTAGTGGTTG	T7E1 PCR

Table 8.6 Sequence of oligo for sgRNA cloning

Oligo name	Sequence
miniCMV-XbaI/AgeI F	CTAGATAATACGACTCACTATAGGGGGATCCACGTATGT CGAGGTAGGCGTGTACGGTGGGAGGCCTATATAAGCAG AGCTCGTTTAGTGAACCGTCAGATCGCCTGGAGGTACC GCCACCA
miniCMV-XbaI/AgeI R	CCGGTGGTGGCGGTACCTCCAGGCGATCTGACGGTTCA CTAAACGAGCTCTGCTTATATAGGCCTCCCACCGTACAC GCCTACCTCGACATACGTGGATCCCCCTATAGTGAGTCG TATTAT
SpCas9 gRNA1 top	ACCGCAAGAAGTACAGCATCGGCC
SpCas9 gRNA1 btm	AACGGCCGATGCTGTACTTCTTGC
SpCas9 gRNA2 top	ACCGTACAGCATCGGCCTGGACAT
SpCas9 gRNA2 btm	AACATGTCCAGGCCGATGCTGTAC
SpCas9 gRNA3 top	ACCGCCGATGCTGTACTTCTTGT
SpCas9 gRNA3 btm	AACACAAGAAGTACAGCATCGGC
SpCas9 gRNA4 top	ACCGCAGAGTTGGTGCCGATGTCC
SpCas9 gRNA4 btm	AACGGACATCGGCACCAACTCTGC
YFP sgRNA6 top	ACCGCGTCGCCGTCCAGCTCGACC
YFP sgRNA6 btm	AACGGTCGAGCTGGACGGCGACGC
YFP sgRNA4 top (SpCas9)	ACCGCCGTCCAGCTCGACCAGGAT
YFP sgRNA4 btm (SpCas9)	AACATCCTGGTCGAGCTGGACGGC
YFP sgRNA5 top (SpCas9)	ACCGCCGTCCAGCTCGACCAGGA
YFP sgRNA5 btm (SpCas9)	AACATCCTGGTCGAGCTGGACGGC
YFP sgRNA6 top (SpCas9)	ACCGCGTCGCCGTCCAGCTCGACC
YFP sgRNA6 btm (SpCas9)	AACGGTCGAGCTGGACGGCGACGC
LacZ sgRNA1 top (SpCas9)	ACCTGCGAATACGCCCACGCGAT
LacZ sgRNA1 btm (SpCas9)	AACATCGCGTGGGCGTATTCGCA
YFP sgRNA 20nt top (Cas12a)	ACCGTAATTTCTACTCTTGTAGATCGTCGCCGTCCAGCT CGACCAGGTTTTGGCC
YFP sgRNA 20nt btm (Cas12a)	AAAAGGTCGAGCTGGACGGCGACGATCTACAAGAGTAG AAATTAC

YFP sgRNA 23nt top (Cas12a)	ACCGTAATTTCTACTCTTGTAGATCGTCGCCGTCCAGCTCGACCTTTTGGCC
YFP sgRNA 23nt btm (Cas12a)	AAAAGGTCGAGCTGGACGGCGACGATCTACAAGAGTAGAAATTACC
LacZ sgRNA 20nt top (Cas12a)	ACCGTAATTTCTACTCTTGTAGATCGAATACGCCCACGCGATGGTTTTGGCC
LacZ sgRNA 20nt btm (Cas12a)	AAAACCATCGCGTGGGCGTATTCGATCTACAAGAGTAGAAATTAC
LacZ sgRNA 23nt top (Cas12a)	ACCGTAATTTCTACTCTTGTAGATCGAATACGCCCACGCGATGGGTATTTTGGCC
LacZ sgRNA 23nt btm (Cas12a)	AAAATACCCATCGCGTGGGCGTATTCGATCTACAAGAGTAGAAATTACC
YFP sgRNA (SapI) top (SaCas9)	ACCGTACGTCGCCGTCCAGCTCGAC
YFP sgRNA (SapI) btm (SaCas9)	AACGTCGAGCTGGACGGCGACGTAC
LacZ sgRNA (SapI) top (SaCas9)	ACCGCTTTGCGAATACGCCCACGCG
LacZ sgRNA (SapI) btm (SaCas9)	AACCGCGTGGGCGTATTCGCAAAGC
YFP sgRNA1 top (CjCas9)	ACCGCGAGCTGGACGGCGACGTAAAC
YFP sgRNA1 btm (CjCas9)	AACGTTTACGTCGCCGTCCAGCTCGC
YFP sgRNA2 top (CjCas9)	ACCGTCGCCGTCCAGCTCGACCAGG
YFP sgRNA2 btm (CjCas9)	AACCCTGGTCGAGCTGGACGGCGAC
LacZ sgRNA top (CjCas9)	ACCGTTGCGAATACGCCCACGCGATG
LacZ sgRNA btm (CjCas9)	AACCATCGCGTGGGCGTATTCGCAAC
SpA F	aattcAATAAAAGATCTTTATTTTCATTAGATCTGTGTGTTGGTTTTTTGTGTA
SpA R	CGCGTACACAAAAAACCAACACACAGATCTAATGAAAATAAAGATCTTTTATTG
M20FWD	ACCGGGTCGCCGTCCAGCTCGACC
M20REV	AACGGTCGAGCTGGACGGCGACCC
M18FWD	ACCGCGACGCCGTCCAGCTCGACC
M18REV	AACGGTCGAGCTGGACGGCGTCGC
M16FWD	ACCGCGTCCCCGTCCAGCTCGACC
M16REV	AACGGTCGAGCTGGACGGGGACGC
M14FWD	ACCGCGTCGCGGTCCAGCTCGACC

M14REV	AACGGTCGAGCTGGACCGCGACGC
M12FWD	ACCGCGTCGCCGACCAGCTCGACC
M12REV	AACGGTCGAGCTGGTCGGCGACGC
M10FWD	ACCGCGTCGCCGTCGAGCTCGACC
M10REV	AACGGTCGAGCTCGACGGCGACGC
M8FWD	ACCGCGTCGCCGTCCACCTCGACC
M8REV	AACGGTCGAGGTGGACGGCGACGC
M6FWD	ACCGCGTCGCCGTCCAGCACGACC
M4FWD	AACGGTCGTGCTGGACGGCGACGC
M4REV	ACCGCGTCGCCGTCCAGCTCCACC
M2FWD	AACGGTGGAGCTGGACGGCGACGC
M2REV	ACCGCGTCGCCGTCCAGCTCGAGC

Table 8.7 Sequence of gBlocks

gBlock name	**Sequence**
(gB1)U6_Cas12a_sgRNA_scaffold	gctagcGGTACCACGCGTgagggcctatttcccatgattcctt catatttgcatatacgatacaaggctgttagagagataattggaatta atttgactgtaaacacaaagatattagtacaaaatacgtgacgtaga aagtaataatttcttgggtagtttgcagttttaaaattatgttttaaaatgg actatcatatgcttaccgtaacttgaaagtatttcgatttcttggctttatat atcttGTGGAAAGGACGAAACACCGTAATTTCTAC TCTTGTAGATggaagagcgagctcttctTTTTGGGCCC GCGGCCGCgaattc
(gB2)U6_SaCas9_sgRNA_scaffold	gctagcGGTACCACGCGTgagggcctatttcccatgattcctt catatttgcatatacgatacaaggctgttagagagataattggaatta atttgactgtaaacacaaagatattagtacaaaatacgtgacgtaga aagtaataatttcttgggtagtttgcagttttaaaattatgttttaaaatgg actatcatatgcttaccgtaacttgaaagtatttcgatttcttggctttatat atcttGTGGAAAGGACGAAACACCggaagagcgagct cttctgttttagtactctggaaacagaatctactaaaacaaggcaaaa tgccgtgtttatctcgtcaacttgttggcgagattttttGGGCCCGC GGCCGCgaattc
(gB3)U6_CjCas9_sgRNA_scaffold	gctagcGGTACCACGCGTgagggcctatttcccatgattcctt catatttgcatatacgatacaaggctgttagagagataattggaatta atttgactgtaaacacaaagatattagtacaaaatacgtgacgtaga aagtaataatttcttgggtagtttgcagttttaaaattatgttttaaaatgg actatcatatgcttaccgtaacttgaaagtatttcgatttcttggctttatat atcttGTGGAAAGGACGAAACACCggaagagcgagct cttctGTTTTAGTCCCTGAAGGGACTAAAATAAAG AGTTTGCGGGACTCTGCGGGGTTACAATCCCC

	TAAAACCGCTTTTTTGGGCCCGCGGCCGCgaattc

Appendix 2 Materials and experiment set up

Table 8.8 Chemicals and reagents

Chemicals and reagents	Supplier	Catalogue No.
Dulbecco's Modified Eagle Medium (DMEM)	Life Technologies	11965118
Iscove's Modified Dulbecco's Medium (IMDM)	Life technologies	12440061
RPMI 1640 medium	Life technologies	11875119
Dulbecco's Phosphate Buffered Saline (DPBS)	Life technologies	14190250
Fetal Bovine Serum (FBS)	Bovogen	SFBS
penicillin-streptomycin	Life Technologies	15140122
GlutaMAX	Promega	35050-061
Opti-MEM	Life Technologies	11058021
FuGENE-HD transfection reagent	Promega	E2311
Lipofectamine 2000 transfection reagent	Life Technologies	11668019
0.25%Trypsin-EDTA	Life Technologies	25200-072
Disodium EDTA	Sigma-Aldrich	6381-92-6
Dimethyl Sulfoxide (DMSO)	Sigma	D2650-100 mL
PEG-it™ Virus Precipitation Solution	System Biosciences	#LV810A-1
Puromycin dihydrochloride	Thermo Fisher	A1113803
polybrene	Sigma-Aldrich	H9268-5G
Sodium Chloride	AMRESCO	0241-2.5KG
Trizma base	Sigma	T1503-1KG
Glycine	Sigma	G8898-1KG
Sodium azide (NaN3)	Sigma	S2002-100g
NaH2PO4	Sigma	S0751-500G
Calcium chloride dihydrate ($CaCl_2 \cdot 2H_2O$)	Sigma	223506-500G
Agarose	Sigma	A9539-250G
Ampicillin sodium salt	Sigma	A9518-5G
Bovine Serum Albumin	Sigma	A4503-50G
HEPES (500g)	Santa Cruz Biotechnology	sc-29097A
Glycerol	Sigma	G5150-1L
UltraPure™ DNase/RNase-Free Distilled Water	Life Technologies	10977015
DEPC-treated water	Invitrogen	AM9920
Virkon 5gm Tablets x 10 Tabs	MedShop Australia	MED1610661
2-Mercaptoethanol	Life Technologies	21985-023
4% paraformaldehyde	ProSciTech	N/A
TRITON X-100	Sigma	T8787-50ML
SOC outgrowth medium	Sigma	S1797-10X5ML
LB Broth Base	Life Technologies	12780-029
LB broth with agar	Sigma	L2897-1KG
TAE buffer (50x)	Thermo Scientific	#B49
NuPAGE MES SDS running buffer (20X)	Invitrogen	NP0002
TE buffer (Ph 8.0, 500 mL)	Life technologies	AM9849

Sodium Dodecyl Sulfate (SDS)_	Invitrogen	15525017
Tween 20	Sigma	P9416-50ML
SYBR Safe-DNA Gel Stain	Invitrogen	S33102
1KB plus DNA ladder	Life technologies	10787018
Gel loading Dye Purple (6x)	NEB	#B7025S
NuPAGE® LDS Sample Buffer (4X)	Invitrogen	0007
Novex® sharp pre-stained protein standard	Invitrogen	LC5800
Cell Lysis Buffer	Thermo Fisher Scientific	89900
T4 DNA ligase	NEB	M0202S
Alkaline Phosphatase, Calf Intestinal (CIP)	NEB	M0290S
T7 Endonuclease I	NEB	M0302S
T4 Polynucleotide Kinase (PNK)	NEB	M0201S
DAPI	Sigma	D9542-5MG
Anti-Cas9 Antibody, clone 7A9	Millipore	MAC133
HA-probe Antibody (F-7)	Santa Cruz Biotechnology	sc-7392
mouse monoclonal β-actin antibody	Millipore	MAB 1501
HRP-conjugated goat anti-mouse secondary antibody	Life Technologies	A-11045
recombinant SpCas9 protein	New England Biolabs	M0386S
NuPAGE™ Novex™ 4-12% Bis-Tris Protein Gels	Life Technologies	NP0321BOX
Skim milk powder	Woolworth	#2885
OCT compound	Tissue-Tek	4583

Table 8.9 Consumables

Consumables	**Supplier**	**Catalogue No.**
15 mL Falcon® polypropylene centrifuge tube	Corning	352097
50 mL Falcon® polypropylene centrifuge tube	Corning	352070
6 well TC plates	in vitro technologies	FAL353046
Falcon 100 x 20 mm TC culture dish	in vitro technologies	FAL353003
PCR tubes	Thermo Fisher Scientific	AM12230
1.5 mL Eppendorf tube	Thermo Fisher Scientific	AM12450
Qubit assay tubes	Invitrogen	Q32856
14 mL polypropylene round-bottom tube	In vitro technologies	352059
Serological pipette sterile	Costar	N/A (5, 10, 25, 50 mL)
Sterile filter pipette tips	Corning Axygen	N/A (10, 20, 200, 1000 µL)
Cryogenic vials 2.0 mL	Corning	430659
T75 cell culture flasks	in vitro technologies	FAL353136
T175 cell culture flasks	in vitro technologies	FAL353112
T225 cell culture flasks	in vitro technologies	FAL353138
Countess™ Cell Counting Chamber Slides	Life Technologies	C10228
Millex-HV 0.45 µm filter	Millipore	SLHV004SL
polyvinylidene difuoride membranes	BIO-RAD	162-0177
Nunc-Immuno™ MicroWell™ 96 well solid plates	Sigma-Aldrich	M9410-1CS
Flow cytometry tubes	BD Falcon	367 526

FLEX glass slides	Dako	
Stericup-GP 0.22 µm PES 500mL	Millipore	SCGPU05RE
Hamilton syringe (10 µL)	Sigma	24530
Coverslips (22 x 22 mm)	TRAJAN/Grale	CS2222100
Corning® cell lifter	Sigma	CLS3008-100EA
30-gauge needle	Terumo	22-272-115
White cardboard boxes	Interpath	CVB100
2ml aspirating pipette	in vitro technologies	FAL357558

Table 8.10 Commercial kits

Commercial Kits	**Supplier**	**Catalogue No.**
QIAquick PCR purification kit (250)	Qiagen	28106
Qiaprep spin miniprep kit (250)	Qiagen	27106
HiSpeed Plasmid Maxi Kit (10)	Qiagen	12262
QIAfilter Plasmid Mega Kit (5)	Qiagen	12281
Fast SYBR Green Master Mix	Thermo Fisher Scientific	4385612
Purelink HiPure Precipitator Module	Life Technologies	K2100-22
Qubit™ dsDNA BR Assay Kit	Invitrogen	Q32853
Amersham ECL Prime Western Blotting Detection kit	GE Healthcare	RPN2232
RNeasy Mini Kit (250)	Qiagen	74106
Pierce™ BCA Protein Assay Kit	Thermo Scientific™	23227
TaKaRa AAVpro Purification Kit (AAV2)	Scientifix	6232
TaKaRa AAVpro Purification Kit (All Serotypes)	Scientifix	6666
DNA Clean & Concentrator kit	Zymo Research	D4033
Taqman RNA Reverse Transcription Kit	Invitrogen	N8080234
Quick-DNA™ MidiPrep Plus Kit	Zymo Research	D4075
Quick-DNA™ MiniPrep Plus Kit	Zymo Research	D4068
Papain dissociation system	Worthington Biochemical Corporation	LK003153
Puregene® Core Kit A	Qiagen	Lot No. 8570335
Puregene® Proteinase K (650 µL)	Qiagen	158918
RNase A Solution	Qiagen	158922

Table 8.11 Plasmid origin

Plasmid name	**Source**	**Addgene No.**	**Purpose**
pX551	Feng Zhang lab	#60957	AAV plasmid expressing Cas9 under mecp2 promoter
pX552	Feng Zhang lab	#60958	AAV plasmid for sgRNA cloning, expressing GFP under hsyn promoter
pHpa-trs-KS-Luci	Original plasmid from Prof Douglas M. McCarty, Center for Gene Therapy, Nationwide Children's Hospital,		CMV for subcloning

	USA		
pX601-AAV-CMV::NLS-SaCas9-NLS-3xHA-bGHpA;U6::BsaI-sgRNA	Feng Zhang lab	#61591	A single AAV vector expressing SaCas9 and its sgRNA
pY010 (pcDNA3.1-hAsCpf1)	Feng Zhang lab	#69982	plasmid expressing hAsCpf1 under CMV promoter
pX404-CjCas9	Feng Zhang lab	#68338	plasmid expressing CjCas9 under CMV promoter
AAV-U6-sgRNA-hSyn-mCherry	Alex Hewitt lab	#87916	AAV plasmid for sgRNA cloning, expressing mCherry driven by hSyn promoter (replaced the GFP in pX552 from Zhang lab with mCherry)
AAV-U6-YFP sgRNA2-hSyn-mCherry	Alex Hewitt lab	Ref [20]	AAV plasmid with YFP KO sgRNA, expressing mCherry driven by hSyn promoter
AAV-U6-LacZ sgRNA-hSyn-mCherry	Alex Hewitt lab	Ref [20]	AAV plasmid with LacZ KO sgRNA, expressing mCherry driven by hSyn promoter
pXX2	A gift from Prof Ian Alexander	N/A	AAV2 production
pXX6	A gift from Prof Ian Alexander	N/A	AAV2 production
7m8	John Flannery & David Schaffer lab	#64839	AAV7m8 production
pMD2.G	Didier Trono	#12259	Lentivirus production
pCMV D8.91	RNAiCore; Academia Sinica, Taipei, Taiwan	N/A	Lentivirus production

Table 8.12 Cell lines

Cells	**Source**	**Catalogue No.**
Human Embryonic Kidney 293A (HEK293A) cell	Life Technologies	R70507
HEK293FT cell	Life Technologies	R70007
Subcloning Efficiency DH5a competent cell	Life Technologies	18265017
Endura Electro Competent Cells	Lucigen	75852
OCM-1	From Prof. Dr. G.P.M. Luyten, Rottterdam University Hospital, Rotterdam	
HEK293D cell	A gift from Prof Ian Alexander (Children's Medical Research Institute, Australia)	
HEK293A-YFP cell	Generated by transducing HEK 293A cells with pAS2.EYFP.puro lentivirus (RNAiCore;Academia Sinica)	

Table 8.13 Animal origin

Animals	**Source**

Thy1-YFP transgenic mice [B6.Cg-Tg(Thy1-YFP)16Jrs/J]	Obtained from the Jackson Laboratory (mouse stock number: 003709; Bar Harbor, ME, USA) and bred at the animal facility of the Menzies Institute for Medical Research
CMV-Cre::Rosa26-YFP transgenic mice	Animal Services, Menzies Institute for Medical Research
C57BL/6 mice	Animal Services, Menzies Institute for Medical Research

Table 8.14 Drugs used for animal study

Drugs	**Source**
0.5% Tropicamide Eye Drops (Mydriacyl)	Alcon
Proxymetacaine hydrochloride Eye Drops (Alcaine)	Alcon
Ocular lubricant (Systane)	Alcon
Ketamine/ Xylazine	Animal Services, Menzies Research Institute Tasmania

Table 8.15 Equipment

Equipment	Supplier	Model/Catalogue No
Thermal cycler	Bio-Rad	T100™
Countess Automated Cell Counter	Invitrogen	C10227
Nanodrop spectrophotometer	Thermo Fisher Scientific	Nanodrop 1000
Qubit Fluorometer	Invitrogen	Qubit® 2.0
Ultrasonic cell disruptor	Qsonica	MISONIX Microson XL 2000
Microplate reader	TECAN	Infinite M1000 Pro
Invitrogen Mini Gel Tank	Invitrogen	A25977
XCell II™ Blot Module	Life Technologies	EI9051
Amersham Imager 600	GE Healthcare	29-0834-61
Flow cytometer	BD Bioscience	FACSCanto II
Leica Modulation Contrast Microscope	Leica	Leica DMIRB
Zeiss Axio Imager Microscope	Zeiss	N/A
Centrifuge	Eppendorf	5430R
Microcentrifuge	Eppendorf	5424
UMP3 Ultra Micro Pump	World Precision Instruments	UMP3-3
Mr. Frosty™ Freezing Container	Thermo Fisher Scientific	5100-0001
Cryostat	Leica, Germany	CM1850
Virtual Slide Microsope	Olympus	VS120
Phase contrast microscope	Nikon	TE2000-U
Digital Dry Bath	Benchmark	BSH1002
Spectral-domain Optical coherence tomography	Bioptigen	Envisu R2200 VHR
StepOnePlus™ Real-Time PCR System	Applied Biosystems	4376600
Milli-Q Biocel Water Purification System	Millipore	Milli-Q Biocel

Table 8.16 Software and online resources

Purpose	Software/Website
CRISPR	https://benchling.com http://crispr.mit.edu/ https://www.synthego.com/ Cas-OFFinder
Molecular biology tools	https://www.neb.com/tools-and-resources
FACS analysis	FlowJo®
Bioinformatic analysis	CRISPRAnalyzeR gProfiler ULCAN FastQC (http://www.bioinformatics.babraham.ac.uk/projects/fastqc) BBTools (https://jgi.doe.gov/data-and-tools/bbtools/)
Cell counting, image analysis	Image J
Statistics and plot	GraphPad Prism 7.0

Table 8.17 Reagent and equipment setup

Cell culture Cell growth medium for HEK293 cells: Complete DMEM: DMEM + 10% FBS + 5 mL GlutaMAX stock + 5 mL Pen/Strep stock Freezing medium: FBS+10% DMSO Cell growth medium for OCM-1 cells: RPMI 1640+10% FBS + 5 mL GlutaMAX stock + 5 mL Pen/Strep stock Cell culture medium for HEK293D for AAV production: One week before AAV production, HEK293D cells were cultured in complete DMEM medium. After that, cells were maintained in Pen/Strep free medium. Growth medium: DMEM+10% FBS Transfection medium: IMDM+10% FBS Maintenance medium: DMEM+2% FBS
Molecular Biology Liquid LB with ampicilin (1 L): 20g of Lennox L Broth base in 1 L of distilled water. Autoclave at 121c for 15 min and cool to room temperature. Upon use for bacterial culture, add ampicillin to a final concentration of 100 μg/mL. LB agar plate with ampicilin (1 L): 35g of Lennox LB Broth with agar in 1 L of distilled water. Autoclave at 121ºC for 15 min and allow the mixture to cool down to around 55 ºC before adding ampicillin to a final concentration of 100 μg/mL. Pour 20~25 mL of LB agar per petri dish in a sterile fume hood. Cool down until solidified. Place the lids, invert the plates and store at 4 ºC.

Western blot

10 x Transfer Buffer (500 mL)：
Tris-29.1 g, Glycine-14.6 g, 10% SDS-18.75 mL in 500 mL with distilled water

1x Transfer buffer （500mL）:
10x transfer buffer-50 mL, methanol-100 mL, distilled water-350 mL

1 x TBS-T:
1M Tris pH 7.5 20 mL, 5M NaCl 60 mL, 10% Tween 20 10 mL, million Q 1910 mL.

Blocking buffer (5% skim milk, 50 mL):
2.5 g skim milk in 50 mL 1xTBS-T buffer.

Primary antibody:
Add desired amount of primary antibody to 10 mL primary antibody dilution buffer (10mL TBS-T with 2% BSA and 10% NaN_3).

Secondary antibody:
Add desired amount of HRP-conjugated secondary antibody (e.g. 1:5000) in 5% non-fat milk.

AAV production

2 x HBS:
NaCl 8.182 g (280 mM final)
HEPES 5.958 g (50 mM final)
Make up to 500 mL with distilled water after adjusting to pH 7.1 and autoclave.

0.15 M NaH_2PO4:
10.647 g in 500 mL distilled water. Adjust to pH 7.1 and autoclave.

2 M $CaCl_2$
29.404 g of $CaCl_2 \cdot 2H_2O$ in 100 mL distilled water. Autoclave.

FACS

FACS buffer:
Make DPBS-2 mM EDTA solution, then add BSA to a concentration of 1% w/v. Adjust pH to 7.45 and sterilize using a Stericup-GP 0.22 μm bottle.

Appendix 3 AAVs and titration

Table 8.18 AAVs and titration

AAV2	**Vector**	**Titration (vg/mL)**
AAV2-SpCas9	pX551	$8.18x10^{12}$
AAV2-YFP sgRNA2	pX552-hsyn1-mCherry-YFP sgRNA2	$8.97x10^{12}$
AAV2-YFP sgRNA6	pX552-hsyn1-mCherry-YFP sgRNA6	$4.81x10^{12}$
AAV2-SpCas9 sgRNA -YFP sgRNA2	pX552-hsyn1-mCherry-Cas9 sgRNA4 -YFP sgRNA2	$1.47x10^{13}$
AAV2-SpCas9 sgRNA -YFP sgRNA6	pX552-hsyn1-mCherry-Cas9 sgRNA4 -YFP sgRNA6	$1.89x10^{13}$
AAV2-SpCas9 sgRNA -LacZ sgRNA	pX552-hsyn1-mCherry-Cas9 sgRNA4 -LacZ sgRNA	$1.21x10^{13}$
AAV7m8	**Vector**	**Titration (vg/mL)**
AAV7m8-SpCas9	pX551-miniCMV-SpCas9	$5.13x10^{14}$
AAV7m8-SaCas9	pX551-miniCMV-SaCas9	$5.48x10^{14}$
AAV7m8-Cas12a	pX551-miniCMV-Cas12a	$6.22x10^{14}$
AAV7m8-CjCas9 (CMV)	pX551-CMV-CjCas9	$1.61x10^{15}$
AAV7m8-CjCas9 (miniCMV)	pX551-miniCMV-CjCas9	$3.53x10^{14}$
AAV7m8-YFP sgRNA5 (SpCas9)	pX552-CMV-mCherry-YFP sgRNA5 (SpCas9)	$2.31x10^{14}$
AAV7m8-YFP sgRNA 20nt (Cas12a)	pX552-CMV-mCherry-YFP sgRNA 20nt (Cas12a)	$1.06x10^{15}$
AAV7m8-YFP sgRNA (SaCas9 dual)	pX552-CMV-mCherry-YFP sgRNA (SaCas9)	$1.22x10^{14}$
AAV7m8-YFP sgRNA2 (CjCas9)	pX552-CMV-mCherry-YFP sgRNA2 (CjCas9)	$1.26x10^{15}$
AAV7m8-YFP sgRNA (SaCas9 single)	pX601-miniCMV-SaCas9-U6-YFP sgRNA	$2.55x10^{14}$
AAV7m8-mCherry	pX552-CMV-mCherry	$1.58x10^{14}$

Appendix 4 Animal groups

Table 8.19 Animal groups for time course of SpCas9 expression (Chapter 3 study)

Animal groups (C57BL/6)*	Number
AAV2-SpCas9+AAV2-YFP sgRNA2	39
AAV2-SpCas9+AAV2-SpCas9 sgRNA/YFP sgRNA2	37

*Left eye was injected. Right eye was control with no injection.

Table 8.20 Animal groups for YFP disruption (Chapter 3 study)

Animal groups (Thy1-YFP transgenic mice)*	Number
AAV2-SpCas9+AAV2-YFP sgRNA2	17
AAV2-SpCas9+AAV2-SpCas9 sgRNA/YFP sgRNA2	17
AAV2-SpCas9+AAV2-SpCas9 sgRNA/LacZ sgRNA	15

Animal groups (Thy1-YFP transgenic mice)*	Number
AAV2-SpCas9+AAV2-YFP sgRNA6	9
AAV2-SpCas9+AAV2-SpCas9 sgRNA/YFP sgRNA6	10
AAV2-SpCas9+AAV2-SpCas9 sgRNA/LacZ sgRNA	10

*Left eye was injected. Right eye was control with no injection.

Table 8.21 Animals for CRISPR comparison study (Chapter 4 study)

Animal groups (CMV-Cre::Rosa26-YFP transgenic mice) #	Number
AAV7m8-SpCas9+AAV7m8-YFP sgRNA5 (SpCas9)	20
AAV7m8-SaCas9+AAV7m8-YFP sgRNA (SaCas9 dual)	20
AAV7m8-YFP sgRNA (SaCas9 single)+AAV7m8-mCherry	20
AAV7m8-Cas12a+AAV7m8-YFP sgRNA 20nt (Cas12a)	20
AAV7m8-CjCas9+AAV7m8-YFP sgRNA2 (CjCas9)	20
AAV7m8-CjCas9(miniCMV)+AAV7m8-YFP sgRNA2 (CjCas9)	21
AAV7m8-mCherry	29

both eyes were injected with the same AAV7m8-CRISPR/Cas in one animal.

Appendix 5 Uncropped agarose gel and western blot images.

Figure 3.3

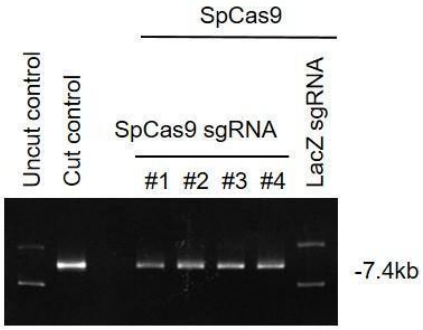

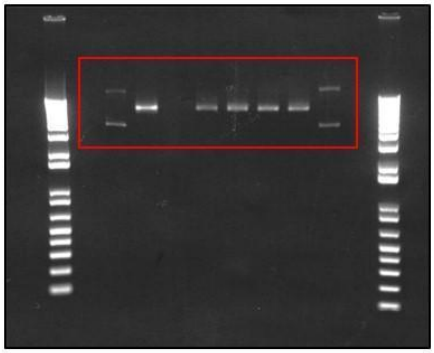

Figure 3.4

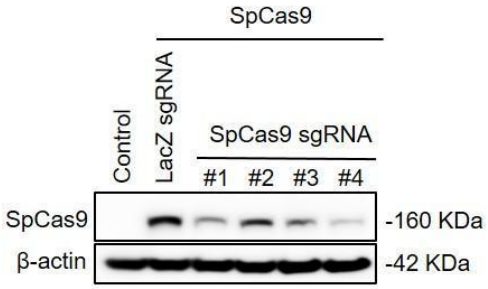

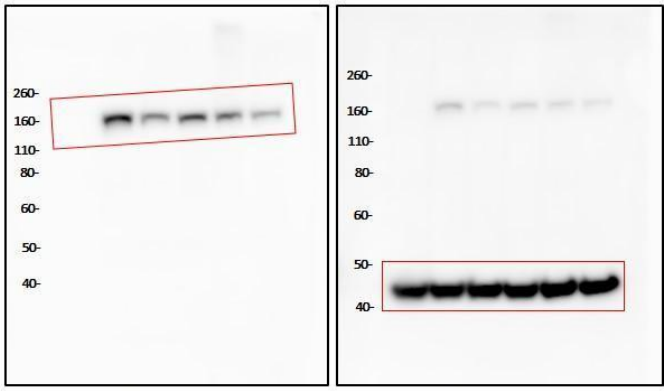

Figure 3.5

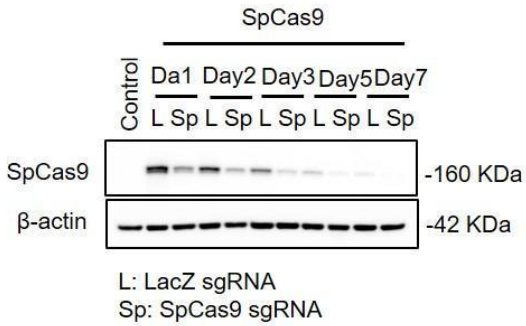

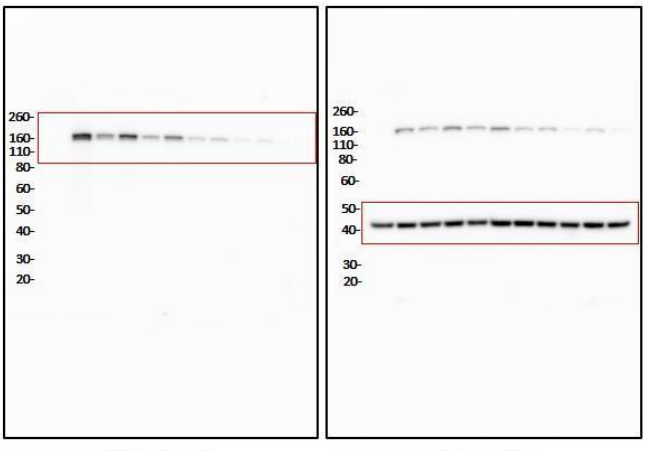

Figure 3.8

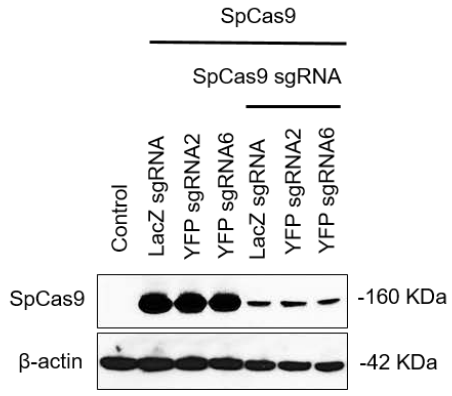

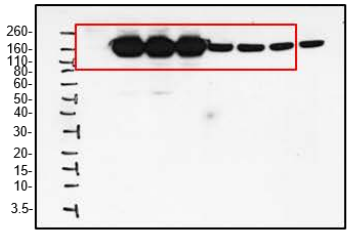

mouse anti-SpCas9

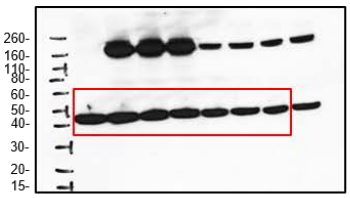

mouse anti-β-actin

Figure 4.6

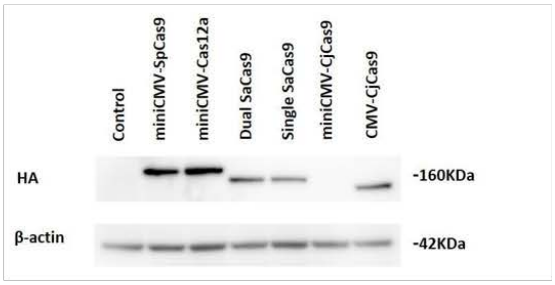

Mouse HA tag antibody (F-7)

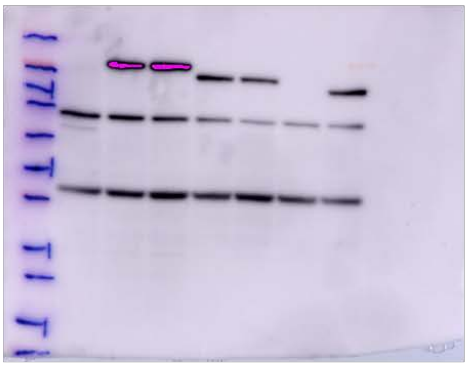

Over exposure one with ladder

Figure 3.12 B

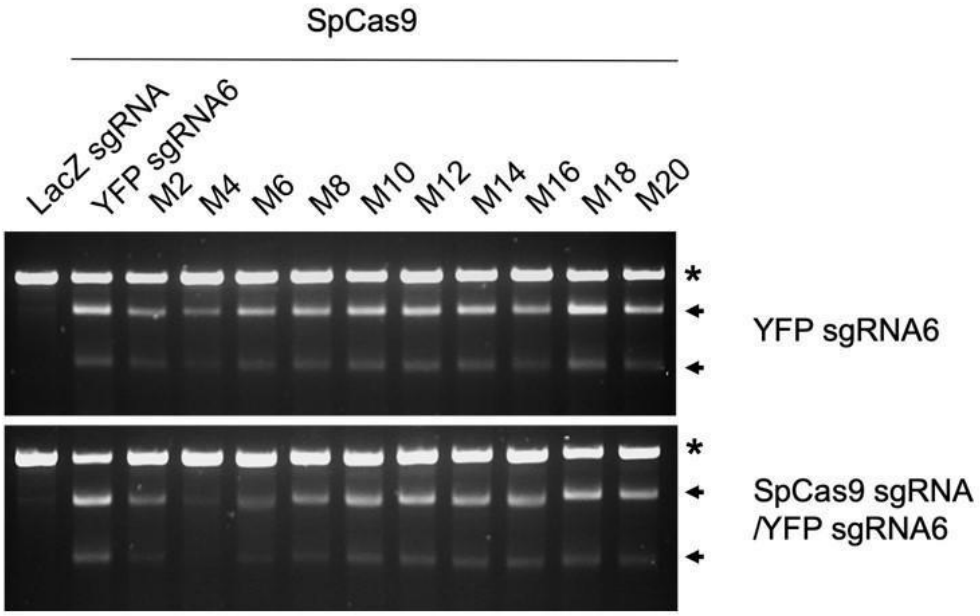
SpCas9
LacZ sgRNA
YFP sgRNA6
M2
M4
M6
M8
M10
M12
M14
M16
M18
M20
YFP sgRNA6
SpCas9 sgRNA
/YFP sgRNA6

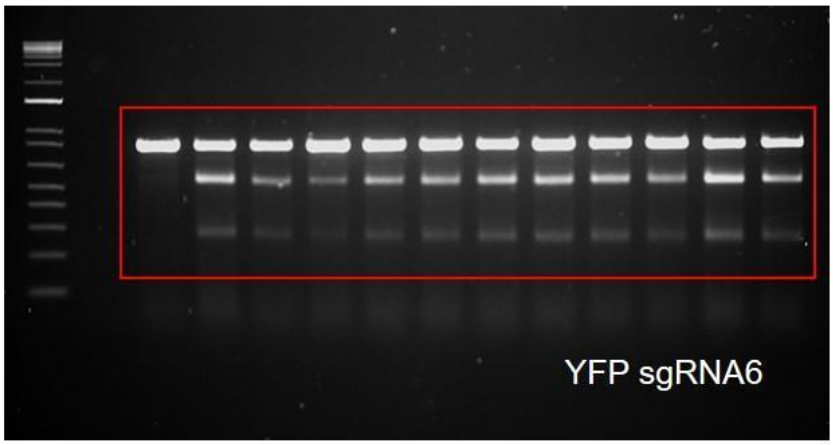
YFP sgRNA6

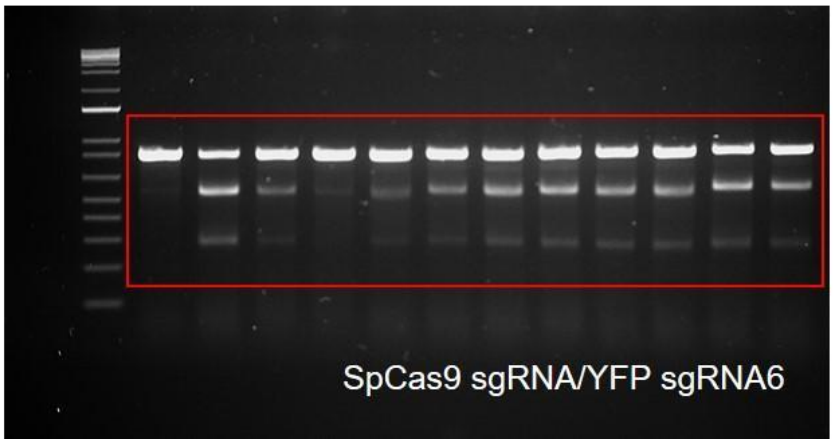
SpCas9 sgRNA/YFP sgRNA6